SECTION I

RESEARCH IN PROGRESS

NUCLEAR REACTIONS -- EXPERIMENTAL

HIGH ENERGY GAMMA RAY PRODUCTION IN ^{2}H AND ^{4}He INDUCED REACTIONS AT 25 AND 53 MeV/A

C.L. Tam, J. Stevenson, W. Benenson, J. Clayton, Y. Chen, E. Kashy, A.R. Lampis, D.J. Morrissey, M.Samuel, and J.S.Winfield

Since the discovery[1,2] of high energy gamma ray production in heavy-ion collision, there have been a number of experiments[3-7] carried out by various groups to study different systems in order to gain some understanding into its production mechanism. The characteristic features of the gamma ray spectra are the exponentially decreasing energy spectra and a slightly forward peaked angular distribution which can be attributed to an isotropic emission from a moving source having velocity close to the nucleon-nucleon center-of-mass velocity.

Several models have been proposed[8-15] to explain the possible mechanism responsible for these unexpectedly large gamma ray yields at high energy. One such model is the coherent nucleus-nucleus bremsstrahlung mechanism[8], which predicts a quadrupole angular distribution and a Z^2 dependence of the gamma ray cross section. It should become dominant for heavy systems. Other models suggest that gamma rays come from the incoherent neutron-proton bremsstrahlung[9-14] within the two colliding nuclei. A different approach was to attributes the gamma rays to the statistical emission of a recoiling nuclear fireball.[15] In this case, the angular distributions should be isotropic.

Here we report measurements of gamma rays produced in ^{2}H and ^{4}He induced heavy-ion reactions. The detectors used were three gamma ray telescopes, each consisting an active BaF_2 scintillator converter followed by a stack of 8 (or 13 in the third telescope) plastic Cerenkov detectors. The energies of the gamma rays were determined by the sum of the weighted light output from the Cerenkov detectors as well as from the active converter. Each telescope was surrounded by anticoincidence shields against cosmic ray muons.

Figure 1 shows the gamma ray energy spectra measured at $\theta_{lab} = 90°$ for all the reactions we studied. They all possess that characteristic exponential fall off in the form $Ae^{-E/T}$, with slope parameters independent of targets. In Table I, we show the fitted values of the inverse slopes T. Also shown are the values of β extracted from the data assuming isotropic emission, as well as the values for the nucleon-nucleon and nucleus-nucleus center-of-mass velocities of the projectile-target system.

Figure 2 is a comparison of energy spectra at $\theta_{lab} = 90°$ for the three different beams on a Pb target showing the slope difference for different beam energies.

Table I: Parameters obtained from best fit to the gamma ray spectra. Also shown, for comparison with the β_{exp} extracted from the spectra, are the nucleon-nucleon (β_{NN}) and the nucleus-nucleus (β_{Ns-Ns}) center-of-mass velocities for each projectile-target system.

Beam Ion	Target	E/A(MeV)	T(MeV)	β_{exp}	β_{NN}	β_{Ns-Ns}
He	C	25	6.9	0.03	0.11	0.049
He	Zn	25	6.3	0.05	0.11	0.013
He	Pb	25	6.0	0.06	0.11	0.004
d	C	53	10.2	0.10	0.16	0.040
d	Zn	53	8.9	0.12	0.16	0.010
d	Pb	53	8.6	0.16	0.16	0.003
He	C	53	12.7	0.10	0.16	0.07
He	Zn	53	11.1	0.13	0.16	0.019
He	Pb	53	11.5	0.12	0.16	0.006

The gamma ray angular distributions of all the systems we studied were shown in Fig. 3, for

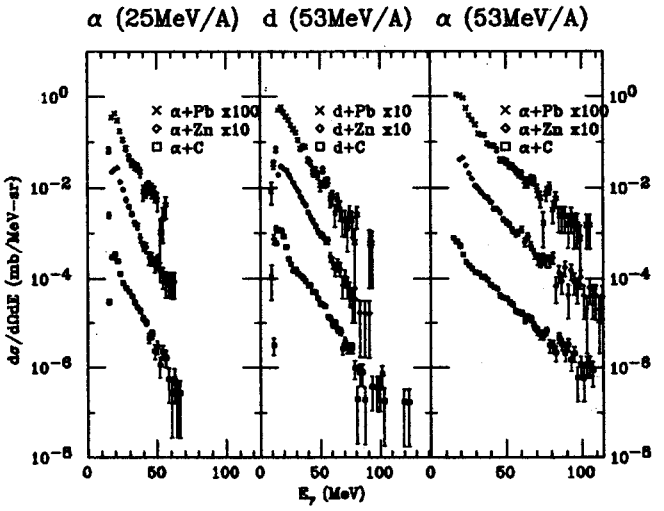

Fig. 1: Gamma ray energy spectra at θ_{lab} = 90° for the three beams and three targets we measured.

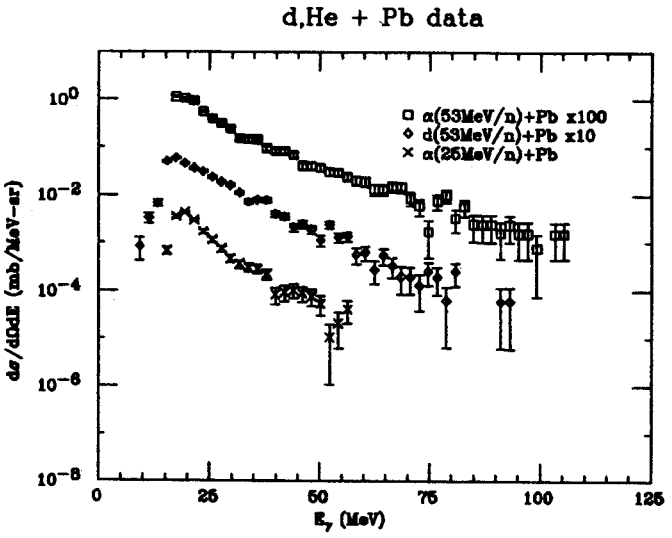

Fig. 2: Comparison of gamma ray energy spectra at θ_{lab} = 90° for ^{2}H(53MeV/A), ^{4}He(25MeV)/A and ^{4}He(53MeV/A) on Pb targets.

gamma ray energy above 30 MeV. They all appears to be slightly forward peaked, and do not change with different energy cuts.

To conclude, all our data have exponentially falling energy spectra and slightly forward peaked angular distributions. The slope parameters are roughly independent of target.

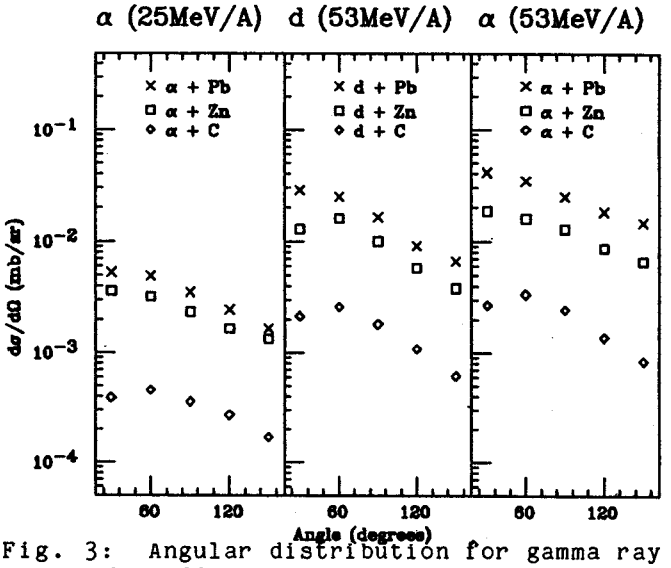

Fig. 3: Angular distribution for gamma ray energy above 30 MeV for all the systems.

References

1. E. Grosse et al., in Proceedings of the International Workshop on Gross Properties of Nuclei and Nuclear Excitations XIII, Hirschegg, Austria, 1985.
2. K. B. Beard et al., Phys. Rev. C32,1111(1985).
3. J. Stevenson et al., Phys. Rev. Lett. 57, 555 (1986).
4. M. Kwato Njock et al., Phys. Lett. 175B, 125 (1986).
5. N. Alamanos et al., Phys. Lett. 173B, 392 (1986).
6. E. Grosse et al., Europhysics Lett. 2, 9 (1986).
7. R. Hingmann et al., Phys. Rev. Lett. 58, 759 (1987).
8. D. Vasak, B. Muller, and W. Greiner, J. Phys. G Nucl. Phys. 11, 1309 (1985).
9. B. A. Remington, M. Blann, and G. F. Bertsch, Phys. Rev. C35, 1720 (1987).
10. C. M. Ko, G. F. Bertsch, and J. Aichelin, Phys. Rev. C31, 2324 (1985).
11. W. Bauer, W. Cassing, U.mosel, and M. Tohyama, Nucl. Phys. A456, 159 (1986).
12. W. Bauer, G. F. Bertsch, W. Cassing, and U. Mosel, Phys. Rev. C34, 2127 (1986).
13. K. Nakayama, and G. F. Bertsch, C34, 2190 (1986).
14. D. Neuhauser, and S. E. Koonin, Nucl. Phys. A462, 163 (1987).
15. H. Nifenecker, and J. P. Bondorf, Nucl. Phys. A442, 478 (1985).

HIGH ENERGY GAMMA RAY PRODUCTION IN THE REACTION OF ^{136}Xe + Sn AT E/A =66, 89, AND 124 MeV

J. Clayton, J. Stevenson, W. Benenson, Y. Chen, E. Kashy, A.R. Lampis, M. Mohar, D.J. Morrissey, T.K. Murakami, M. Samuel, B. Sherrill, C.L. Tam, and J.S. Winfield

High energy gamma ray production ($20<E_\gamma<120$ MeV) in heavy ion collisions has recently been investigated by several groups[1-6]. The important characteristics of the photon spectra are an exponentially decreasing energy spectrum and a slightly forward peaked angular distribution. The spectra are consistent with isotropic emission in a frame near the nucleon-nucleon center of momentum velocity.

Theoretically, the proposed gamma ray production mechanisms include: nucleus-nucleus bremsstrahlung[7-9], neutron-proton bremsstrahlung[10], and statistical decay[11].

We report the results from an inclusive measurement of gamma rays with energies ($20 < E_\gamma < 160$ MeV), produced in the reaction ^{136}Xe + Sn. We studied the production at three incident beam energies 66, 89, and 124 MeV/A. The experiment was performed at Lawerence Berkeley Laboratory, using the Bevalac. A self supporting, .38 mm thick, natural tin target was used. In the experiment, two gamma ray telescopes, consisting of an active barium flouride converter followed by a stack of eight Cerenkov plastic elements, were used. The detectors were located at various angles 30° - 90°(D1), and 90°- 150°(D2) to measure the angular distribution.

In this energy regime one must consider the contribution due to photons coming from the decay of the neutral pion. We have made a preliminary estimate of the photon spectra from the pion decay, by assuming that in the nucleon-nucleon center of momentum, the neutral pions are emitted isotropically with an exponential energy spectrum in this frame[12]. To obtain an estimate of the neutral pion cross section, we used the data of Sullivan et al.[13], who averaged negative and positive pions from the system Ne + NaF at various incident beam energies. We scaled the Ne + NaF data by an empirical $(A_p \times A_t)^{2/3}$ dependence to arrive at a value for the total cross section. This allows us to assess the gamma rays coming from neutral pion decay. In Figs. 1 and 2 we show the background due to the decay of neutral pions at two of the three incident beam energies. Using the invariant cross section, we have transformed the photon spectra from the nucleon-nucleon center of mass system to the lab frame. The calculated spectra were folded with the response function of the detectors before comparison to the experimental data was made. The contribution was the greatest at the highest beam energy (124 MeV/A), representing a contribution of approximately 50% of the total cross section for $E_\gamma>50$ MeV, and at the lowest energy the background was smaller, only 10%.

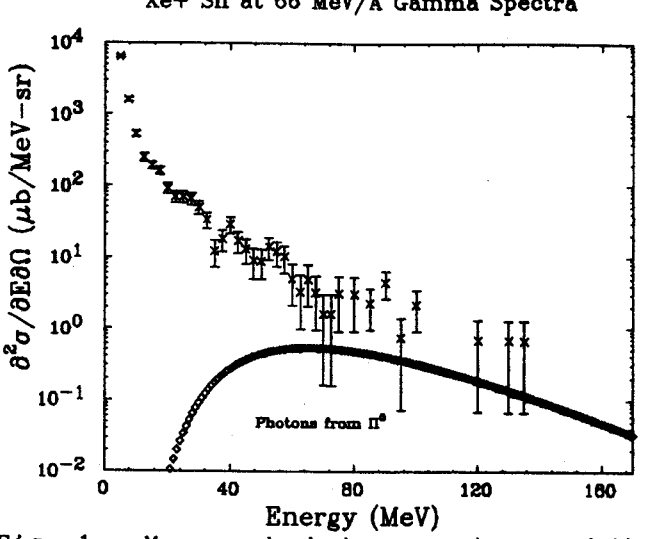

Fig. 1: Measured photon spectra, and the calculated background due to neutral pion decay at 66 MeV/A.

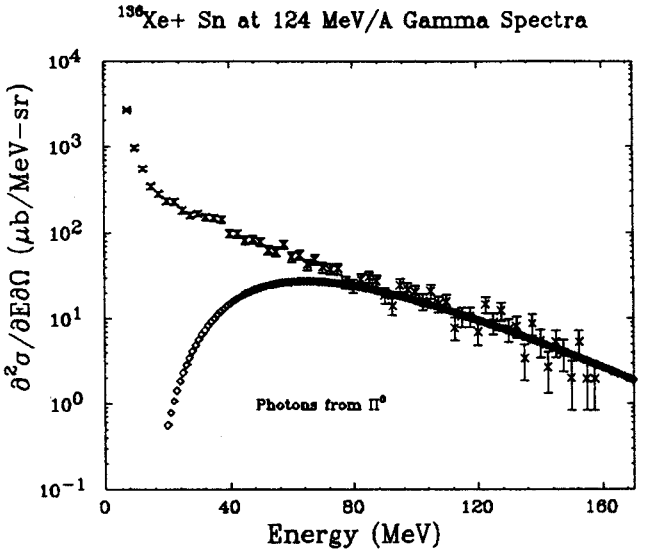

Fig. 2: Measured photon spectra, and the calculated background due to neutral pion decay at 124 MeV/A.

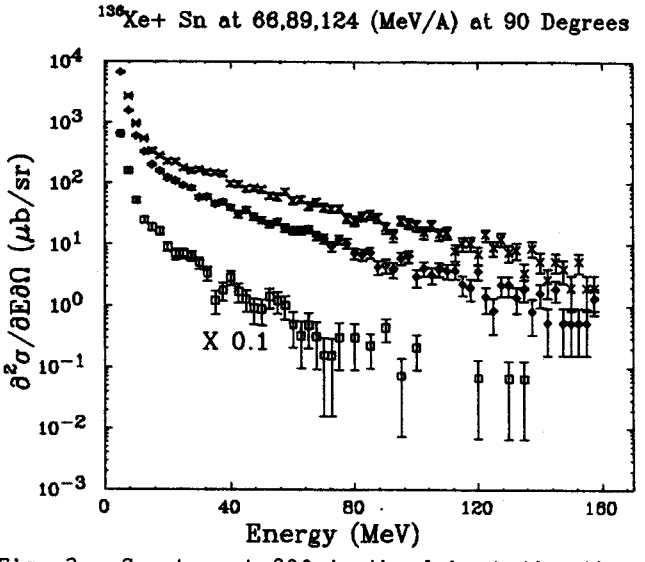

Fig. 3: Spectra at 90° in the lab at the three incident beam energies.

The photon spectra measured in this experiment are similar in their characteristics to data measured at other laboratories. The data shows a slightly forward peaked angular distribution and an exponentially falling energy spectrum. The data at the various beam energies were not only different in magnitude but also in slope (see Table I and Fig. 3). The best-fit parameters displayed in Table I were determined from a least squares fit to the data. Figure 4 shows the energy integrated cross section for $E_\gamma > 40$ MeV; from this plot one can see the forward peaked angular distribution. In the emitting frame we assume that the double differential cross section is given by the following Eq. 1:

$$\frac{\partial^2\sigma}{\partial E\partial\Omega} = A(\,1 + B\cos^2\theta\,)e^{-E/T} \qquad (1)$$

In Eq. 1 the functional dependence is isotropic plus a dipole term. The best-fit parameters were found from Eq. 1 transformed to the laboratory frame. We fit all the angles simultaneously, assuming that A, B, T, and v are free parameters. It can be seen from Table I

Table I

Fitted parameters

E/A (MeV)	A ($\times 10^2$)	B	T (MeV)	$\beta_{(exp)}$	Red-χ^2	fitted region (MeV)
66	1.31	0.22	19.62	.170	.604	40-152
	1.44	0.0	19.35	.178	.605	40-152
89	1.56	0.05	26.70	.191	1.045	40-152
	1.58	0.0	26.70	.190	1.046	40-152
124	3.41	0.30	33.22	.250	1.340	40-152
	3.66	0.0	33.45	.258	1.465	40-152

$\partial^2\sigma/\partial E\partial\Omega = A(1 + B\cos^2\theta\,)\exp(E/T_0)$ in the emitting frame θ_{lab} = 40°, 60°, 90°, 120°, 150°.

that the minimum χ^2 fit always has a nonzero dipole term. However, the statistical significance of this term is small for all three beam energies. The difference in the reduced χ^2 between the fit with B=0 and the best-fit is very small only 5%. Therefore we cannot exclude pure isotropic emission. The best-fit source velocities beta are very close to the center of mass velocities.

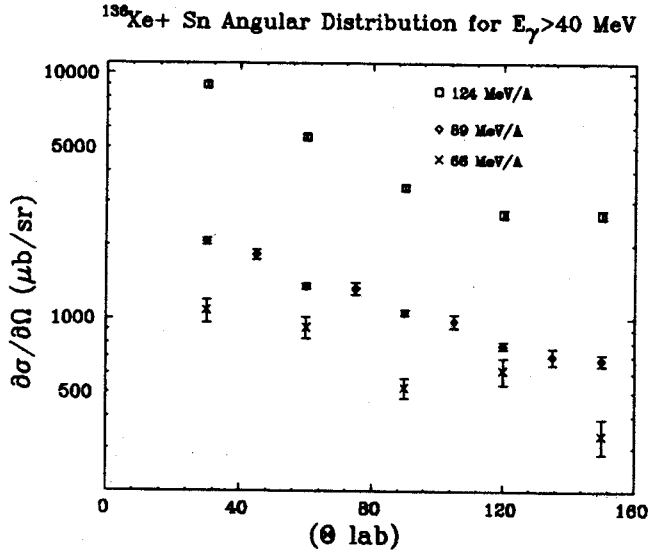

Fig. 4: Energy integrated cross sections plotted as function of lab angle.

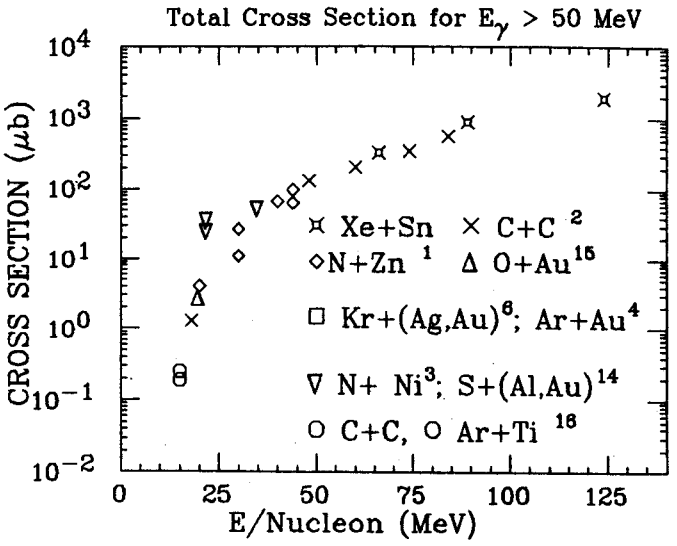

Fig. 5: Total cross section plotted as a function of the incident beam energy. The cross section is normalized to the system N + Zn.

With the estimate of the contribution from neutral pion decay, we have been able to extract new information on the total cross section for high energy gamma rays at these beam energies. Fig. 5 shows the comparison of the systematics of this data, to results measured at other facilities. The total cross section has been corrected for the contribution due to gamma rays coming from neutral pion decay. We have made a first attempt to assess the background from neutral pion decay, and we are currently pursuing better methods to calculate this contribution.

References

1. J. Stevenson et al., Phys. Rev. Lett. 57, 555 (1986).
2. E. Grosse et al., Europhys. Lett. 2, 9 (1986).
3. N. Alamanos et al., Phys Lett. B 173, 392 (1986).
4. M. Kwato Njock et al., Phys. Lett. B 175, 125 (1986).
5. R. Hingmann et al., Phys. Rev. Lett. 58, 759 (1987).
6. R. Bertholet et al., Nucl. Phys. (1987) to be published.
7. C.M. Ko, G. Bertsch and J. Aichelin, Phys. Rev. C 31, 2324 (1985).
8. E.M. Nyam, Phys. Lett. B 136, 143 (1984).
9. D. Vasak et al., Nucl. Phys. A428 (1984) 291c.
10. W. Bauer, G. Bertsch, W. Cassing, U. Mosel Phys. Rev. C 34, 2127 (1986).
11. H. Nifenecker and J.P. Bondorf, Nucl. Phys. A442, 478 (1985).
12. M.P. Budiansky, Ph.D. thesis, Lawerence Berkeley Laboratory (1981).
13. J.P. Sullivan, Phys. Rev. C 36, 1200 (1986).
14. J. Stachel et al.,(1987) to be published.
15. K. Wolf et al, Gull Lake Conference (1987).
16. K. Hanold et al., MSU-NSCL Annual Report 1987 pg. 6.

HIGH ENERGY γ-RAYS FROM THE $^{12}C + ^{12}C$ AND $^{40}Ar + ^{48}Ti$ SYSTEMS AT 15 MeV/NUCLEON

K. Hanold and D.J. Morrissey

γ-rays with energies in the region of 10 to 30 MeV were measured with $^{12}C^{3+}$ and $^{40}Ar^{10+}$ beams at the National Superconducting Cyclotron Laboratory (NSCL) at Michigan State University. The targets were a natural carbon foil (99% ^{12}C), 53.3 mg/cm^2, and an isotopically enriched (approximately 99%) ^{48}Ti target, 0.923 mg/cm^2, respectively. The γ-rays were observed in a set of four 7.6 cm x 7.6 cm cylindrical bismuth germanate (BGO) scintillation detectors. The BGO detectors were placed around a small scattering chamber at 30, 60, 90, 150 deg (lab) at a distance of 0.80 m. The beam was stopped in a Faraday cup surrounded by ~200 liters of water and approximately 3 m from the target. All the detectors were shadowed from the Faraday cup by two 15 cm thick lead walls positioned along the beam pipe. High energy neutrons and charged particles are copiously produced in these reactions. Therefore, time-of-flight with respect to the beam pulse is necessary to separate the γ-rays from these particles. In addition, neutron attenuators (20 cm nylon bars) were placed in front of each BGO detector to lower the counting rate due to the unwanted neutrons and charged particles. We calibrated the response function and the efficiencies of the BGO detectors for high energy γ-rays, as well as the attenuation in the nylon bars at the Tagged Photon Facility of the University of Illinois. The attenuation is approximately constant above 10 MeV. The γ-ray spectra for the reaction of $^{12}C+^{12}C$ are shown in Fig. 1. The spectra from the heavier system (Fig. 2) resemble those reported by Hingmann, et al.[1] for the reaction of ^{40}Ar with ^{148}Gd and by Herrmann[2] for the $^{92}Mo+^{92}Mo$ system. However, the spectra from the present study do not have any clear indication of giant dipole radiation (GDR) near 18 MeV.

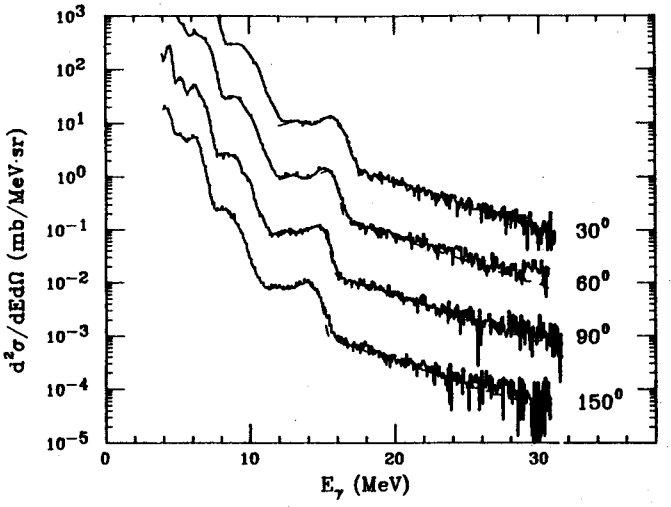

Fig. 1: The measured γ-ray spectra from the $^{12}C + ^{12}C$ reaction, labeled by laboratory angle, along with the fitted function. The difference between the data and the function is sufficiently small that the function is difficult to see under the data. The data for angles less than 150° were offset from one-another by a factor of ten for clarity.

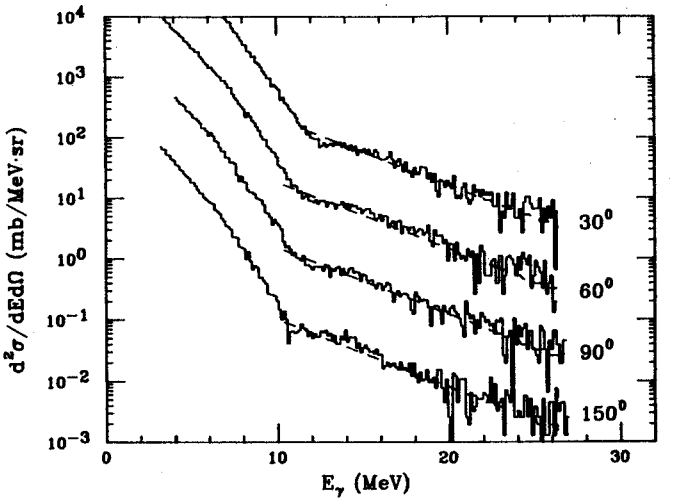

Fig 2: Similar to Fig. 1 but for the $^{40}Ca+^{48}Ti$ system.

The γ-ray spectra from the four angles were simultaneously fit to the sum of Doppler-shifted projectile and target velocity discrete lines (each using the calibrated BGO response

function) and an underlying exponential using a nonlinear least squares technique.[3] The exponential function, representing the contribution from high energy γ-rays, with an angular distribution of the form:

$$(a + b \cos(\theta_{lab}))\exp(-E_\gamma/E_0)$$

was used to fit the data. Two discrete transitions with energies above 10 MeV were observed in the ^{12}C reaction. These discrete lines are produced by the decay of the 15.1 MeV states in ^{12}C and ^{13}N (not distinguishable in this work) and a 12.7 MeV transition in ^{12}C [4,5]. The fit is shown as a dashed curve.

The angle and energy integrated cross section for $E_q \leq 20$ MeV was found to be 34 microbarns for the $^{12}C+^{12}C$ system and to be 604 microbarns for the $^{40}Ar+^{48}Ti$ system. Extrapolating the fitted function beyond the measured region, the integrated cross section of γ-rays with $E_\gamma \leq 50$ MeV, scaled to the $^{14}N+Zn$ reaction by assuming that the cross section in proportional to the overlap of two hard spheres, was found to be 0.25 microbarns and 0.19 microbarns for the light and heavy systems, respectively. The difference between the scaled cross sections is most likely due to the large extrapolation of the fitted function. However, notice that both small values are consistant with the results obtained with conversion-electron telescopes. The slope parameters of the high energy exponentials were slightly different, 4.9 and 4.0 MeV, light and heavy systems respectively. These values are also consistent with the previously established trend that the exponential slope is approximately 1/3 of E_{proj}/nucleon. The exponential energy distribution was found to be isotropic in a frame moving with a velocity of 0.08 ± 0.02 c in a separate analysis. This velocity is consistent with emission from the center of mass system. An isotropic angular distribution in the center of mass system lends support to the production of high energy γ-rays by incoherent proton-neutron collisions[6].

References

1. R. Hingmann, et al., Phys. Rev. Lett. 58, 759 (1987).
2. N. Herrmann, Ph.D. Thesis, Univerität Heidelberg, 1987, and Gesellschaft für Schwerionenforschung report, GSI-87-17.
3. The computer code ORGLS, for Oak Ridge General Least Squares, was modified to run under the VAX/VMS operating system and interactive graphics were incorporated. This code finds the minimum chi-squared value by using the derivatives of chi-squared with respect to the parameters of an arbitrary user-defined function.
4. F. Ajzenberg-Selove, Nucl. Phys. A433, 54 (1985).
5. F. Ajzenberg-Selove, Nucl. Phys. A449, 36 (1986).
6. K. Nagayama and G. Bertsch, Phys. Rev. C 34, 2190 (1986).

CORRELATIONS BETWEEN HIGH ENERGY GAMMA RAYS AND LIGHT FRAGMENTS IN HEAVY ION COLLISIONS

A.R. Lampis, J. Stevenson, W. Benenson, J. Clayton, D. Cebra, Y. Chen, D. Fox[a], E. Kashy, D.J. Morrissey, M. Samuel, R. Smith[b], C.L. Tam, G.D. Westfall, K. Wilson, and J.S. Winfield

The discovery[1, 2] of high-energy gamma-ray production in heavy-ion collisions was an unexpected result and stimulated a large amount of theoretical and experimental work aimed at understanding the production mechanism. Most recent models of high-energy gamma-ray production assume that the the gamma rays are produced by incoherent bremsstrahlung from individual proton-neutron collisions during the heavy-ion collision. Most models have been suprisingly successful at predicting the general features of the inclusive high-energy gamma-ray data such as the near isotropy of the angular distribution, the magnitude of the cross-section, and the beam energy dependence. Thus inclusive high-energy gamma-ray measurements have not been very stringent tests of heavy-ion collision models.

There have been several experiments performed to study high-energy gamma-rays in coincidence with heavy fragments. Hingmann et al.[3] studied high-energy gamma-ray production from the reaction $^{40}Ar+^{158}Gd$ at a beam energy of E/A=44 MeV and also detected charged fragments in an array of parallel plate avalanche chambers (PPAC). Hingmann et al. concluded that the high-energy gamma-ray production was associated with central collisions. Another coincidence experiment was performed by Herrmann et al.[4], who studied high-energy gamma-ray production in the reaction $^{92}Mo+^{92}Mo$ at a beam energy of E/A=19.5 MeV in coincidence with pairs of heavy fragments which were detected in a 2π PPAC in the forward hemisphere. They concluded that the gamma rays at this bombarding energy came from statistical emission from the excited fragments rather than from nucleon-nucleon bremsstrahlung.

In the experiment discussed here, we took an alternative approach and studied light fragments in coincidence with high-energy gamma rays. The principal motivation behind this experiment was to measure the charged-particle multiplicity associated with high-energy gamma-ray production. If high-energy gamma-ray production occurs only in central collisions, then the average charged particle multiplicity should be greater for high-energy gamma-ray emission than for emission of other particles such as protons, deuterons, and tritons.

The gamma-ray detectors used in this experiment were the Cerenkov range telescopes used by Stevenson et al.[5] to measure inclusive production of high energy gamma rays. In the present experiment two gamma-ray detectors were placed at laboratory angles of 60° and 120° on the same side of the beam. Each detector subtended a solid angle of 125 msr.

The light charged particle detectors were plastic scintillator "phoswich" detectors. Each phoswich detector consisted of a 0.15 cm thick fast plastic ΔE (Bicron BC-412) followed by a 12.7 cm plastic E scintillator (Bicron BC-444). Fourteen of the phoswiches were grouped in pairs and covered the angular range from 30° to 120° in the plane defined by the gamma-ray detectors but on the opposite side of the beam. The phoswich detectors subtended a total solid angle of 250 msr. The resolution was sufficient to separate cleanly the hydrogen isotopes, and to resolve easily helium from hydrogen.

The events which were included in the multiplicity counts were restricted to hydrogen isotopes with energy greater than 30 MeV and were also restricted to 14 of the in-plane phoswiches. The gamma rays considered for the multiplicity measurement included energies above 20 MeV only, since lower energy gamma rays are known to come from decay of the giant dipole

resonance and statistical emission. The multiplicity measurement was further restricted to gamma rays in the forward (60°) detector. In order to have a standard for comparison, the coincidence data between charged particles were used to construct the multiplicity of charged particles (Z=1,E>30 MeV). It was then possible to compare the charged particle (Z=1, E>30 MeV) multiplicity associated with high-energy gamma rays and that associated with charged particles (Z=1, E>30 MeV). This comparison is shown in Fig. 1. For the purpose of comparison, the charged particle and gamma-ray singles data (defined to be M=1), are set equal. It is clear from Fig. 1 that the charged particle multiplicity distribution associated with gamma rays and that associated with charged particles are very similar: the yields for M=2 are equal within 10%. The similarity of the multiplicity distributions suggests that the production probability of high energy gamma rays and charged particles as a function of impact parameter is rather similar. This indicates that high-energy gamma-ray production is not restricted to central collisions.

Figure 2 compares the energy spectrum of protons observed at 30° , 60°, and 90° to protons observed in coincidence with high-energy (E_γ>20 MeV) gamma rays detected in the 60° detector. The slope of the inclusive and coincidence proton spectra are nearly identical at all angles, and the angular distributions are quite similar. This again indicates that charged particle and high-energy gamma-ray production have similar impact parameter dependences.

This conclusion although different from that of Hingmann et al.[3], is not in conflict with their original data since Hingmann et al. did not compare high-energy gamma ray and

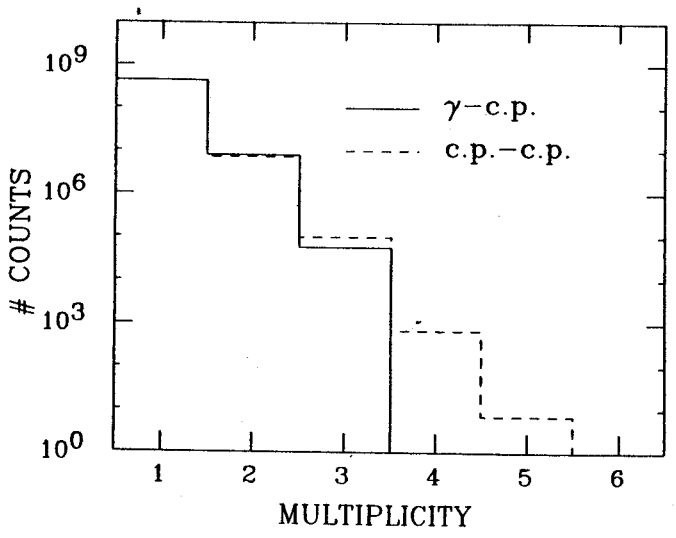

Fig. 1: Comparison of the multiplicity of light (Z=1) fragments with E>30 MeV observed in coincidence with a high-energy gamma ray(E_γ>20 MeV, θ=60°) or with another light (Z=1) fragment. The data for the multiplicity associated with high-energy gamma rays has been multiplied by 900.

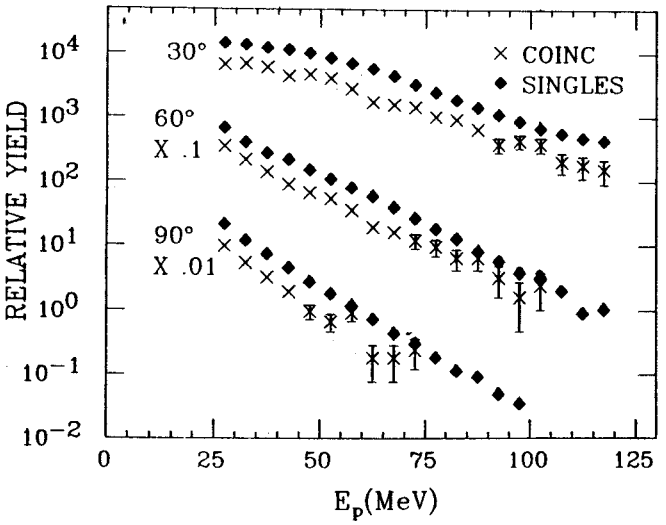

Fig. 2: Proton energy spectra measured at laboratory angles of 30°, 60°, and 90°. Diamonds are singles proton spectra, and crosses are proton spectra measured in coincidence with a high energy gamma ray (E_γ>20 MeV) observed at a lab angle of 60°. The coincidence data have been multiplied by 6 X 10^5.

charged particle production. The results of Herrmann et al.[4] relate to a much lower beam energy and heavier system and should not be compared to the present data.

---

a. Current address: Los Alamos National Laboratory, Los Alamos, New Mexico 87545
b. Current address: Department of Physics, University of Padua, Padua, Italy.

References

1. E. Grosse, in Proceedings of the International Workshop on Gross Properties of Nuclei and Nuclear Excitations XIII, Hirschegg, Austria, 1985 Edited by H. Feldmeier (Gesellschaft fur Schwerionenforschung and Institut fur Kernphysik, Technische Hochschule, Darmstadt, West Germany, (1985).
2. K.B. Beard, W. Benenson, C. Bloch, E. Kashy, J. Stevenson, D.J. Morrissey, J. van der Plicht, B. Sherrill, and. J.S. Winfield, Phys. Rev. C32, 1111 (1985).
3. R. Hingmann, W. Kuhn, V. Metag, R. Muhlahans, R. Novotny, A. Ruckelshausen, W. Cassing, B. Haas, J.P. Vivien, A. Boullay, H. Delagrange, H. Doubre, C. Gregoire, and Y. Schutz, Phys Rev. Lett. 58, 759 (1987).
4. Herrmann et al. GSI preprint (1987).
5. J. Stevenson, K.B. Beard, W. Benenson, J. Clayton, E. Kashy, A. Lampis, D.J. Morrissey, M. Samuel, R.J. Smith, C.L. Tam, and J.S. Winfield, Phys. Rev. Lett. 57, 555 (1986).

VERY-HIGH-ENERGY LIGHT ION PRODUCTION NEAR θ=0° IN ^{40}Ar COLLISIONS AT E/A = 20 AND 30 MeV/u

S. Shaheen[a], F.D. Becchetti[a], D.A. Roberts[a], J.W. Jänecke[a] and A. Nadasen[a]

Very-high-energy protons, alpha particles and other light ions have been observed in reactions induced by 20 and 30 MeV/nucleon ^{40}Ar beams at the Michigan State University NSCL. A large BGO detector (4.2 cm dia. x 15 cm), utilizing TOF, and large NaI detectors (up to 10 cm square x 40 cm deep), utilizing TOF and PSD were used to detect energetic L.I.s near θ=0°. The latter were produced in a thick stopping target (usually Ta) or a combination of an upstream thin target and downstream stopping target with TOF used for target identification. Both techniques allowed measurements at θ=0°. As in previous measurements using ^{16}O, ^{32}S and ^{58}Ni[1] protons and alpha particles are observed near θ=0° with a large fraction (≥ one half) of the beam energy i.e. with many times the beam velocity. A fit to the data using a moving source model (Fig. 1) requires $v_{source} \rightarrow v_{projectile}$ and a source "temperature" ($T_s \approx$ 10-30 MeV), which is much larger than the nuclear fermi energy (T_f). The α-energy endpoints of the (HI,α) data appear to be roughly correlated with (HI,α) two-body transfer Q-values hence suggesting a transfer mechanism[2] or similar processes as a source for the most energetic α particles ($E \rightarrow E_{beam}$).

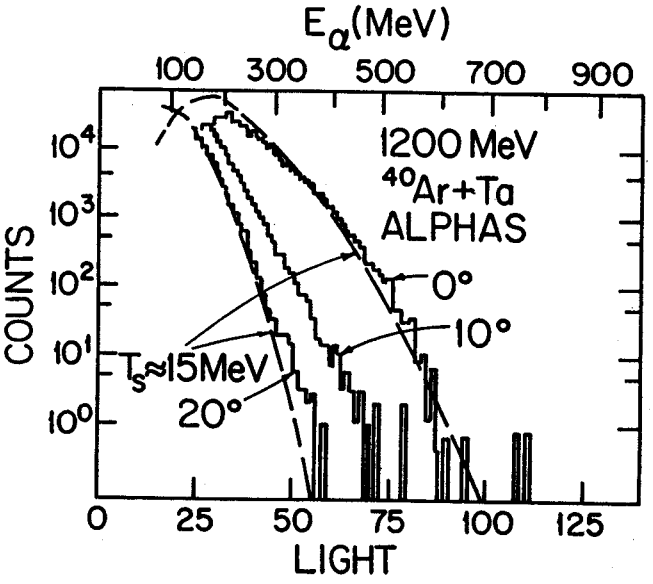

Fig. 1: Alpha particle spectra and moving-source model fits ($v_s = v_{projectile}$) for ^{40}Ar + Ta at E/A = 30 MeV/u. The quantity T_s is the apparent source "temperature" required to fit the data.

a. University of Michigan, Ann Arbor, Michigan.

References

1. MSU NSCL Annual Report (1986) p. 18; P. Schulman, et al. BAPS 31,840(1986).
2. C. Borcea et al. Nucl. Phys. A351,312(1981).

NEUTRON EMISSION IN ^{14}N + Ag REACTIONS AT 35 MEV/NUCLEON

F. Deak[a], A. Galonsky, C.K.Gelbke, L. Heilbronn, J. Kasagi[b], A. Kiss[a], W. Lynch, T. Murakami, B. Remington[c], H.R. Schelin[d], Z. Seres[e], M.B. Tsang, X. Yang and G. Zhang.

This report presents preliminary results from our study of the emission of neutrons in ^{14}N + Ag reactions at E/A = 35 MeV. We have extracted temperatures from inclusive neutron spectra. These values will increase our knowledge of the systematics of temperatures obtained from spectral distributions of light particles[1-4].

Energy spectra of neutron singles from the reaction Ag(^{14}N,nX) have been obtained employing time-of-flight techniques. The K500 cyclotron provided $^{14}N^{5+}$ beams at 35 MeV per nucleon. The cyclotron period was 52.42 ns, and the time-averaged beam intensity was about 2 x 10^9/sec. The experimental set-up is shown in Fig. 1. Most of the apparatus and techniques used in the present experiment have been described in detail elsewhere[4-6], so only the essential features will be described in this report. Twenty three neutron detectors were placed in the horizontal plane at angles between 15° and 160° and at distances ranging from 1.1m to 4.5m. Most of the detectors consisted of ~1 liter of liquid scintilator (NE213 or BICRON 501) contained in a sealed glass cell about 12.7 cm in diameter and 7.6 cm thick. Their intrinsic resolution was about 0.8ns. In front of each detector (at angles $\leq$64°) was a 6mm thick NE102A proton veto paddle. The target was a self-supporting rolled foil of natural silver, 3.9 mg/cm^2 thick, positioned at 45° with respect to the beam. The in-beam background contributions to the spectra were measured by taking data with shadow bars between the target and the neutron detectors. The background contribution was typically less than 20% of the total, but for the highest energies it was much larger. The neutron kinetic energy was determined by timing against

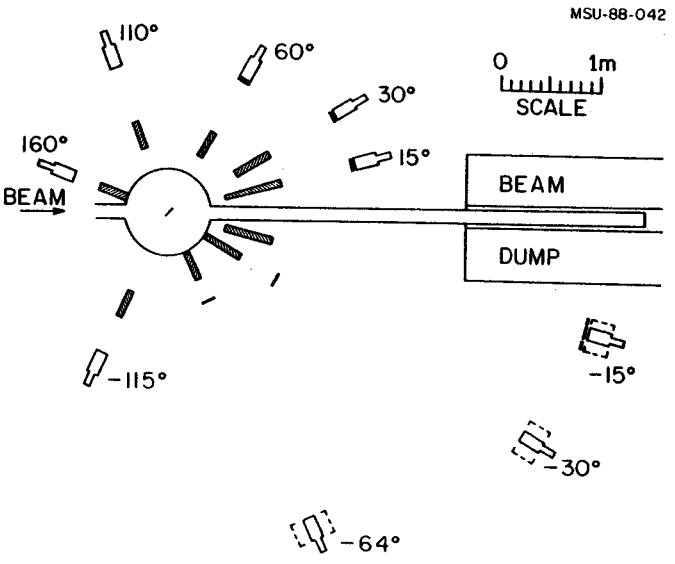

Fig. 1: Experimental set-up.

the cyclotron rf signal. Neutrons were distinguished from gamma-rays by pulse shape discrimination using two QDC's[7]. For each event the following information was written onto magnetic tape: detector number, light output in equivalent electron energy, the two QDC signals and the time-of flight. The data were written onto tape with the CAMAC multiparameter data acquisition system which employed an MC 68010 microprocessor.

Typical time-of-flight spectra for neutrons and gamma rays are shown in Fig. 2. For each spectrum the background obtained with a shadow-bar has been subtracted. The time resolution of the system (scintillation counter and beam pulse length) obtained from the gamma ray peak is 1.3 ns FWHM.

The kinetic energy of the neutrons was determined from their time-of-flight measured relative to the gamma ray peak position. The efficiency for each detector was calculated with

a Monte Carlo code developed by Cecil et al[8]. Figure 3 shows the resulting energy spectra in the form of absolute cross sections $d^2\sigma/dEd\Omega$ for five angles. Attenuation of the neutrons by material lying between the target and the detector was taken into account.

The spectral shapes suggest the existence of three distinct components. The low energy component is nearly isotropic and dominates at the backward angles. It corresponds to neutrons evaporated from a thermally equilibrated target-like source. The high energy component originates from a source of preequilibrium neutrons, a source called the intermediate-rapidity source. It appears thermal in shape and has a much flatter slope than the target-like component. The third component can be attributed to sequential decays from projectile-like-fragments. It appears as a bump only at forward angles and is centered around the energy, 35 MeV, corresponding to the velocity of the incident projectile.

Assuming that each source emits neutrons isotropically with a Maxwellian distribution in its rest frame, the sum of the three contributions[9] was fitted to the data using a χ^2 minimization procedure with the parameters N_i (normalization constant), T_i (nuclear temperature) and ϵ_i (kinetic energy per nucleon) as free parameters where "i" identifies the source. The resulting fits are shown by the solid lines in Fig. 3. The dashed lines correspond to the fit using the target-like source only and the dotted lines to using the target-like and intermediate-rapidity sources. The source parameters corresponding to the solid lines are listed in Table I.

It has to be noted that considering the projectile-like-fragments source as a Maxwellian distribution is an oversimplification. In fact, analysis of projectile-like-fragment contributions[10] shows that neutron decay of a few slightly unbound states plays an important (non-Maxwellian) role.

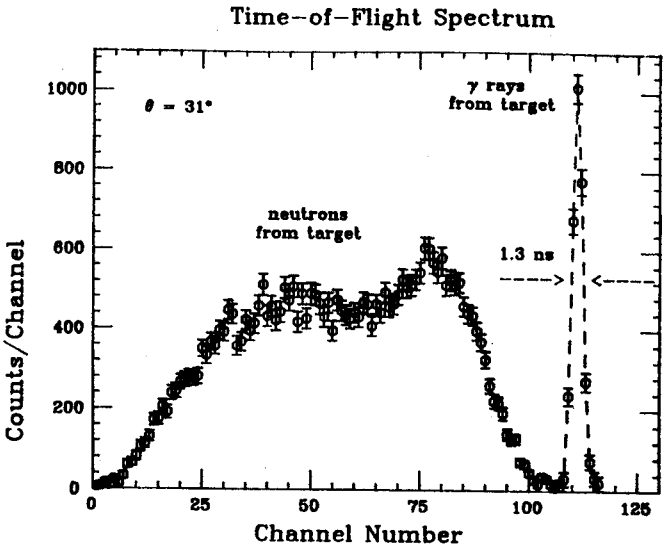

Fig. 2: Typical neutron and gamma-ray time-of-flight spectrum. The calibration is 0.246 ns/channel.

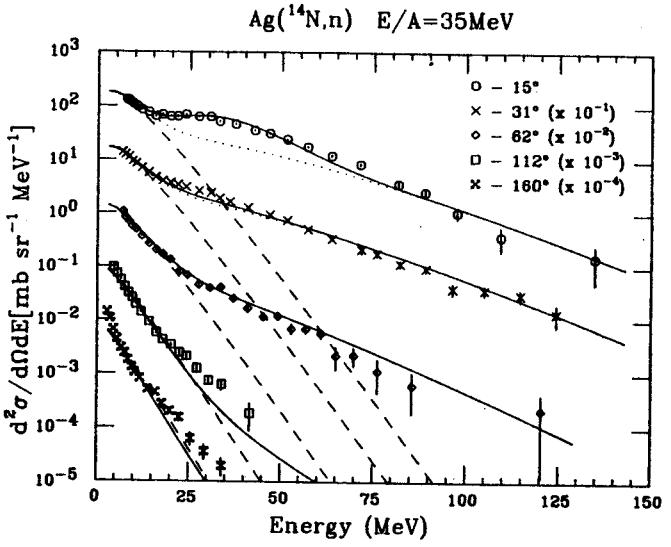

Fig. 3: Single inclusive cross sections for neutrons emitted in ^{14}N + Ag reactions at E/A = 35 MeV. The curves are moving source fits obtained by using only a target-like source (dashed curves), by adding an intermediate-rapidity source (dotted curves), and by adding to those two a projectile-like source (solid line).

Another observation is that these inclusive spectra show a behaviour similar to that seen in earlier exclusive measurements.

The next steps in the analysis will be: a) the comparison with proton singles spectra taken at the same energy and same system, b) application of different models such as the Boltzmann-Uehling-Uhlenbeck equation, the Fermi-Jet model, and the Harp-Miller-Berne model.

Table I: Moving source parameters used for the fits shown by the solid lines in Fig. 1. The normalization constants N_i are given in units of mb/sr.

Source	T_i (MeV)	E/A (MeV/A)	N_i
TLS	4.04	0.45	134.90
IRS	11.10	12.83	5.64
PLS	2.20	30.11	19.64

a. Eötvös University, Budapest, Hungary.
b. Tokyo Institute of Technology, Japan.
c. Lawrence Livermore Laboratory.
d. Centro Tecnico Aeroespacial and FAPESP, Brazil.
e. Central Research Laboratory, Budapest, Hungary.

References

1. C.B. Chitwood et al. Phys. Rev. C 34, 858(1986).
2. Z. Chen et al. Phys. Rev. C 36, 2297(1987).
3. E. Holub et al. Phys. Rev. C 33, 143(1986).
4. B.A. Remington et al. Phys. Rev. C 34, 1685(1986).
5. F. Deak et al. 1986 NSCL Ann. Rep. p.4.
6. F. Deak et al. Nucl. Phys. A64,133(1987).
7. J. Heltsley et al. Nucl. Instr. & Meth. in Phys. Res. A263, 441(1988).
8. R.A. Cecil et al. Nucl. Instr. Meth. 161, 439(1979).
9. T.C. Awes et al. Phys. Lett. B 103, 417(1981).
10. A. Kiss et al. Phys. Lett. B 184 149 (1987).

TARGET MASS DEPENDENCE OF NEUTRON EMISSION IN ^{14}N COLLISIONS WITH C, Ni, AND Ho

A. Kiss,[a] G. Caskey,[b] F. Deak,[b] A. Galonsky, L. Heilbronn, B. Remington,[c] and Z. Seres[d]

We have conducted a series of exclusive measurements on the target dependence of neutron emission. The exclusivity somewhat separates the spectra into their various components. Furthermore, with no Coulomb barrier effects, we are able to make relatively model-independent observations of the target mass dependence.

The neutron spectra were measured in coincidence with fragments of Li, Be, B, and C from three targets--carbon, nickel, and holmium. The projectile was ^{14}N at an energy of 35 MeV/nucleon. The experiment[1] was conducted with the K500 cyclotron.

Figures 1 and 2 show typical neutron spectra for the C, Ni, and Ho targets. In each figure the shapes of the three spectra, especially above 15 MeV, are very similar to each other even though the targets have widely different masses. The low energy parts of the spectra, especially the enhancements in Fig. 2, are target dependent. For the nickel target the enhancement is less pronounced than for the holmium target, and for carbon it is quite small.

The colinear (target, Si telescope, and neutron detector on a straight line) and near-colinear spectra contain dominant contributions from neutron decay of excited fragments wherein the daughter fragment is the coincident PLF.[2,3] The peak structures between 15 and 40 MeV in Fig. 1 have this origin, and they occur with about the same relative strength for all three targets. For the colinear geometry, a major share of the coincident events come from decay of one or a few discrete states of the excited parent fragment. Regardless of whether the target was C, Ni, or Ho, the relative velocity spectra for a given coincident isotope are similar to each other. For each element: Li, Be, B, and C, Table I lists the relative contributions of individual isotopes to the colinear neutron-fragment coincidences at -10°. We see from this table that the distribution amongst the isotopes of one element does not change drastically with target, but that there is a trend toward greater population of the heavier isotopes as the target mass increases.

Table I.--Isotope abundance distributions and relative neutron multiplicities for neutron-fragment coincidences with the -10° colinear geometry for carbon, nickel, and holmium targets ($E_{PLF} \geq 9$ MeV/u, $E_n \geq 4$ MeV). The relative multiplicities tell the number of neutrons which come from the parent of the indicated isotope for targets of nickel and holmium relative to the number for a target of carbon.

	Isotope abundance distributions			Relative neutron multiplicities	
	C	Ni	Ho	M(Ni)/M(C)	M(Ho)/M(C)
PLF					
^{6}Li	45±6%	37±5%	32±5%	0.79±0.16	0.80±0.16
^{7}Li	54±7%	59±8%	61±8%	0.67±0.47	0.73±0.47
^{8}Li	1.3±%	3.4±2	7.1±3.5%		
^{7}Be	66±3%	63±3%	28±5%		
^{9}Be	11±3%	11±3%	24±4%	1.04±0.25	1.37±0.34
^{10}Be	23±3%	26±3%	48±4%		
^{10}B	19±5%	15±4%	13±4%	0.99±0.2	0.89±0.2
^{11}B	80±5%	81±5%	86±5%	0.98±0.5	1.00±0.5
^{12}B	1.1±.7	3.8±1.5	1.61%		
^{11}C	12±3%	14±3%	6±3%	0.98±0.18	0.34±0.2
^{12}C	76±6%	73±6%	82±6%	0.92±0.18	0.81±0.17
^{13}C	12±3%	14±3%	13±3%		

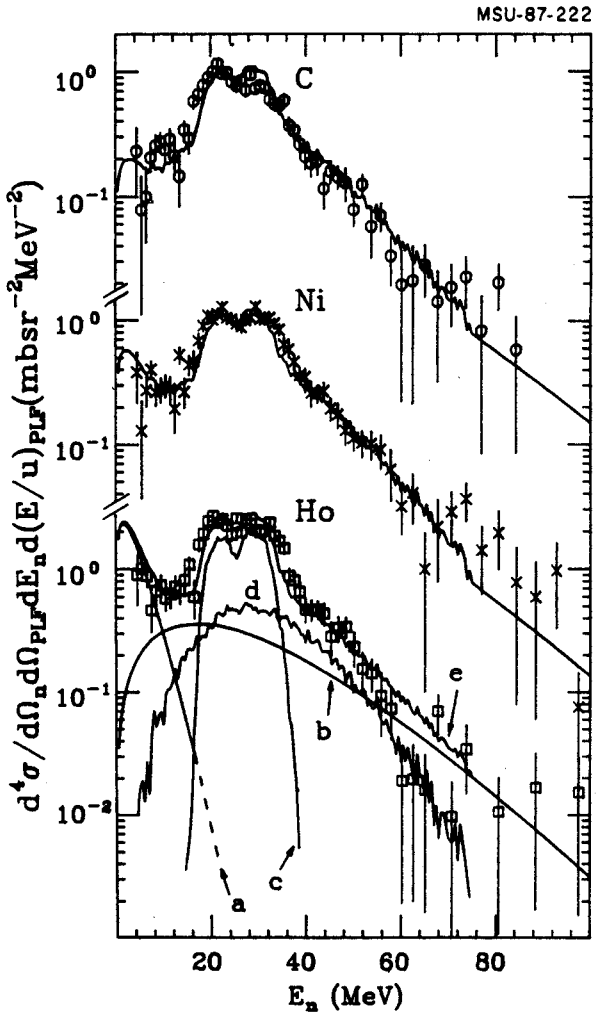

Fig. 1: Energy Spectra of neutrons from the carbon, nickel, and holmium targets at -10° in coincidence with projectile-like fragments of lithium at -10° and within the 23-30 MeV/u energy bin. The curves give the sum of the calculated contributions from three moving sources. The source parameters (Tables I and II) were determined from these spectra and from spectra at seven other angles. For the holmium target we also show the individual contributions--a from a target-like source, b from an intermediate-rapidity source, and c and d from a projectile-like source. c gives the part from the lowest neutron-unstable states of ^{7}Li and ^{8}Li, and d gives the thermal part. The fluctuations result from the Monte-Carlo calculations used for c and d. The sum of the contributions is given by e.

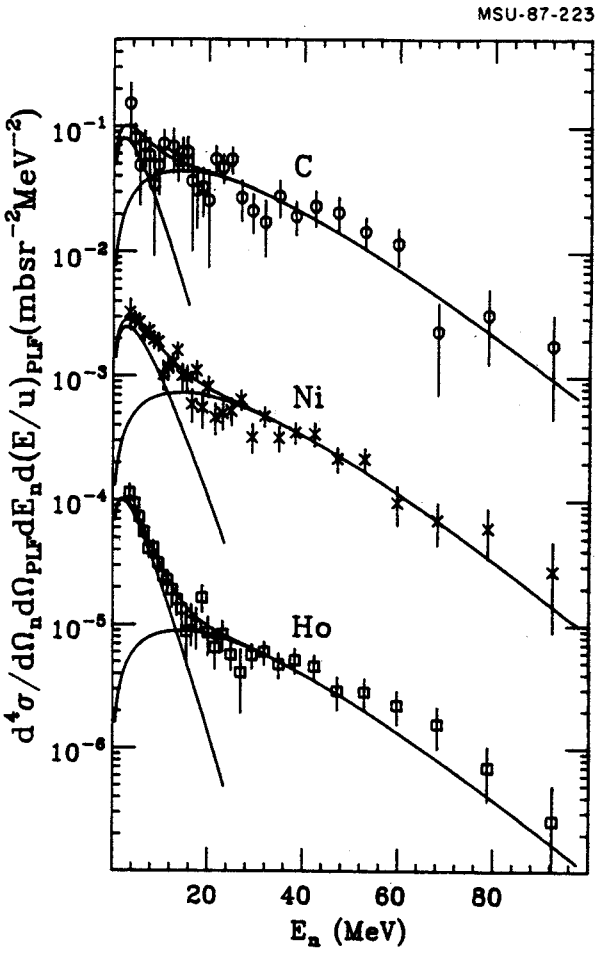

Fig. 2: Energy Spectra of neutrons for the carbon, nickel, and holmium targets at -30° in coincidence with lithium PLF's at +23° and within the 9-16 MeV/u energy bin. The curves show the contributions from the intermediate rapidity source (dominating at higher energies), from the target-like source, and from the sum of them. The source parameters (Table III) were determined from these spectra and from spectra at six other angles.

As in Refs. 1 and 4, the spectra of neutrons at the seven angles furthest from the angle of the coincident fragment (the non-colinear spectra) were fitted by two moving thermal sources--the IR source and the TLF source. The fit parameters were the kinetic energy/nucleon (E/A), the angle, the temperature, and the strength or multiplicity of each source. The parameter values for the fits

shown in Figs. 1 and 2 are given in Tables II and III, respectively. Such a fit was made for each of the six fragment angles, four fragment elements, and four or five fragment velocity bins, giving a total of about 100 fits for each target. Although the concept of the TLF source may not have any clear physical meaning for a target nucleus as light as carbon, we needed the contribution from this kind of source for the description of the low energy parts of the spectra (see Fig. 2) and therefore included it.

Table II. Parameter values of the IR (intermediate-rapidity) and TL (target-like) moving source contributions to the fits shown in Fig. 1.

		Strength	E/A	Temp	Ang
target	source	$mb/sr^{-2}MeV^{-2}$	MeV/nuc	MeV	deg
Carbon	IR	9.6	10.1	9.3	8
	TL	5.3	0.64	2.2	10
Nickel	IR	13.7	7.4	9.5	3
	TL	21.9	0.28	2.45	-4
Holmium	IR	28.2	10.3	8.2	4
	TL	108	0.13	2.4	5

Table III. Parameter values of the IR (intermediate-rapidity) and TL (target-like) moving source fits shown in Fig.2.

		Strength	E/A	Temp	Ang
target	source	$mb/sr^{-2}MeV^{-2}$	MeV/nuc	MeV	deg
Carbon	IR	6.0	6.6	10.5	0
	TL	3.4	0.51	2.6	-2
Nickel	IR	9.6	6.5	10.4	1
	TL	12.8	0.59	3.2	2
Holmium	IR	11.7	6.3	10.3	2
	TL	56.5	0.24	2.9	-13

For the IR source the values of E/A scattered around 8.5 MeV with a deviation of about 2.5 MeV. The values of temperature were roughly the same as the E/A values. There is no significant trend in the values for any of the target nuclei as a function of either the PLF energy/nucleon or the PLF identity. The mean value of T_{IR} for the carbon target is around 7 MeV, which is somewhat lower than for the Ni and Ho targets. This result is independent of the angle of the PLF. All IR temperatures are consistent with an average value of 9 ± 2.5 MeV.

For the TLF source the values of E/A were 1 MeV for the Ni and Ho targets[1,4] and < 3 MeV for the C target. The TLF temperatures for the Ho target are between 2 and 2 1/2 MeV and for Ni between 2 and 3 1/2 MeV. For both targets the temperature drops with increasing fragment velocity.

We have evaluated M_{TLF}/M_{IR} ratios for all cases where the neutron multiplicities were available. The results show that the ratio is approximately independent of PLF angle and of PLF energy. We have found that for all three targets the ratio tends to be bigger for lighter coincident PLF-s. M_{TLF}/M_{IR} lies between 6 and 3 for the Ho target (in-plane case) and between 2 and 1 for the Ni target. For the C target the ratio is less than 0.6. Since the contribution from the TLF source for the C target is so small, the source parameters were less well determined than for the heavier targets. Nevertheless, the temperature values are in the same range.

The $(E/A)_{IR}$ and T_{IR} values were found not to depend on the identity, energy, or angle of the coincident fragment (see also Refs. 1 and 4). One may suppose that the IR neutron emission occurs at an early stage of the reaction, whereas the fragment departs later. This idea can be used to develop a stripping-pickup model[4] of peripheral collisions. This model offers a simplified view of a peripheral

collision. First the participant zone develops in the interaction of an abraded part of the projectile with an approximately equal mass from the target nucleus. This zone emits the IR nucleons. Later the coincident PLF is formed from the projectile spectator by a decelerating mass pick-up from the hot participant zone.

The mass of the IR source A_{IR} is given by

$$A_{IR} = \{\frac{A_{PROJ}\, v_0}{v_{IR} \cos\theta_{IR}} + \frac{A_{PLF}\, v_0}{v_0 - v_{IR}\cos\theta_{IR}}\} - \{\frac{v_0\, A_{PLF}}{v_{IR}\cos\theta_{IR}\,(v_0 - v_{IR}\cos\theta_{IR})}\} v_{PLF} \cos\theta_{PLF} \quad (1)$$

For each case the quantities on the right side of this equation are known from measurement or as fit parameters; hence in the stripping-pickup model A_{IR} is determined. We cannot test the model directly through Eq. 1, since A_{IR} is not one of the fit parameters. However, we note that the temperature of the IR source seems to be independent of all PLF parameters. Therefore, M_{IR}, the source multiplicity, which is one of the fit parameters, should be proportional to A_{IR}. To test whether M_{IR} is indeed proportional to A_{IR}, we plot M_{IR} vs A_{IR} computed with Eq. 1 for the C, Ni, and Ho targets. The results are in Fig. 3 where we see a rough linear correlation for the +7°, -10°, +15°, and 15° out-of-plane cases. The proportionality is not present for $\theta_{PLF} = +23°$; 18° seems to represent the transition. The slopes of the correlation in Fig. 3 are about the same for all three targets.

The neutron contribution from the PLF source was obtained from colinear and near-colinear spectra after subtraction of the calculated IR and TLF contributions computed from their fit parameters, which were determined from the neutron spectra at angles away from the colinearity condition. Each neutron spectrum from the PLF source was decomposed into two parts, one from decay of the excited fragment via discrete neutron unbound states with known energies, and another via many densely-packed states summing up to a Maxwellian distribution.[2,3] In several cases Monte Carlo

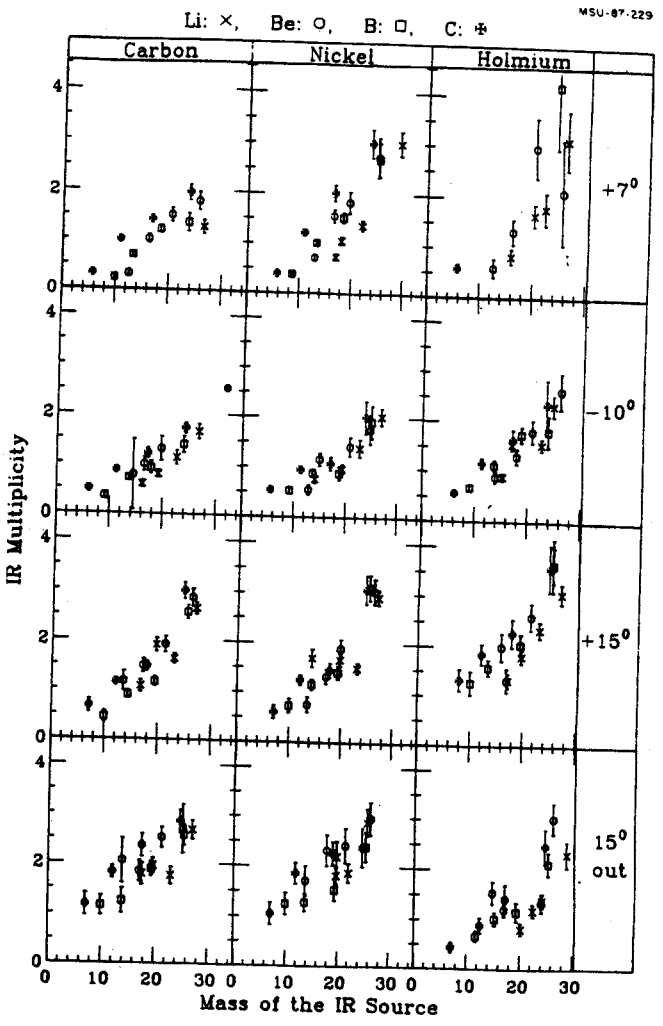

Fig. 3: Dependence of the IR multiplicity on the estimated mass of the participant zone for the carbon, nickel, and holmium targets for PLF angles ≤ 15°. The values of A_{IR} were obtained from eq. (1). Symbols for the PLF's are defined at the top.

calculations[3] were performed for the description of the colinear and near-colinear energy spectra of the neutrons as weighted sums of the contributions from the different isotopes. The abundances of the individual isotopes are listed on the left side of Table I.

The curves in Fig. 1 give the spectra due to the TLF, IR, and PLF sources. For the Ho target we show the individual contributions. Curves c and d are results of empirically normalized Monte Carlo calculations. The twin

peaks in curve c account for neutrons from forward and backward decay of the lowest neutron-unstable states of ^{7}Li and ^{8}Li (2.255 MeV and 7.456 MeV).[5] The broad bump, curve d, is the contribution from a Maxwellian source with 2.5 MeV temperature. The agreement between experiment and calculation in Fig. 1 is typical of all the cases. It is worth remembering that the curves are not just fits to the data of Fig. 1; curves a and b were computed with parameters determined from fitting spectra at seven non-colinear angles.

For the -10° colinear data, the right side of Table I displays neutron multiplicties from the Ni and Ho targets in comparison to those from the C target. The relative multiplicities allow us to compare the degree of excitation of a given fragment for the different targets. The more a fragment is excited, the greater is the probability that the excitation energy exceeds the neutron separation energy, and the greater the number of coincident neutrons.[6,7] The many multiplicity ratios consistent with 1.0 in Table I indicate that the parent isotope comes out of the collision with an average excitation energy which is the same for the three targets. The only contrary case is $^{12}C^{*} \rightarrow {}^{11}C+n$, where the relative multiplicity is only 0.3 for the Ho target.

In summary then, it must be said that for the projectile used here, 35 MeV/u ^{14}N, the properties of the IR and PLF sources have little, if any, dependence on the target.

---

a. Eötvös Lorand University, Budapest, Hungary.
b. Donnelly Corp., Holland, Michigan.
c. Lawrence Livermore National Laboratory.
d. Central Research Laboratory, Budapest.

References

1. B.A. Remington, G. Caskey, A. Galonsky, C.K. Gelbke, L. Heilbronn, J. Heltsley, M.B. Tsang, F. Deak, A. Kiss, Z. Seres, J. Kasagi, and J.J. Kolata, Phys. Rev. C 34, 1685 (1986).
2. A. Kiss, F. Deak, Z. Seres, G. Caskey, A. Galonsky, L. Heilbronn, B.A. Remington, and J. Kasagi, Phys. Lett. B 184, 149 (1987).
3. F. Deak, A. Kiss, Z. Seres, G. Caskey, A. Galonsky, and B. Remington, Nucl. Instr. Meth. A258, 67 (1987).
4. F. Deak, A. Kiss, Z. Seres, G. Caskey, A. Galonsky, B. Remington, C.K. Gelbke, M.B. Tsang, and J.J. Kolata, Nucl. Phys. A464, 133 (1987).
5. F. Ajzenberg-Selove, Nucl. Phys. A413, 1 (1984).
6. C.K. Gelbke and D.H. Boal, "Dynamical and statistical aspects of intermediate energy nucleus-nucleus collisions", Progress in Particle Physics 19, 1987, p. 37.
7. J. Pochodzalla, C.K. Gelbke, W.G. Lynch, M. Maier, D. Ardouin, H. Delagrange, H. Doubre, C. Gregoire, A. Kyanowski, W. Mittig, A. Peghire, J. Peter, F. Saint-Laurent, B. Zwieglinski, G. Bizard, F. Lefebvres, B. Tamain, J. Quebert, J.P. Viyogi, W.A. Friedman, and D.H. Boal, Phys. Rev. C 35, 1695 (1987).
8. G. Caskey, L. Heilbronn, B. Remington, A. Galonsky, F. Deak, A. Kiss, and Z. Seres, Phys. Rev. C March (1988) and A. Kiss, F. Deak, Z. Seres, G. Caskey, A. Galonsky, B. Remington, "Production of light fragment isotopes from collisions of ^{14}N ions of 35 MeV/u with carbon, nickel, and holmium targets", (to be published).

ANALYSIS OF SOME PROJECTILE FRAGMENTATION COLLISIONS

Z. Seres,[a] G. Caskey,[b] F. Deak[c], A. Galonsky, L. Heilbronn, A. Kiss[c], and B. Remington[d]

The Goldhaber model of fragmentation[1] works well at high projectile energies, but from E/A ≈ 100 MeV[2] and below[3-6] the momentum spectra become asymmetric; the low-momentum side of the peak becomes broader. This broadening is probably evidence of contributions from processes other than pure fragmentation[5-9], i.e., from interaction-plus-fragmentation.

Several attempts have been made to include processes other than direct fragmentation, such as delayed fragmentation[9], fragmentation + sequential decay[8], breakup + fusion[10], and transfer from stripping[11], from the surface[5], from the overlap region[7], and with damping[12]. Presumably some combination of these effects leads to the low energy side of the QE peak, though no comprehensive treatment yet exists. In a re-analysis of some fragment data[6] obtained with an ^{14}N beam at E/A = 35 MeV bombarding a target of ^{165}Ho, we developed an "interaction + fragmentation" parametrization that covers the full energy range. The fragment angle was always 10°.

An analytic spectral shape was constructed on the basis of three assumptions: 1) that fragmentation produces a Gaussian distribution, as in the Goldhaber model, around momentum p_0 with a standard deviation of σ, 2) that a fraction w results from direct, or clean, fragmentation, the remainder 1-w suffering energy (and momentum) dissipation prior to fragmentation, and 3) that the probability of momentum loss is an exponential function of that loss. Our approach is similar in spirit to that of Friedman and Saloner[9]. The exponential shape is a phenomenological choice based on the appearance of the spectra.

Then the peakform of a multi-step, slightly damped component is the convolution of the Gaussian and exponential probability density functions

$$g(p) = \frac{g_0}{\sqrt{2\pi\sigma^2}} \exp\left[-\frac{(p-p_0)^2}{2\sigma^2}\right]$$

and $$f(p,p') = \frac{1}{q} \exp\left[-\frac{p'-p}{q}\right].$$

The complete spectrum is

$$F(p) = w\, g(p) + (1-w) \int_p^\infty g(p')\, f(p,p')\, dp'. \quad (2)$$

The first term is the one-step, direct fragmentation part, and the second term is the multi-step damped part. Figure 1 ,for example, shows the ^{10}B spectrum and the fit. The parameters of the fit are p_0, σ, w, q, and g_0. They are listed in Table I for ^{10}B and for eight other fragment isotopes. To fit the spectra

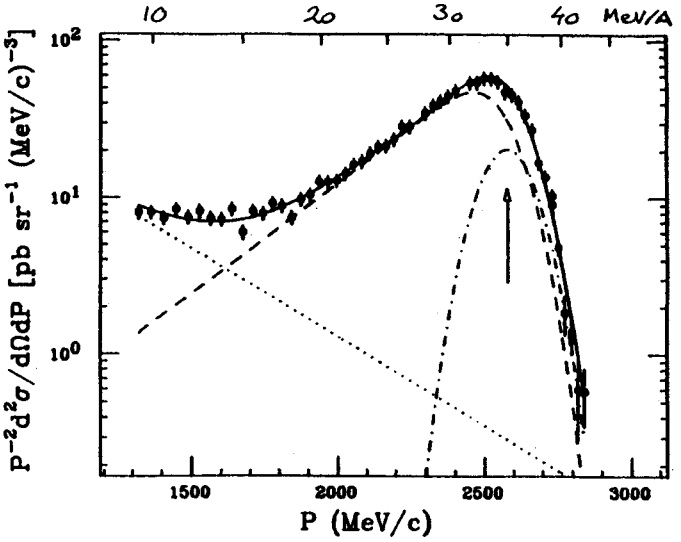

Fig. 1: The invariant momentum spectrum of ^{10}B fragments at 10° from the ^{14}N + ^{165}Ho reaction at E/A = 35 MeV. The full line is the fitted analytical form. The dot-dashed line is the direct fragmentation, the dashed line is the damped fragmentation, and the dotted line is the contribution of strongly-damped reactions. The arrow indicates the parameter p_0, the peak of the direct fragmentation component.

Table I.

Parameters of the direct and damped fragmentation.

Detected fragment	Missing nucleons	$E(p_0)/A$ [MeV]	σ [MeV/c]	w	q [MeV/c]	g_0 [x100]
^{7}Be	3p,4n(^{7}Li)	35.73	99±3	0.152±0.018	307±29	377±13
^{9}Be	3p,2n(^{5}Li)	34.43	64±3	0.022±0.022	388±39	212±13
^{10}Be	3p,1n(^{4}Li)	33.98	62±4	0.000±0.012	472±53	101± 8
^{10}B	2p,2n(^{4}He)	35.00	89±2	0.160±0.016	307±18	286± 8
^{11}B	2p,1n(^{3}He)	34.54	79±2	0.035±0.011	402±16	339± 8
^{12}B	2p	34.15	83±5	0.034±0.020	452±67	29± 2
^{11}C	1p,2n(^{3}H)	35.48	81±2	0.286±0.014	315±15	133± 3
^{12}C	1p,1n(^{2}H)	35.00	56±1	0.312±0.015	245± 8	411± 8
^{13}C	1p	34.61	52±2	0.101±0.012	292±13	117± 3

down to the lowest momenta, where strongly-damped reactions dominate, the function $h\beta \exp(-\beta p)$ was included in all fits. As can be seen in Fig. 1 this component contributes only about 1% in the region of the direct fragmentation peak.

We next investigate the physical significance of the parameters.

1. p_0 - The parameter p_0 gives the peak position of the direct fragmentation component. It is indicated by an arrow in Fig. 1. It is clear that p_0 does not correspond to the peak of the experimental spectrum; it applies only to the direct fragmentation part. The striking thing about p_0 is that it is approximately independent of Q-value. One may think of direct fragmentation as occuring in two steps. In the first step the projectile, in the vicinity of the target, splits into the detected fragment and the remainder. Then the remainder may interact more strongly with the target. In this picture the kinetic energy of the fragment is affected by the Q-value for breakup of the projectile. For a ^{14}N projectile and the fragments we detected this Q-value is as low as -4 MeV/nucleon. We should, but did not, see a 4-MeV/nucleon shift to lower energy. On the other hand, if we assume a simple two-body reaction, e.g., $^{14}N + ^{165}Ho \rightarrow ^{168}Tm + ^{11}B$, Q/A = -0.85 MeV. For eight of our nine fragments this two-body, one-step process gives Q/A between +0.1 MeV and -1.4 MeV, a range that is consistent with observation. The ninth fragment, ^{7}Be, yields Q/A = -2.65 MeV. While not conclusive, the near-constancy of p_0 favors the one-step process.

2. σ - The width of the direct fragmentation distribution σ agrees with that obtained by fitting a Gaussian to the high-momentum side only of the asymmetric experimental peak [4]. The collection of σ values is fitted by eq. 1 with $\sigma_0 = 45 \pm 2$ MeV/c.

3. w - The probability for direct fragmentation w ranges from 0.0 to 0.31 (see Table 1). The largest values occur when the nucleons stripped from the projectile have a constituency of ^{3}H or ^{2}H; the next largest for ^{4}He and ^{7}Li; and the smallest values when the stripped nucleons form no bound system.

4. q - The probability of a given momentum loss is determined by the damping momentum, parameter q. The degree of damping increases monotonically with q. The damping momentum is around 350 MeV/c, and it has a decreasing trend with Z/A. Whether we consider the entire data set, isobar pairs within the set, or isotope triplets within the set, q decreases with increasing Z/A. This dependence is consistent with a picture in which the projectile and the fragment follow a Coulomb trajectory. The key

idea is that the acceleration due to the Coulomb force is determined by two factors, the value of Z/A and the distance of closest approach. The acceleration depends directly on Z/A, but inversely on the distance of closest approach, and therefore on the impact parameter. A fragment of small Z/A, for example, requires a small impact parameter to receive sufficient acceleration to end up at 10°. The smaller is Z/A, the smaller must be the impact parameter of the collision and, therefore, the greater the interaction and damping momentum q. Such a trend is in agreement with the predictions of Harvey and Murphy.[7]

In summary then, by using an "interaction plus fragmentation" model we have separated fragment spectra in peripheral collisions into a direct and a damped part. The systematics of the peak momentum of the direct part and of the degree of damping of the damped part indicate that Coulomb deflection and impact parameter selection play a key role in determining the spectra. We conclude that the smaller the Z/A of the detected fragment, the smaller the impact parameter of the reaction.

---

a. Central Research Laboratory, Budapest, Hungary.
b. Donnelly Corp., Holland, MI 49423.
c. Eötvös Lorand University, Budapest, Hungary.
d. Lawrence Livermore National Laboratory, Livermore, California.

References

1. A.S. Goldhaber, Phys. Lett. 53B (1974) 306.
2. J.D. Silk, H.D. Holmgren, D.L. Hendrie, T.J.M. Symons, G.D. Westfall, P.H. Stelson, S. Raman, R.L. Auble, J.R. Wu, and K. Van Bibber, Phys. Rev. C 37, 158 (1988).
3. S. Wald, S.B. Gazes, C.R. Albiston, Y. Chan, B.G. Harvey, M.J. Murphy, I. Tserruya, R.G. Stokstad, P.J. Countryman, K. Van Bibber, and H. Homeyer, Phys. Rev. C 32, 894 (1985).
4. M.N. Namboodiri, R.K. Choudhury, J.B. Natowitz, K. Hagel, L. Adler, P.L. Gonthier, H. Simon, S. Kniffen, R. Patton, E. Tomasi, C. Ngo, C. Mazur, and M. Ribrag, Phys. Rev C 28 (1983) 460.
5. Y. Blumenfeld, PH. Chomaz, N. Frascaria, J.P. Garron, J.C. Jacmart, J.C. Roynette, D. Ardouin, and W. Mittig, Nucl. Phys. A455 (1986) 357.
6. G. Caskey, B. Remington, L. Heilbronn, A. Galonsky, F. Deák, A. Kiss, and Z. Seres, Phys. Rev. C, March, 1988.
7. Bernard G. Harvey, Nucl. Phys. A444, 498 (1985); B.G. Harvey and M.J. Murphy, Phys. Lett. 130B, 373 (1983).
8. K.W. McVoy and M. Carolina Nemes, Z. Phys. A295, 177 (1980).
9. W.A. Friedman and D. Saloner, Phys. Rev. C 23, 2532 (1981).
10. T. Udagawa, D. Price, and T. Tamura, Phys. Lett. 116B, 311 (1982).
11. H. Utsunomiya, Phys. Rev. C 32, 849 (1985).
12. M.C. Mermaz, F. Auger and B. Fernandez, Phys. Rev. C 28, 1587 (1983).
13. Handbook of Mathematical Functions with Formulas, Graphs, and Mathematical Tables, Edited by M. Abramowitz and I.A. Stegun, National Bureau of Standards, Applied Mathematics Series 55, p.932, 1966, Washington D.C.

POPULATION IF HIGH SPIN STATES BY QUASI-ELASTIC AND DEEP INELASTIC COLLISIONS

H. Takai[a], C.N. Knott[a], D.F. Winchell[a], J.X. Saladin[a], M.S. Kaplan[a], L. de Faro[a], R. Aryaeinejad, R.A. Blue, R.M. Ronningen, D.J. Morrissey, I.Y. Lee[b], and O. Dietzsch[c]

Reactions induced by ^{22}Ne + ^{170}Er have been studied at a bombarding energy of 10 MeV/A, about twice the Coulomb barrier energy. Arrays of gamma-ray and particle detectors allowed identification of both the target-like fragment (TLF) and the projectile-like fragment (PLF) for a number of reaction channels. Both PLF-gamma and gamma-gamma coincidence events were recorded. The purpose of the experiment was to assess the usefulness of the various reaction mechanisms, quasi-elastic collisions, incomplete fusion, massive transfer, breakup fusion, and deep inelastic collisions, for excitation of high spin states in the TLF and more particularly for investigations of nuclei on the neutron rich side of the valley of stability. The apparatus, shown schematically in Fig. 1, included six silicon ΔE-E particle telescopes located at $\theta = 30$ deg and equally spaced in ϕ on a cone about the beam direction. Gamma rays were detected in elements of the Pittsburgh gamma detector array composed of five high-purity, Compton-supressed germanium detectors and a fourteen-element BGO sum-energy and multiplicity spectrometer (SMS).

The germanium detectors were placed in the horizontal plane at angles of 72.3, 92.3, 101.2, 142.2 and 145.0 degrees with seven SMS elements clustered above and seven elements below the target to cover a total solid angle of about 30% of 4π.

The resolution of the particle telescopes allowed identification of PLFs ranging from ^{6}Li to ^{24}Mg. Relative to elastic scattering those reaction channels with PLF yields of 1% or more include only single nucleon transfer on the "pick up" side but extend clearly to ^{11}C as a product of "stripping". The role of various reaction mechanisms contributing to the PLF

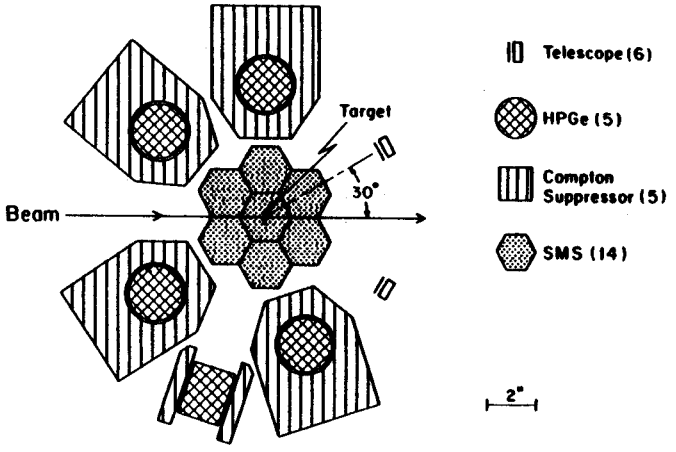

Fig. 1: Top view of the experimental apparatus showing the various types of detectors and their arrangement.

yields can perhaps best be shown by 2-dimensional intensity contour maps of PLF energy as a function of gamma-ray fold observed in the SMS detectors. Figure 2 shows these maps for a number of different identified PLFs. Using standard calibration procedures, it is possible to derive the gamma-ray multiplicity M from the detected coincidence fold K. Both quantities are indicated in the figure. It should be noted that K and M here refer to the sum of the folds and multiplicities for cascades from the TLF and PLF fragments.

For PLFs close to the projectile mass the Fig. 2 contours reveal a well-defined maximum corresponding to quasi-elastic processes. As more nucleons are transferred this maximum broadens and then disappears as one moves from oxygen to nitrogen isotopes. The disappearance of the QE peak is probably due to proton shell effects which favor the stripping of clusters with Z of two or less. Similar neutron shell closure effects may be responsible for the unusually strong population of ^{15}N among the nitrogen isotopes. Starting in ^{19}O the deep-

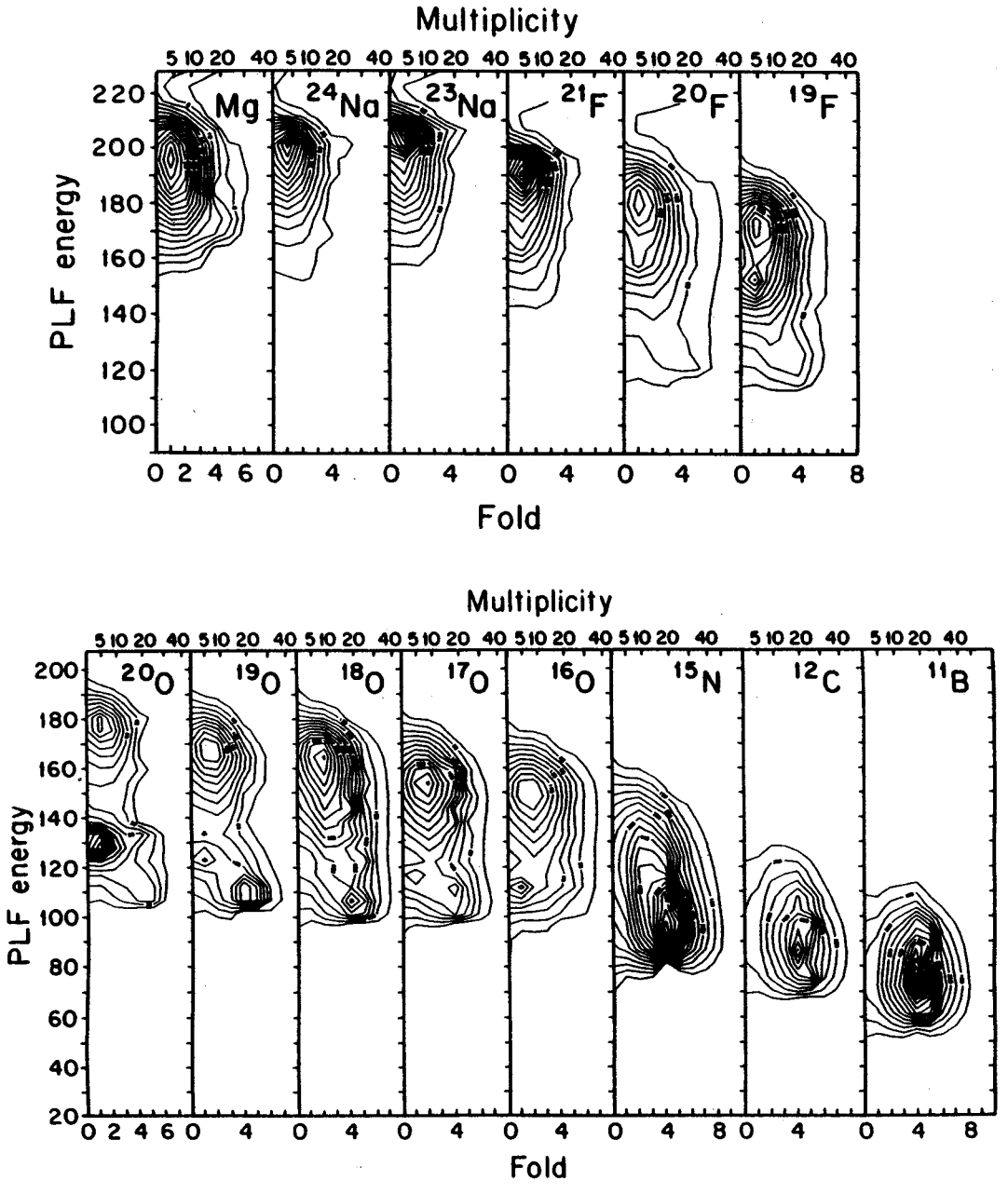

Fig. 2: PLF kinetic energy vs. gamma-ray fold for various PLFs with an approximate multiplicity scale. This figure shows the transition from the predominance of quasi-elastic reactions for heavier PLFs to mainly DICs for the lighter PLFs. The low fold, low energy peak in ^{19}F and some of the oxygen isotopes is the result of pulse pileup in the particle detectors.

inelastic collisions (DIC) are seen in a second maximum at considerably lower PLF energy but with higher multiplicity M. For the lightest PLFs only the DIC maximum is observed.

Figure 3 shows spectra of the TLF gamma rays obtained in coincidence with each PLF isotope with Z greater than 6. In each case the spectrum is the sum of the spectra from all five germanium detectors, with the data Doppler corrected on the basis of reaction kinematics. Gamma rays are identified for 12 different TLF isotopes. As expected, the TLFs found in coincidence with the lighter PLFs are "missing" a greater number of neutrons. In the case of the carbon PLFs, the channels in which an alpha particle is part of the unobserved mass are as

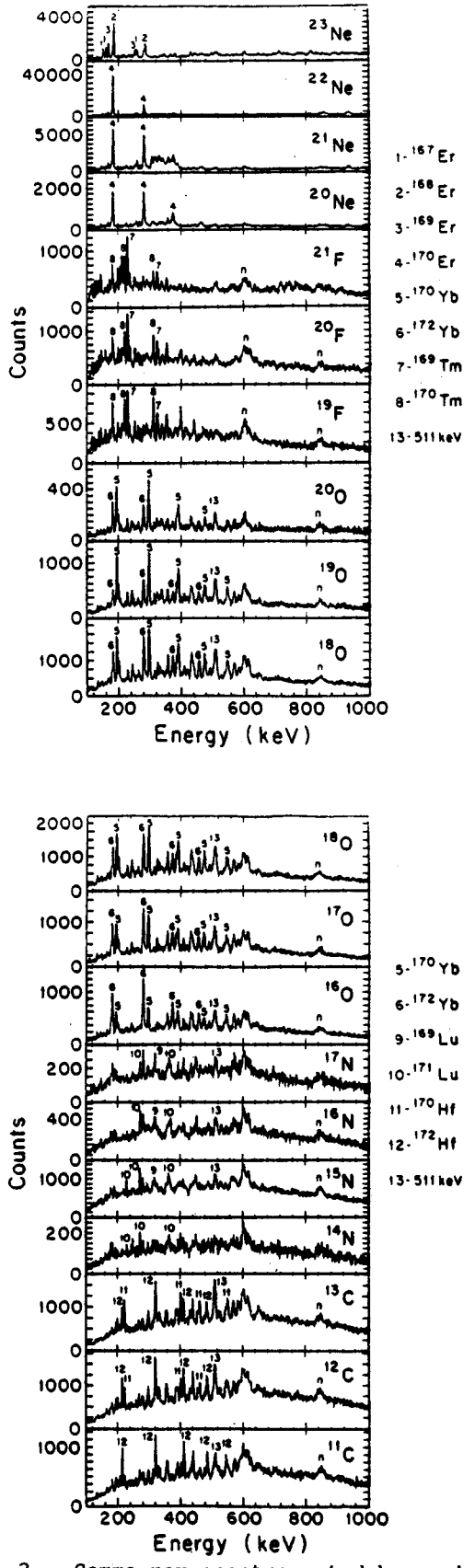

Fig. 3: Gamma-ray spectra gated by various PLF isotopes. Lines associated with selected TLF channels are marked.

strong as channels in which only neutrons are missing. Further gating on PLF energy can, in some cases at least, produce greater selectivity in the TLF coincident gamma spectra. This observed TLF isotope selectivity as a function of PLF energy can be understood in terms of the formation of an initial compound system by the target nucleus and the transferred cluster with subsequent light particle evaporation. A statistical model calculation performed for the ^{18}O PLF channel in coincidence with various Yb isotopes gives satisfactory agreement with the observed relation between PLF energy and relative TLF isotope yields.

From the measured multiplicities, it is possible to estimate the fraction of the initial orbital angular momentum that is transformed into the spin angular momentum of the final fragments. Following the formation of the compound system excitation energy and angular momentum are carried away by the evaporation of neutrons and alpha particles. Statistical calculations as well as a considerable body of experimental data indicate that on the average each neutron carries away about 0.7 units of angular momentum. Once the fragments are stable against particle emission the remaining angular momentum is carried away by gamma emission, mostly via stretched E2 stretched transitions which result in a spin change of 2 units. A small portion of the decays proceed via dipole transitions which, according to statistical calculations, correspond to an average spin change of 0.5 units. With the assumption that the average cascade involves about two dipole transitions we can then determine the total amount of orbital angular momentum transformed into intrinsic angular momentum. The relative intensities as a function of initial spin state for yrast decays in four Yb isotopes formed in coincidence with ^{18}O are shown in Fig. 4. For $^{170,172}Yb$, which are produced by quasielastic reactions the intensity drops off quite rapidly for transitions above the 8^+ state. As we move

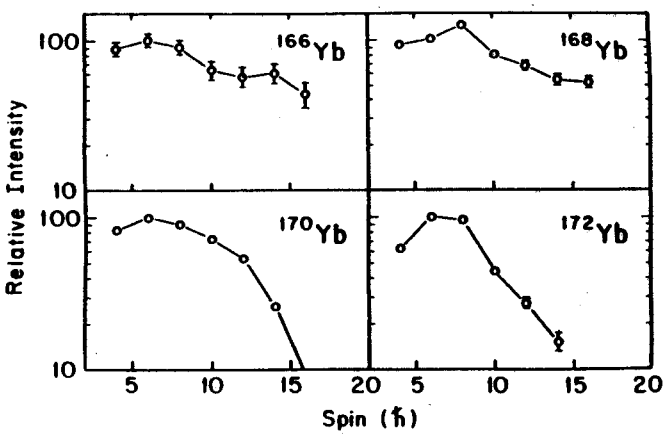

Fig. 4: Relative transition intensities as a function of initial spin for the Yrast lines of four Yb isotopes gated on ^{18}O. The plots are normalized to the 4+ - 2+ transition.

toward isotopes that are populated primarily through DIC the intensities do not fall off as rapidly at higher spins. These results indicate that DIC compares favorably with other methods in its ability to populate high spin states.

This summary has given only a sample of the information that is being derived from the results of this experiment. With regard to the stated aims of the measurements it seems that the selection of events in which DIC are predominant can be a very effective way to study high spin states in regions of the chart of nuclides not accessible by other means. To achieve higher angular momentum transfers, PLFs could be detected at more backward angles, thus selecting fragments from the sticking limit regime. Larger solid angles for particle detection are clearly needed, but resolution to identify the PLFs by Z only should be sufficient. Thus some form of gas counters could replace the silicon telescopes. However, accurate measurement of the PLF scattering angle is highly desirable so that the small (~ 1%) Doppler shift corrections to the TLF gamma energies can be made.

---

a. University of Pittsburgh.
b. Oak Ridge National Laboratory.
c. University of Sao Paulo, Brazil.

EXCITATION FUNCTIONS FOR IMF FORMATION IN THE E/A = 20-50 MeV ^{14}N + ^{nat}Ag, ^{197}Au REACTIONS

D.E. Fields[a], K. Kwiatkowski[a], D. Bonser[a], R.W. Viola[a], V.E. Viola[a], M.B. Tsang, J. Pochodzalla, W.G. Lynch, C.K. Gelbke, D.J. Fields and S.M. Austin

Excitation function measurements were performed for the ^{14}N + ^{nat}Ag and ^{14}N + ^{197}Au systems using beams of E/A = 20, 30, 40 and 50 MeV. Telescopes for detection of Z = 3-14 fragments consisted of gas-ionization chamber/silicon surface barrier/Si(Li) detectors fixed at angles of θ = 60°, 90°, 120° and 165° and a four-element silicon telescope which was rotated from 20° to 40° at each energy. High purity silver and gold targets were employed and all experimental variables were kept constant throughout the experiment, except the forward detector and the beam energy, in order to insure highly systematic data. The results presented here are in good agreement with more limited data sets for this system.[1,2]

The energy spectra obtained in these studies exhibit characteristic IMF features as a function of angle and atomic number; i.e. the spectra evolve from rather flat pre-compound-like behavior at forward angles to steep compound-nucleus-like character at extreme backward angles for all Z values (except near the grazing angle). The most striking feature of the energy spectra is that for energies from E/A = 30 to 50 MeV, the spectral slopes for a given IMF and angle are essentially constant - implying that on the average there is a temperature saturation across this energy range.[3] The only other systematic feature of the spectra is a broadening of the Coulomb peak at forward angles for each fragment type as the energy increases, suggestive of enhanced contributions from sequential decay processes.

In Fig. 1, representative angular distributions for Z = 8 fragments for ^{14}N + ^{nat}Ag provide some initial indication of the relative importance of equilibrated and non-

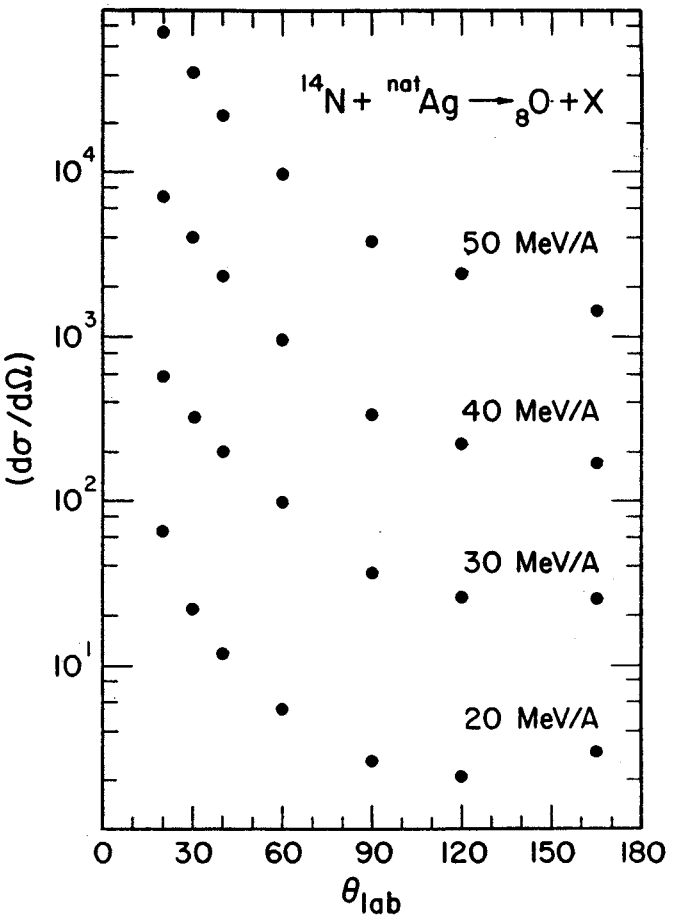

Fig. 1. Angular distributions of oxygen fragments.

equilibrated emission mechanisms in these reactions. Table 1 presents results of a decomposition of these two components into what we shall define as equilibrated (σ_{eq}) and non-equilibrated (σ_{neq}) sources. The basic assumptions of this decomposition are: 1) the differential cross section at 165° arises only from a fully equilibrated source which follows a 1/sin θ angular distribution and 2) the remainder of the cross section arises from non-equilibrium mechanisms. It is apparent in Table 1 that the non-equilibrated component becomes increasingly dominant at higher bombarding

energies, but that nonetheless some equilibrated species persist, even at the highest energies. These same trends are observed for all IMF Z-values, with σ_{neq} being enhanced for the lightest fragments, whereas σ_{eq} is enhanced for the heaviest fragments. Similar behavior is observed in the gold system.

Table 1.

E/A =	20 MeV	30 MeV	40 MeV	50 MeV
σ_{eq}/σ_{neq}<	1.0	0.45	0.27	0.17
τ	2.6	2.9	3.1	3.2

The elemental cross sections for ^{14}N + Ag also exhibit nearly identical behavior at each energy. When fit with a power-law function,

$$\sigma(Z) \propto Z^{-\tau}, \ (Z < 10) \qquad (1)$$

the values of τ (listed in Table 1) show little energy dependence. Only at E/A = 20 MeV is there a meaningful difference. The origin of this difference can be traced to the forward-and backward-angle data; the former yield τ = 2.9 and the latter τ = 2.1. Thus at all energies the values of τ for the σ_{neq} component are essentially identical. The significantly lower value of τ for the σ_{eq} component supports the suggestion that the τ parameter may provide a useful test for changes in reaction mechanisms leading to IMF formation.[4]

In Fig. 2 the excitation functions for emission of Z = 4,6,8, and 10 fragments from the target-like source are presented with the total IMF cross sections for ^{14}N + Ag. For reference, Fig. 2 also shows calculated values for the total reaction cross section,[5] σ_R, and an estimate of the cross section for events which deposit more than 200 MeV of excitation energy, $\sigma(E^*>200$ MeV), which is the approximate

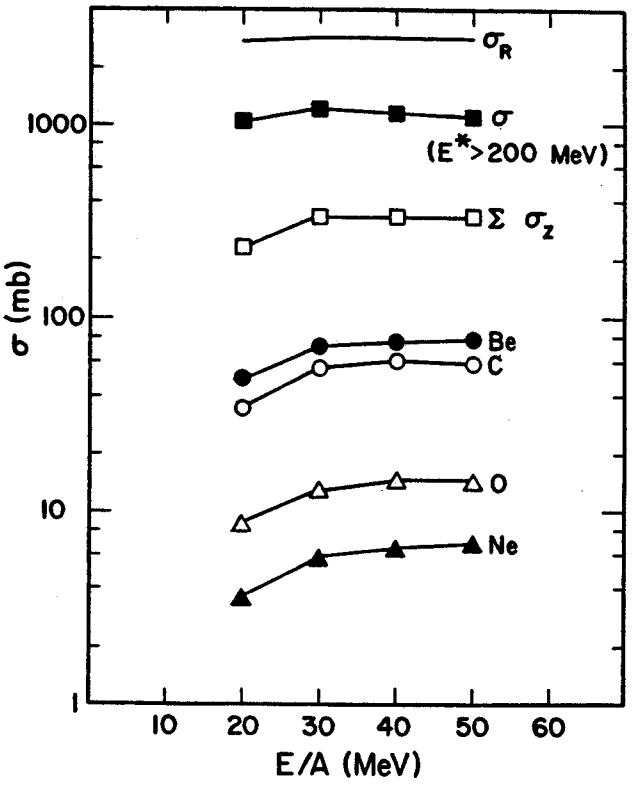

Fig. 2. Cross Sections for IMF production for the ^{14}N + ^{nat}Ag reaction; σ_R is the total IMF value, σR is the calculated reaction cross section from Ref. 5, and $\sigma(E^*>200$ MeV) is derived from data of Ref. 6.

threshold for IMF formation in this reaction. The latter were derived from linear momentum transfer distributions for a ^{238}U target.[6] The most pronounced feature of Fig. 2 is the relative insensitivity of the inclusive cross sections to bombarding energy, once the threshold energy is exceeded. Thus, while increasing E/A of the incoming projectile may broaden the distribution of excitation energy and angular momentum, on the average, mass and energy deposition processes change little. This is most readily understood in terms of the rapid growth in pre-compound nucleon emission in the vicinity of the Fermi energy - which appears to be paralleled by a similar enhancement of IMF emission from non-equilibrated sources relative to fully equilibrated ones (Table 1). It can also be deduced from Fig. 2 that multifragmentation probably does not contribute significantly to IMF production for these

systems, since the multiplicities are much less than unity ($\sigma_{IMF}/\sigma_R < 0.15$). Somewhat different cross section behavior is observed in the ^{14}N + Au system. The IMF cross sections in this case undergo a sharp rise between E/A = 20 and 30 MeV, with a continued, more gentle increase at higher energies. This implies that for this heavier system excitation-energy deposition saturates more slowly.

---

a. Indiana University Cyclotron Facility, Bloomington, IN 47405

References

1. T. Murakami, private communication.
2. C. Bloch, Ph.D. thesis, Michigan State University, 1987.
3. D. Fabris et al., Nucl. Phys. A471, 351 (1987); G. Nebbia et al., Phys. Lett. B176, 20 (1986).
4. N.T. Porile et al., Nucl. Phys. A471, 351 (1987).
5. S. Kox et al., Nucl. Phys. A420, 162 (1984).
6. M. Fatyga et al., Phys. Rev. Let. 55 1376 (1987); Ph.D. thesis, Indiana University, 1986.
7. T. Batsch et al., Phys. Lett. B189, 287 (1987).

ENTROPY PRODUCTION IN INTERMEDIATE ENERGY NUCLEAR COLLISIONS

W.K. Wilson, D. Cebra, C. Djalali, D. Fox, J. Karn, A. Pradhan,
A. Vander Molen, J. Van der Plicht, G. Westfall

The study of the entropy produced in heavy ion-induced reactions on heavy nuclei can shed light on the collective behavior of nuclear matter. Theoretical models[1,2] have suggested that the entropy per baryon, S/A, created in high energy nucleus-nucleus collisions remains nearly constant during the expansion of the system. Thus the measure of entropy could yield information about the hot, dense stage of a nucleus-nucleus reaction. Extraction of the entropy produced in heavy ion reactions at intermediate energies[3] has been achieved by comparison of production cross sections for fragments up to A=14 with quantum statistical[4] and Hauser-Feshbach[5] models. The extracted entropy was found to decrease from 2.4 at 137 MeV/nucleon for 2.0 at 42 MeV/nucleon. It is crucial to measure the entropy produced at energies below 42 MeV/nucleon to verify whether the entropy decreases as one would expect from simple considerations or whether the entropy per baryon remains near the value of 2 observed at 42 MeV/nucleon.

The previous measurement[3] at 42-137 MeV/nucleon concentrated on detecting fragments from an intermediate velocity source (IVFs). At these beam energies IVFs may be separated from fragments arising from spectator sources by appropriate choices of energy and angular range. However, as one lowers the beam energy, the separation between the three sources becomes less well defined. Another method of selecting collisions which produce an intermediate velocity source is to select collisions with a high multiplicity of emitted fragments. Measurements done at high energies demonstrate that central collisions produce an intermediate velocity source of particles corresponding to high multiplicity events.[6]

We report the initial results of an experiment performed at NSCL to study the entropy produced in intermediate energy nucleus-nucleus collisions by measuring all sources of fragments as a function of charged particle multiplicity. The experiment was performed in the 60" scattering chamber (Fig. 1). Fragments with Z from 3 to 12 were detected with Si ΔE-E telescopes from 22.5° to 40° (Fig. 2). For energies ranging from below the coulomb barrier to above the beam energy per nucleon, mass resolution was achieved for A=6-10 (Fig. 3). Light particles were detected with mass resolution for Z=1,2 from 10° to 30° by phoswich telescopes, and from 45° to 165° by phoswich telescopes with Si ΔEs added. Central events were selected using a multiplicity filter consisting of 30 phoswich telescopes arranged in a cone spanning the forward hemisphere 40° from

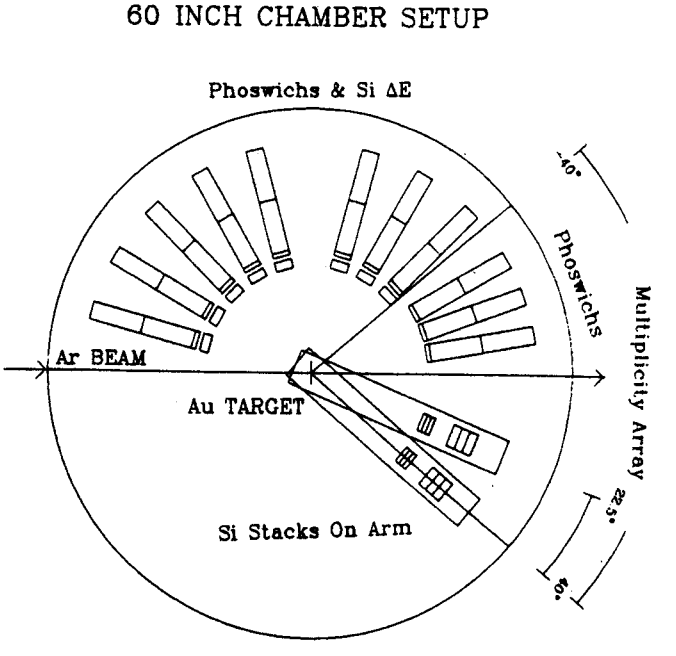

Fig. 1: Experimental setup.

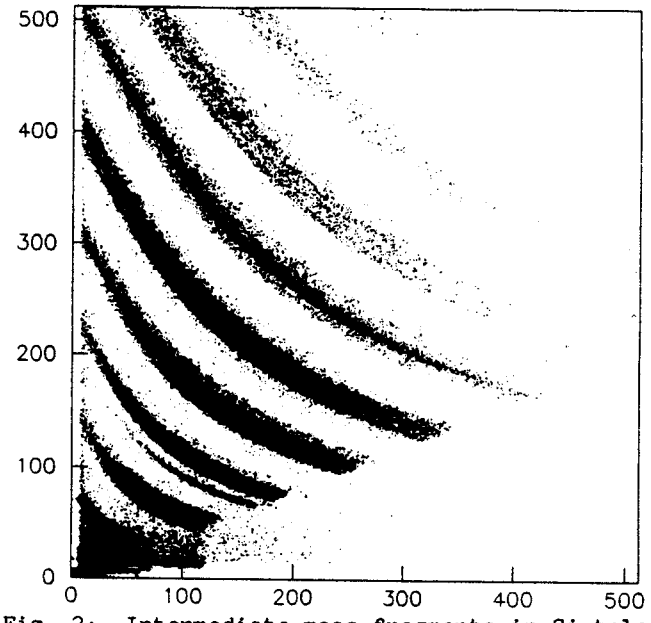

Fig. 2: Intermediate mass fragments in Si tele.

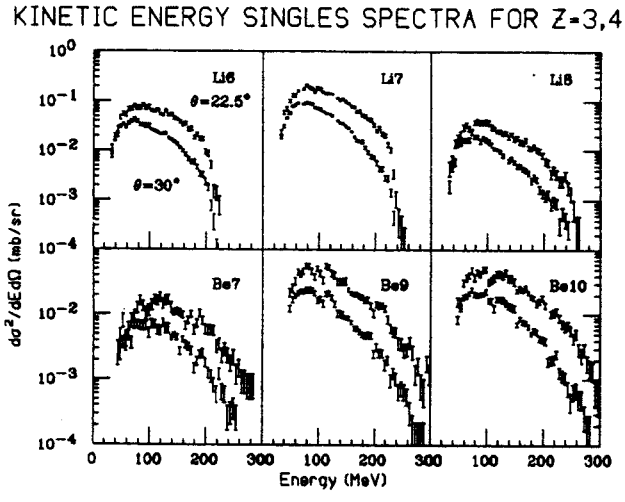

Fig. 3: A sample of IMF inclusive spectra.

the beam axis. These telescopes are capable of Z resolution through Z=7.

We choose 20 and 30 MeV Ar beams on a Au target in order to continue the systematics of ref. 3. Inclusive energy spectra were obtained as well as data triggered on multiplicity greater than 1. The ability of the multiplicity filter to select events in which IVFs dominate is demonstrated by fig. 4 gating on multiplicity > 2 significantly suppresses fragments from the projectile velocity source.

Further analysis of this data, including the determination of the entropy per baryon, is underway.

References

1. J.I. Kapusta and D. Strottman, Phys. Rev. C23, 2514 (1981)
2. G. Bertsch and J. Cugnon, Phys. Rev. C24, 2514 (1981)
3. B.V. Jacak, G.D. Westfall, C.K. Gelbke, L.H. Harwood, W.G. Lynch, D.K. Scott, H. Stöcker, M.B. Tsang, and T.J.M. Symons, Phys. Rev. Lett. 51. 1846 (1983).
4. H. Stöcker, G. Buchwald, G. Graebner, P. Subramanian, J.A. Maruhn, W. Greiner, B.V. Jacak, and G.D. Westfall, Nucl. Phys. A400, 63c, (1983)
5. W.A. Friedman and W.G. Lynch, Phys. Rev. C28, 16 (1983)
6. H.H. Gutbrod, H. Löhner, A.M. Poskanzer, T. Renner, H. Reidesel, H.G. Ritter, A. Warwick, F. Wiek, and H. Wieman, Phys. Lett. 127B, 317 (1983).

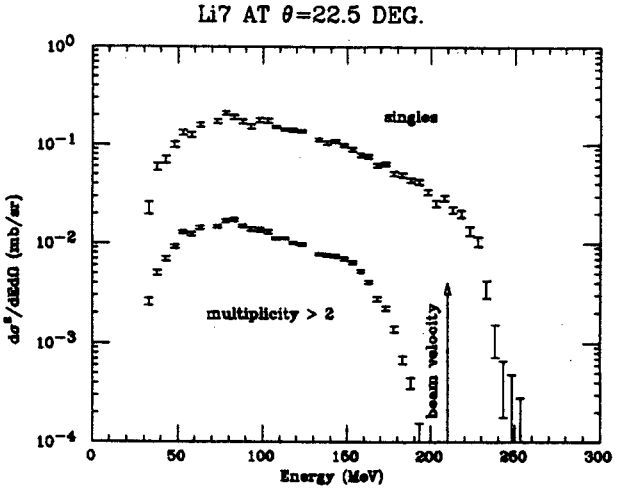

Fig. 4: The effect of multiplicity gating on the projectile velocity source.

^{12}C-INDUCED TRANSFER REACTIONS AT INTERMEDIATE ENERGIES

J.S. Winfield, E. Adamides, S.M. Austin, G.M. Crawley, C.A. Ogilvie, S. Robbins, B. Sherrill, M. Torres and G. Yoo

There is recent interest in whether the distorted wave Born approximation (DWBA), which has been extensively used to describe low energy nuclear transfer reactions, is valid in the intermediate energy regime. At energies well above E/A = 10 MeV, individual nucleon-nucleon interactions are expected to become more important than nucleon-nucleus interactions,[1] which may invalidate the mean field assumptions inherent in the DWBA. Such a breakdown of the DWBA might be manifested by a need for an energy dependence of the effective nucleon-nucleus interaction, although the use of phenomenological optical model potentials might obscure any discernible effect on the cross sections.

A suggestion that the mean field assumptions are breaking down at intermediate energies comes from a study[2] of the ^{208}Pb(^{16}O,^{15}N)^{209}Bi and ^{208}Pb(^{16}O,^{15}O)^{209}Pb reactions at E/A = 50 MeV, for which DWBA calculations overpredict the measured cross sections by a factor of about ten. This discrepancy by far exceeds other anomalies found in DWBA analyses of transfer reactions at or below E/A = 10 MeV that have often been attributed to coupled channels effects. Furthermore, it is not an isolated result: for the same ^{16}O+^{208}Pb system, Olmer et al.[3] had previously noted a trend for DWBA to overpredict cross sections as the bombarding energy was increased from E/A = 6.5 to 20 MeV. At E/A = 20 MeV, σ(DWBA)/σ(expt) ranged from 2 to 3, depending on the particular final state involved.

Other intermediate energy heavy-ion transfer reactions add little or no support to an energy dependence of the σ(DWBA)/σ(expt) ratio.[4,5] In fact the same group that found the large discrepancy in the ^{16}O+^{208}Pb case has recently reported that DWBA calculations do reproduce data for one nucleon stripping reactions induced by E/A = 40 MeV ^{12}C on a ^{208}Pb target.[6] More data at intermediate energies are clearly needed to resolve the situation, and we have begun a systematic study of single nucleon transfer reactions induced by E/A = 50 MeV ^{12}C from the K500 cyclotron at NSCL on a wide mass range of targets. The reactions studied were specifically ^{12}C(^{12}C,^{13}C)^{11}C, ^{27}Al(^{12}C,^{11}B)^{28}Si, ^{40}Ca(^{12}C,^{11}C)^{41}Ca and ^{90}Zr(^{12}C,^{13}N)^{89}Y. The reaction products were analyzed by the S-320 spectrograph with a resolution of about ΔE/E = 1/600. Adequate particle identification was obtained through the energy-loss signal from the ion chambers, time-of-flight relative to the cyclotron rf and the light output from the stopping scintillator.

Monitor detectors were used to determine the relative cross sections for different spectrograph angles. In order to fix the absolute cross sections, we used the integrated current from a Faraday cup, the efficiency of which was determined by measuring elastic scattering from all the targets at small angles. The overall systematic uncertainty in the present data is estimated as ±25%.

A spectrum for the ^{12}C(^{12}C,^{13}C)^{11}C reaction is shown in Fig. 1. Typically, one observes that relatively high spin states tend to be favored.[7] The ground state yield was extracted from a 4-peak Gaussian fit to the spectrum as indicated in Fig. 1 (these data are to be published in Ref. 8). The ground state angular distribution is shown in Fig. 2 together with DWBA predictions from the exact finite-range program SATURN-MARS.[9] The optical model potential used in this calculation was taken from Sahm et al.,[10] and is listed in Table I as

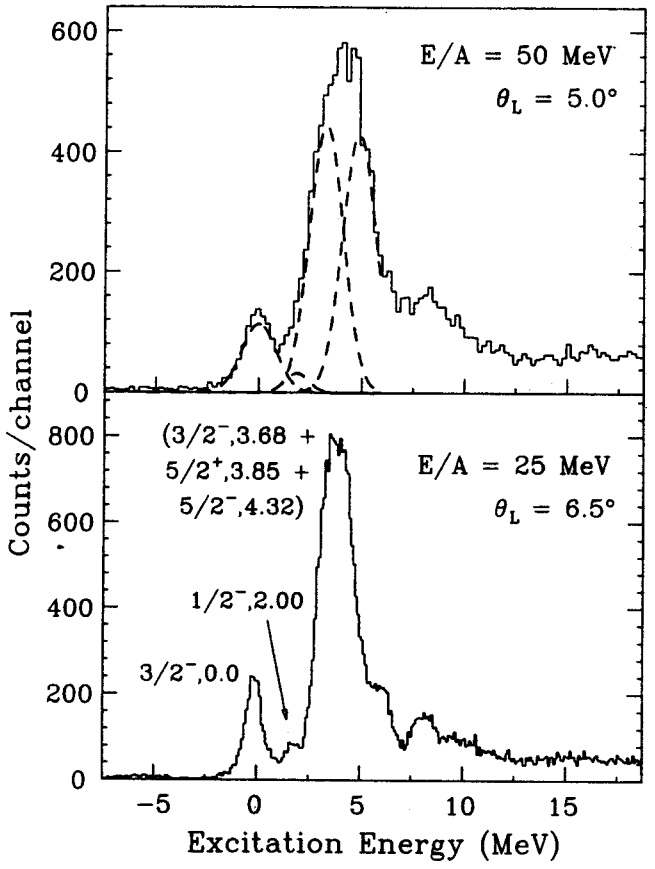

Fig. 1: Spectra of the single neutron transfer reaction induced by ^{12}C + ^{12}C at E/A = 50 and 25 MeV.[8] Low-lying states in ^{13}C and ^{11}C are indicated by spin, parity and excitation energy. The dashed lines in the E/A = 50 MeV spectrum are the results from a 4-fold Gaussian fit.

"C1". Normalization to the data gives a value of 2.6±0.7 for the product of target and projectile spectroscopic factors, $C^2S_1 \times C^2S_2$. This is to be compared with values[8] of between 1.8 and 2.8 for E/A = 10 to 35 MeV and a shell model prediction[8] of 1.8.

A ^{13}N energy spectrum from the reaction $^{90}Zr(^{12}C,^{13}N)^{89}Y$ is shown in Fig. 3. No mutual excitation peaks are observed since the ^{13}N ejectile has no bound excited states. The spectrum is dominated by two peaks, the $1/2^-$ ground state of ^{89}Y and a broad peak next to it which consists of low lying excited states in ^{89}Y, i.e. the $g_{9/2}$, $p_{3/2}$, $f_{5/2}$ and $d_{5/2}$

Table I. Optical model parameters of Woods-Saxon potentials used in the DWBA analyses. Potential depths are in MeV, geometrical parameters are in fm. The columns labeled "System" and "E/A" refer to the elastic scattering from which the potential was obtained.

Label	V	r	a	W	r_w	a_w	Ref.	System	E/A
C1	250	0.814	0.626	231.9	0.789	0.60	10	$^{12}C+^{12}C$	35
C2	120	0.71	0.84	34.02	0.96	0.69	16	$^{12}C+^{12}C$	85
A1	200	0.657	1.054	273.0	0.884	0.658	10	$^{12}C+^{40}Ca$	35
A2	200	0.870	0.75	281.1	0.869	0.678	10	$^{12}C+^{40}Ca$	35
Si	100	0.892	0.905	50.5	0.992	0.780	17	$^{16}O+^{28}Si$	94
Zr	150	0.934	0.781	207.7	0.890	0.834	10	$^{12}C+^{90}Zr$	35

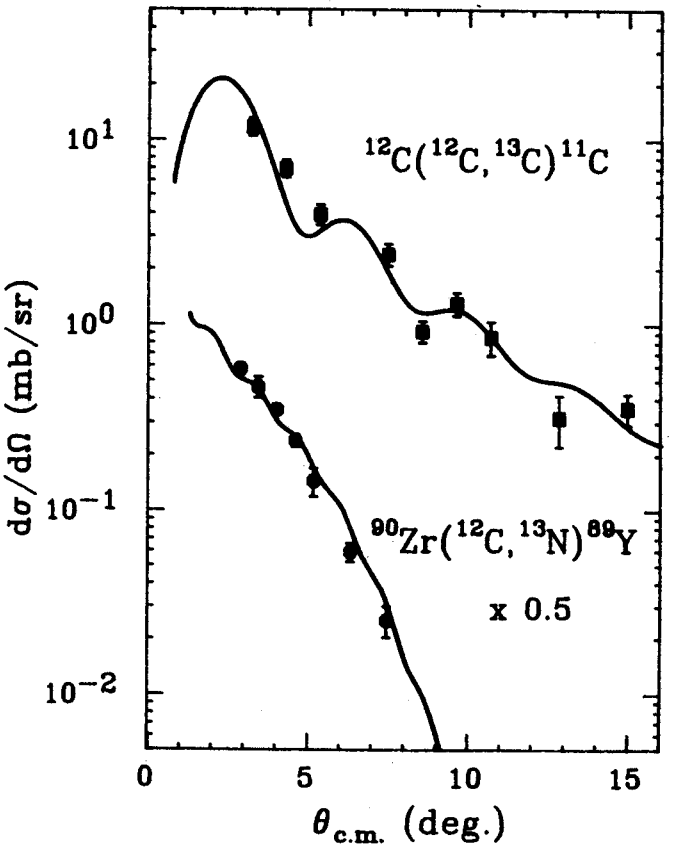

Fig. 2: Angular distributions for $^{12}C(^{12}C,^{13}C)^{11}C$ (g.s.) and $^{90}Zr(^{12}C,^{13}N)^{89}Y$ (g.s.) at E/A = 50 MeV. The curves are finite range DWBA calculations described in the text.

configurations at 0.91, 1.51, 1.74 and 2.22 MeV, respectively. At high bombarding energies, one expects non-spin flip transitions in the final nuclei to be favored over spin flip ones;[7] thus the $p_{3/2}$ $j_>$ state should be weak in comparison to the $j_<$ states. The appearance of the ^{89}Y

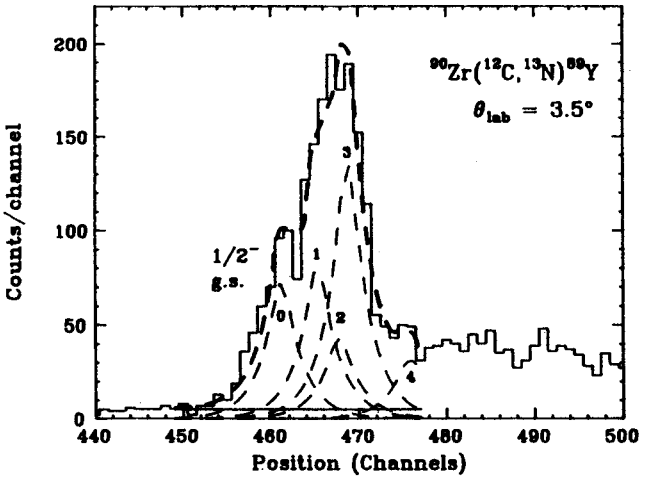

Fig. 3: Spectrum of $^{90}Zr(^{12}C,^{13}N)^{89}Y$ at E/A = 50 MeV. The dashed lines are the results from a 5-fold peak fit to the low-excitation region of the spectra. The unfolded peaks labeled 1 through 3 correspond to the $9/2^+$ 0.91 MeV, $3/2^-$ 1.51 MeV, $5/2^-$ 1.74 MeV excited states of ^{89}Y. The peak labeled 4 is at 3.2 MeV. The solid line is the assumed background in the fitted region.

spectrum is quite similar to that observed by $^{90}Zr(^{13}C,^{14}N)$ at E/A = 30 MeV (Ref. 5) and $^{90}Zr(^{6}Li,^{7}Be)$ at E/A = 10 MeV.[11]

In analyzing the Zr spectra, peaks of Gaussian shape with exponential tails were used. The peak shape was based on those observed in $^{40}Ca(^{12}C,^{11}C)^{41}Ca$ where the ground state is well separated. Two approaches to the peak fitting were followed. In the first method the broad peak next to ground state was fitted by two overlapping peaks. The position of all three peaks was set free for the best fit to the data, with widths held equal and fixed. In the second method a sequence of five peaks corresponding to the first five states in ^{89}Y at the known excitation energies was set free to move as a whole, again with widths set equal and fixed. The two methods gave yields for the ground state which differed by no more than 15% and their weighted average was used for the angular distribution (Fig. 2). The experimental errors include only statistical uncertainties. The calculated DWBA curve shown in Fig. 2 has been obtained with optical model parameters taken from Ref. 10 and listed in Table I as "Zr". The bound state geometry was the same as that used in Refs. 12 and 14. The calculations were normalized to the data in order to extract the product of the spectroscopic factors $C^2S_1 \times C^2S_2$. The DWBA angular distribution is seen to agree fairly well with the shape of the experimental data. If we take the spectroscopic factor for the $^{12}C + p = {}^{13}N$ system from Ref. 11 as 0.48, the resulting spectroscopic factor for the ^{89}Y ground state is 1.4 ± 0.4. Other experiments gave results between 1.1 and 1.9 (Refs. 12-15).

Spectra for single nucleon transfer reactions on the ^{27}Al and ^{40}Ca targets are shown in Figs. 4 and 5. The ground states of the final nuclei are cleanly resolved for both ^{28}Si and ^{41}Ca. The analysis of these data is not yet complete. However, DWBA calculations for the $^{27}Al(^{12}C,^{11}B)^{28}Si_{g.s.}$ and $^{40}Ca(^{12}C,^{11}C)^{41}Ca_{g.s.}$ reactions show a marked sensitivity to the choice of optical model parameters. Calculations with $^{12}C+^{12}C$ potentials ("C1" and "C2" in Table I) gave cross sections roughly 10 times greater than those with $^{12}C+^{40}Ca$

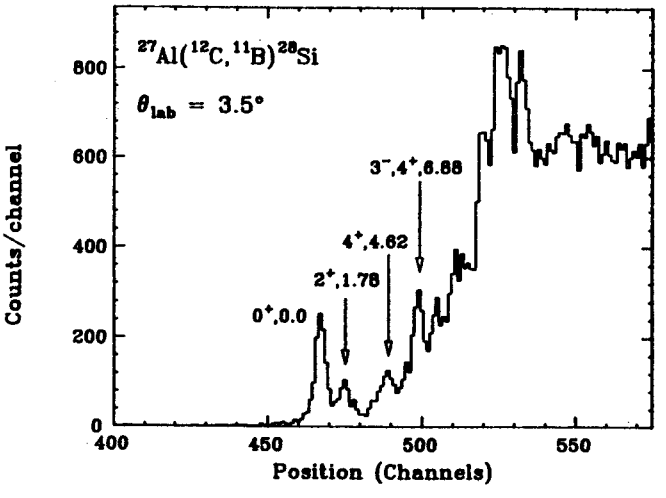

Fig. 4: Spectrum of $^{27}Al(^{12}C,^{11}B)^{28}Si$ at E/A = 50 MeV. Low lying states in ^{28}Si are labeled by spin, parity and excitation energy.

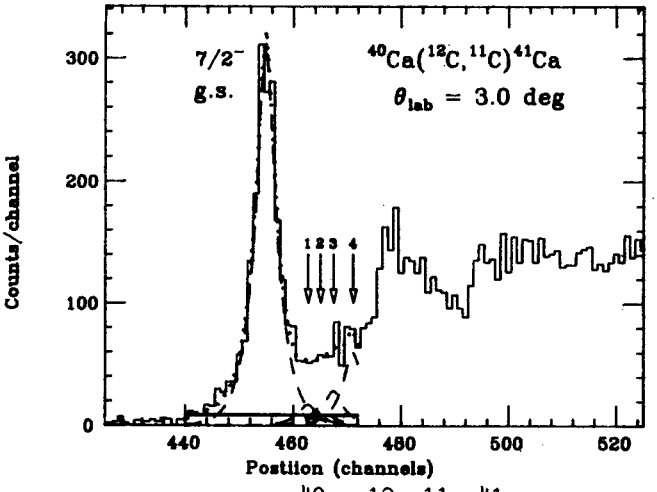

Fig. 5: Spectrum of $^{40}Ca(^{12}C,^{11}C)^{41}Ca$ at E/A = 50 MeV. The dashed (unfolded peaks) and dotted (sum, including background) lines are the results from a 5-fold peak fit to the low-excitation region of the spectra, assuming a background indicated by the solid line. The unfolded peaks labeled 1 through 4 correspond to the $3/2^-$ 1.94 MeV, $3/2^+ + 5/2^+$ 2.5 MeV, $7/2^- + 9/2^+$ 3.1 MeV and 4.01 $11/2^-$ excited states of ^{41}Ca.

potentials ("A1" and "A2" in Table I). A $^{16}O+^{28}Si$ potential ("Si" in Table I) gave an intermediate result. Preliminary indications are that the ^{40}Ca potentials describe the data best both in terms of shape and magnitude.

In summary, single nucleon transfer reactions induced by E/A = 50 MeV ^{12}C projectiles on targets of ^{12}C and ^{90}Zr are well reproduced by standard finite range DWBA calculations. These results are supported by the slightly lower energy work by Mermaz et al.[6] for $^{12}C+^{208}Pb$. In the case of the ^{27}Al and ^{40}Ca targets, we have found a remarkable sensitivity of the DWBA cross sections to the choice of optical model parameters used for the distorted waves. It thus appears that the discrepancy found[2,3] between data and DWBA calculations for $^{16}O+^{208}Pb$ is an anomaly, perhaps associated with the ^{16}O projectile, rather than an indication of the breakdown of the underlying assumptions in DWBA theory.

References

1. R.M. DeVries and J.C. Peng, Phys. Rev. C 22,1055(1980).
2. B. Berthier et al., Phys. Lett. 182B,15 (1986); M.C. Mermaz et al., Z. Phys. A326, 353(1987).
3. C. Olmer et al., Phys. Rev. C 18,205(1978); S.C. Pieper et al., ibid,180.
4. M.A.G. Fernandes et al., Phys. Rev. C 33, 1971(1986).
5. W. von Oertzen, E. Adamides et al., submitted to Nucl. Phys., 1987.
6. M.C. Mermaz et al., DPh-N/Saclay preprint No. 2470, submitted to Phys. Rev. C.
7. D.M. Brink, Phys. Lett. 40B,37(1972); W. von Oertzen, Phys. Lett. 151B,95(1985).
8. J.S. Winfield, S.M. Austin, G.M. Crawley, C. Djalali, C.A. Ogilvie, R.J. Smith, Z. Chen and M. Torres, Phys. Lett. (in press).
9. T. Tamura and K.S. Low, Comput. Phys. Commun. 8,349(1974).
10. C.-C. Sahm et al., Phys. Rev. C 34,2165 (1986).
11. R.J. Peterson and J.J. Hamill, Phys. Rev. C 22,2282(1980).
12. R. Wadsworth et al, J. Phys. G 9,1237 (1983).
13. A. Stuirbrink et al., Z. Phys. A 297,307 (1980).
14. B.M. Preedom, E. Newman and J.C. Hiebert, Phys. Rev. 166,1156(1968).
15. C.D. Kavaloski, J.S. Lilley, D.C. Shreve and N. Stein, Phys. Rev. 161,1107(1967).
16. M. Buenerd et al., Nucl. Phys. A424,313 (1984).
17. P. Roussel, N. Alamanos, F. Auger, J. Barrette, B. Berthier, B. Fernandez, L. Papineau, H. Doubre and W. Mittig, Saclay preprint 1987.

THE (^{6}LI,^{6}LI$^*\gamma$) COINCIDENCE TECHNIQUE FOR SPIN TRANSFER MEAUSREMENTS

N. Anantaraman, E. Adamides, S.M. Austin, D. Morrissey, C.A. Ogilvie, S. Robbins, R. Ronningen, and J.S. Winfield

The probe (^{6}Li,^{6}Li*3.56 MeV,γ) can in principle be used to selectively study the isovector excitation of states in nuclei involving spin transfer. One isolates the $\Delta S=1$, $\Delta T=1$ channel by measuring the outgoing ^{6}Li (1^+,T=0) and the gamma from the deexciting 0^+, T=1 3.56 MeV state.

As a test of this possibility, 35 MeV/nucleon ^{6}Li ions were inelastically scattered from several targets (carbon, ^{24}Mg and ^{90}Zr) and momentum analysed by the S320 spectrometer which was set at 3°. The elastically scattered ^{6}Li nuclei were blocked by a vertical post just in front of the focal plane detector. Gamma rays were detected in four 3"×3" BGO crystals located outside the scattering chamber of the S320. The total solid angle of the BGO's was 276 msr. These BGOs were calibrated with the γ-rays from Pu-Be and ^{60}Co sources, while the spectrometer was calibrated by scanning the elastic scattering peak across the focal plane.

During the experiment a coincidence was required between an S320 event and any of the BGOs. The data were reduced off-line by filtering out only those S320 events that corresponded to the detection of a ^{6}Li particle. The filtered events were further separated into those associated with the same RF pulse as the detected ^{6}Li (real coincidences), and those associated with subsequent pulses (random coincidences). The ratio of real to random coincidences was 2:1.

In order to identify the mutual excitation of the ^{6}Li* 3.56 MeV and known 1^+ states in the target nuclei one must gate on the γ-rays from deexcitation, then project the scattering spectrum from the S320 and examine the energy region of 3.56 MeV plus the known excitation energy of the target state.

Once filtered, the energy-calibrated BGO signals were corrected for the Doppler shift by calculating the velocity of the ^{6}Li detected by the S320. The random coincidences that are present in the real time peak will be falsely corrected since the velocity of their source is unknown. To approximately account for this, both the 'real' and the random filtered sets of events were Doppler-corrected by taking their source to be an outgoing ^{6}Li.

The corrected random BGO spectra are then subtracted from the corrected real BGO spectra. An example of the difference is shown in Fig. 1 for the ^{24}Mg target. A significant background surrounds the energy region of 3.56 MeV. The number of counts in this region is commensurate with the expected cross-section (estimated from the (^{6}Li,^{6}He) cross-section[1]) and the BGO detection efficiency, though it is difficult to identify a peak arising from the decay of ^{6}Li(3.56 MeV). When a gate is applied to this region , no strong enhancement of known 1^+ states of the target nuclei was observed in the S320 position spectra.

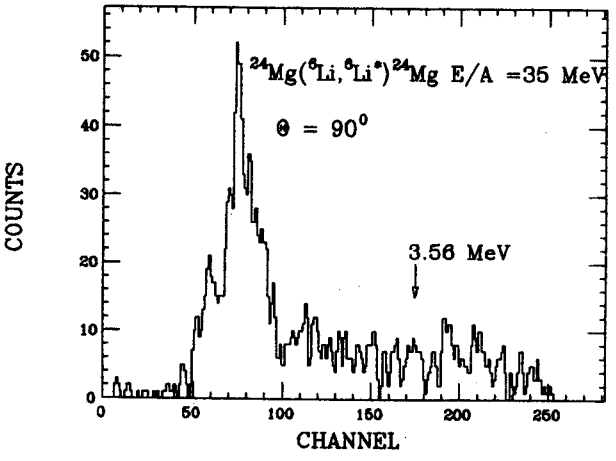

Fig. 1: An example of a BGO spectrum that has been corrected for the Doppler shift and random coincidences. The region near 3.56 MeV is indicated.

These problems probably stem from the high γ background present in the filtered spectra, making it difficult to correct for random coincidences, the generally low statistics and real to random rates. In future experiments detectors subtending a larger solid angle should be used and more shielding must be placed around extraneous sources of γ-rays, such as the beam dump. Other improvements could include higher resolution detectors surrounded by veto-shields to further improve the signal to background ratio.

References

1. N. Anantaraman et al., Phys. Rev. Lett. 57, 2375 (1986)

POLARIZATION, DYNAMICS AND NON-EQUILIBRIUM COMPLEX FRAGMENT EMISSION

M.B. Tsang, W.G. Lynch, R.M. Ronningen, Z. Chen, C.K. Gelbke, T. Nayak, J. Pochodzalla[a], F. Zhu, M. Tohyama, W. Trautmann[b], and W. Dünnweber[c]

To explore the relationship between reaction dynamics and fragment formation, we have measured the circular polarization of γ-rays associated with the emission of intermediate mass fragments for ^{14}N induced reactions on ^{154}Sm at E/A = 35 MeV. Metallic self-supporting ^{154}Sm targets of 4 mg/cm^2 areal density were bombarded with ^{14}N ions of 490 MeV incident energy. Two telescopes, each consisting of three Si detectors of 30μm, 50μm, and 2000μm thickness, were placed at the polar and azimuthal laboratory angles of θ=35°, φ=0° and θ=35°, φ=180° to detect intermediate mass fragments ($3 \leq Z \leq 11$) at angles much larger than the grazing angle. The circular polarization of coincident γ-rays emitted along the reaction normal was measured with two forward scattering polarimeters[1] positioned at θ=90°, φ=90° and θ=90°, φ=270°. The polarimeters had in-beam analyzing powers of 0.95±0.1%. In our sign convention, positive circular γ-ray polarizations correspond to negative deflection angles and vice versa.

The measured energy spectra of fragments with $3 \leq Z \leq 6$ and the circular polarizations of coincident γ-rays are shown in Fig. 1. The energy spectra exhibit nearly exponential slopes, indicating that contributions from projectile fragmentation are small. In contrast to the negligible polarizations expected for purely statistical fragment production mechanisms, positive polarizations are observed for all particles, indicating the importance of reaction dynamics. Such positive polarizations are consistent with fragment emission after deflection by the attractive nuclear mean field to negative emission angles. The polarizations increase monotonically with increasing fragment energy. The largest observed polarizations,

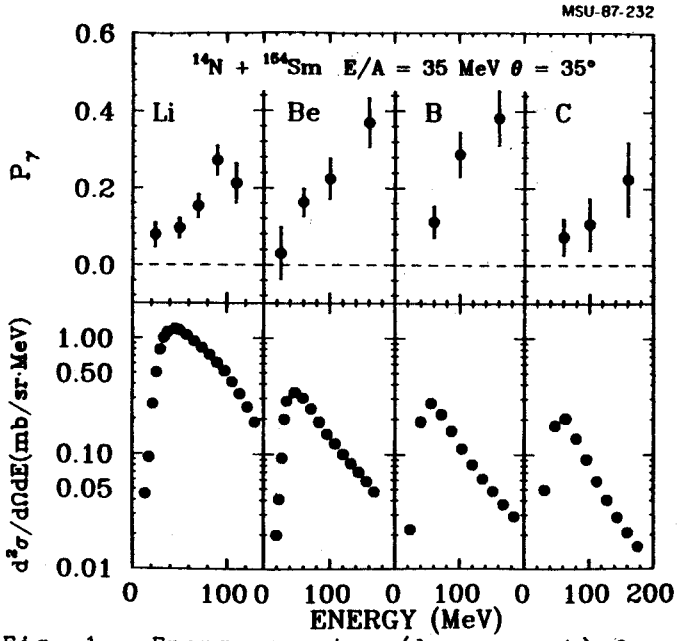

Fig. 1: Energy spectra (lower part) for intermediate mass fragments emitted at 35° in ^{14}N induced reactions on ^{154}Sm at E/A=35 MeV. The corresponding γ-ray circular polarizations (upper part) are shown as functions of the fragment kinetic energy.

P_γ=0.4, however, are considerably less than the maximum polarization, P_γ=0.7-0.8, for purely negative angle scattering when contributions from non-aligned spins and from non-stretched γ-ray transitions are taken into account.[2] The reduced polarizations for low energy fragments can partly be attributed to contributions from compound nuclear emission,[3] for which vanishing polarizations are expected. However, such processes make negligible contributions to the spectra at energies greater than 10·A MeV. Since intermediate mass fragments are preferentially emitted perpendicular to the total angular momentum,[4] the polarization of $P_\gamma \leq 0.4$ for E/A≥10 MeV implies that more than 20% of these intermediate mass fragments are emitted to positive angles.

Some insights can be gained by examining the mass dependence of the γ-ray polarizations. Figure 2a shows the circular polarizations measured[5] for non-equilibrium light particles at θ ≈ 30° as functions of the ejectile energy per nucleon. For fixed ejectile velocity, the polarizations are nearly proportional to the ejectile mass. Such a dependence is predicted by phase-space models, such as the coalescence model, in which the cross section for a fragment of mass A is proportional to the A^{th} power of the nucleonic phase space density.[6] The dashed, dot-dashed, and dotted lines in Fig. 2a are obtained by scaling the solid line, drawn here for α particles, to protons, deuterons, and tritons, respectively, according to the coalesence relationship. Except for fragment energies less than 16·A MeV, where Coulomb effects modify the coalescence relations,[6] the qualitative trends of the measured polarizations and therefore the relative proportions of positive and negative angle scattering are well reproduced.

Figure 2b shows the γ-ray polarizations for the heavier fragments, Z≥3, as functions of the ejectile energy per nucleon. Here, the solid line describes the polarizations for α particles as in Fig. 2a. Clearly the polarizations for the heavier fragments do not increase linearly with fragment mass as expected from the trends established by the light particle measurements. Coalescence model predictions for ^{9}Be and ^{12}C are indicated by the dashed and dash-dotted lines in the figure, respectively. The coalescence model overpredicts the mass dependence of the polarizations for the heavier fragments.

While the polarizations for the heavy fragments do not follow the trends established by the light particles, they are comparable to γ-ray polarizations for heavy fragments detected near the grazing angle in strongly damped reactions at much lower bombarding energies.[2,7] The properties of such fragments have been

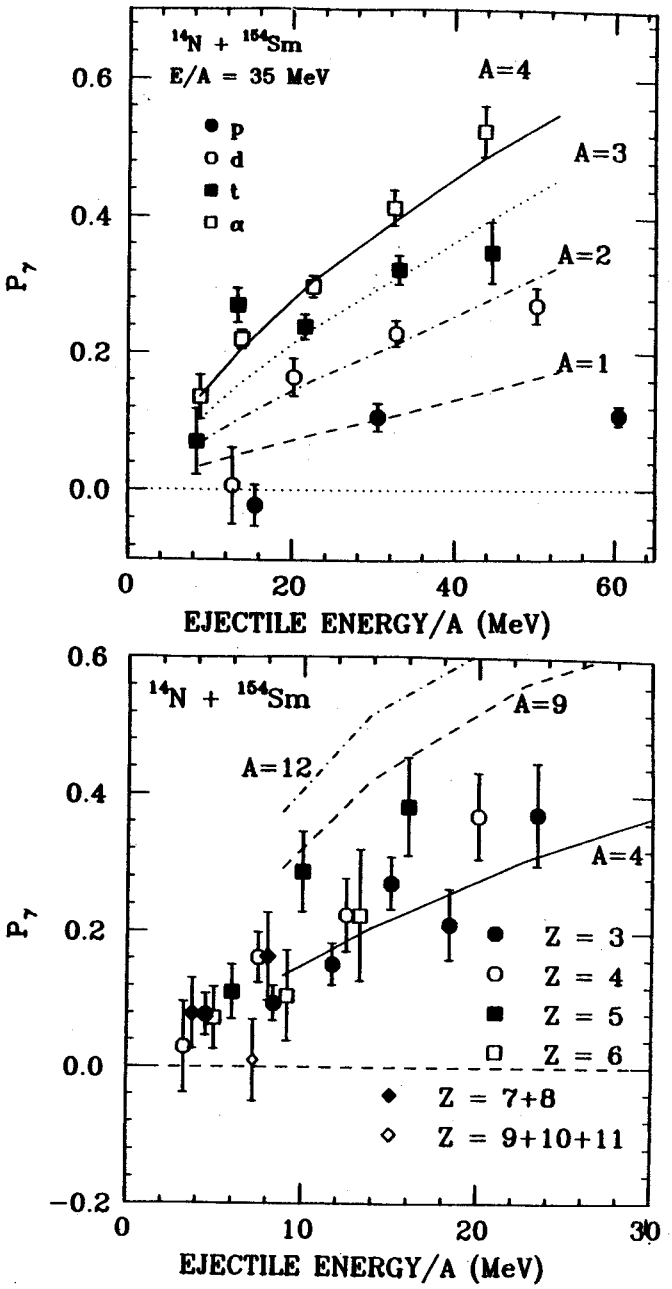

Fig. 2: a.) Polarizations for light particles emitted at 30° as functions of the ejectile energy per nucleon. The lines correspond to coalescence model calculations described in the text. b.) Polarizations for intermediate mass fragments emitted at 35° as functions of the ejectile energy per nucleon. The lines correspond to coalescence model calculations described in the text.

reproduced by trajectory calculations in which the observed fragment is assumed to be the projectile-like residue.[8,9] We have explored

this production-mechanism with the Boltzmann equation and have calculated the deflection function for projectile-like residues given in Table 1.[10,11] These calculations cannot reproduce the experimental polarizations. Agreement with the experimental polarizations might be obtained if the fragments were dispersed over a large angular range by statistical fluctuations.

Table 1: The deflection function (mean scattering angle), mean mass, mean energy per nucleon, and mean angular momentum per nucleon for projectile-like fragments calculated with the Boltzmann equation.

b (fm)	<A>	θ_{cl}	E/A(MeV)	<ℓ>/A
7.0	2.	-53°	6.	5.
7.5	7.	-27°	12.	6.
8.0	9.	-19°	15.	7.
9.0	12.	-2°	25.	9.
10.0	13.	6°	28.	10.

a. Institut für Kernphysik, Johann-Wolfgang-GSI, Darmstadt, W. Germany.
b. Goethe Universität, Frankfurt, West Germany.
c. Universität München, Garching, W. Germany.

References

1. W. Trautmann, Nucl. Instr. and Meth. 184, 449 (1981).
2. W. Trautmann, et al., Nucl. Phys. A422, 418 (1984).
3. M.A. McMahan, et al., Phys. Rev. Lett. 54, 1995 (1985).
4. D.J. Fields, et al., Phys. Rev. C34, 536 (1986).
5. M.B. Tsang, et al., Phys. Rev. Lett. 57, 559 (1986).
6. T.C. Awes, et al., Phys. Rev. C24, 89, (1981).
7. W. Dünnweber et al., Phys. Rev. Lett. 52, 1405 (1984).
8. W. Dünnweber and K.M. Hartmann, Phys. Lett. 80B, 23 (1978).
9. S.Y. Lee et al., Phys. Rev. C30, 887 (1984).
10. J. Aichelin and G. Bertsch, Phys. Rev. C31, 1730 (1985).
11. M.B. Tsang, et al., to be published.

OBSERVATION OF A NON-SPHERICAL PION SOURCE IN HEAVY-ION COLLISIONS*

Crowe/Rasmussen Collaboration (LBL)[a], including Wm. C. McHarris

In principle, pion interferometry can probe the space-time geometry of the interaction region in relativistic heavy-ion collisions. Since pions are created in the interaction region of the collision, a measurement of their source parameters tests the collision geometry of models, containing pion production and absorption, that yield parameters for nuclear equations of state.[1]

The interferometry method is based on the symmetry of the outgoing pionic wavefunction, resulting in intensity interference,[2,3] in which the probability for detecting a pair of pions having similar momenta is enhanced to an extent determined by the source geometry. Assuming the pion source can be described by a Gaussian space-time distribution, symmetric about the beam axis, the correlation function becomes[4]

$$C_2 = 1 + \lambda \exp[-(q_\perp^2 R_\perp^2 + q_\parallel^2 R_\parallel^2 + q_0^2 \tau^2)/2],$$

where the four-momenta, radius, and lifetime parameters have their usual meanings, and λ allows for correlations from effects other than Bose statistics[5] (unity in their absence).

Experimentally the correlation function is defined,

$$C_2 = A \frac{\frac{d^6\sigma}{dp_1^3\, dp_2^3}}{\frac{d^3\sigma}{dp_1^3}\,\frac{d^3\sigma}{dp_2^3}}$$

where A is a normalization constant. In principle, one measures $d^6\sigma/dp_1^3 dp_2^3$, the two-pion inclusive cross-section, and $d^3\sigma/dp^3$, the single-pion inclusive cross-section, fitting the resulting C_2 to the first equation to extract the parameters. In practice, only the two-pion inclusive cross-section is measured, and the denominator is determined by "event mixing," pairing pions from distinct events. Residual correlations are then removed by an iterative procedure.

Data were taken at the LBL Bevalac JANUS spectrometer,[6] with the beam consisting of 1.70-AGeV ^{56}Fe ions directed onto a ≈1-g/cm^2 of natural Fe or stainless steel. Pairs of pions were detected in the spectrometer near $\theta_{lab} = 0°$ and 45° with respect to the beam. Fig. 1 shows accepted single-pion Monte Carlo tracks on a rapidity vs $p_\perp$ plot.

Particle trajectories were identified by effective-edge track reconstruction and making

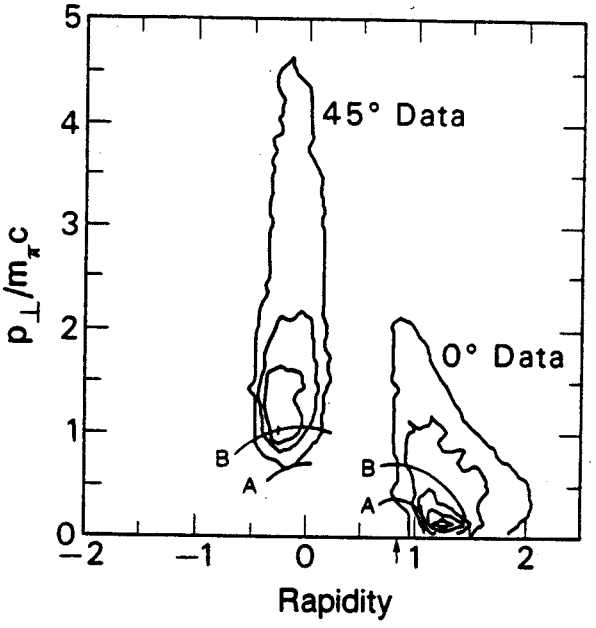

Fig. 1: Rapidity vs $p_\perp$ (in units of pion mass) contour plots for single-pion Monte Carlo tracks for 0° and 45°. The pions were weighted by an exponential distribution in the pion energy (cm). A denotes the lower momentum cut; B, the higher momentum cut. The arrow indicates the beam rapidity.

cuts on the TOF's and ADC's. The momenta were determined through a Chebyshev polynomial expansion in the MWPC wire numbers, the coefficients derived from a fit to simulated pion tracks. The data were corrected for the Coulomb interaction with a momentum-correction formula.[7] A Gamow correction compensated for the final-state Coulomb interaction between two pions.[6] (These corrections produced changes of up to three standard deviations.)

Momentum cuts were applied to the data as shown in Fig. 1 and Table I. The cut on the projectile-frame momentum for the 0° data, $|\vec{p}_{proj}|$>50 MeV/c, was made to remove pions with velocities near those of projectile fragments. Otherwise, a large Coulomb attraction would invalidate a separate pion-pion Coulomb correction. The cut on the cm-frame momentum for the 45° data, $|\vec{p}_{cm}|$>100 MeV/c, was imposed by the spectrometer acceptance. The more stringent cuts were made to study the dependence of source parameters on pion momentum. The corrected correlation functions were fitted to the first equation above, yielding the parameters plus a normalization constant for each data set. In Fig. 2 we show the correlation function for the 45° data with the $|\vec{p}_{cm}|$>100 MeV/c cut projected onto the $q_\perp$ axis, in order to show the quality of its Gaussian fit.

Our measured source parameters are listed in Table I with 1σ statistical uncertainties and, where calculated, systematic uncertainties. Systematic errors were examined by generating Monte Carlo data for the 0° $|\vec{p}_{proj}|$>50 MeV/c case, and analyzing these data using the same programs used to analyze the experimental data. Also, the experimental data were tested for track-finding biases by refitting them with the requirement that $q_\perp, q_{||}$>10 MeV/c; this cut removes the 10% which have the smallest spatial separations and which are hardest to resolve. The two bias estimates give good agreement. For the 45° data (except for λ), systematic uncertainties are not shown, as they are

	45° $\|\vec{p}_{cm}\|$ > 100 MeV/c		45° $\|\vec{p}_{cm}\|$ > 150 MeV/c	
	Experiment	CASCADE	Experiment	CASCADE
$R_\perp$(fm)	4.0 ± 0.5	4.2 ± 0.3	4.3 ± 0.6	4.2 ± 0.2
$R_{\|\|}$(fm)	$1.5^{+0.5}_{-0.9}$	3.0 ± 0.2	$1.5^{+0.5}_{-1.0}$	2.9 ± 0.2
τ(fm/c)	$1.7^{+1.5}_{-1.7}$	3.3 ± 0.6	$0.1^{+2.6}_{-0.1}$	3.2 ± 0.6
λ	$0.66 \pm 0.05 \pm 0.1$	1.00 ± 0.02	$0.58 \pm 0.06 \pm 0.1$	0.98 ± 0.02
χ^2/ NDF	381/403	1099/1082	362/345	1112/1039
Events	8300	-	6900	-

	0° $\|\vec{p}_{proj}\|$ > 50 MeV/c		0° $\|\vec{p}_{proj}\|$ > 100 MeV/c	
	Experiment	CASCADE	Experiment	CASCADE
$R_\perp$(fm)	$4.8 \pm 0.2 \pm 0.1$	4.0 ± 0.1	$4.7 \pm 0.3 \pm 0.2$	4.4 ± 0.1
$R_{\|\|}$(fm)	$2.7 \pm 0.3 \pm 0.3$	3.3 ± 0.1	$2.1 \pm 0.5 \pm 0.8$	2.3 ± 0.1
τ(fm/c)	$2.7 \pm 0.6 \pm 0.4$	4.3 ± 0.2	$3.5 \pm 0.6 \pm 0.3$	4.4 ± 0.2
λ	$0.88 \pm 0.03 \pm 0.1$	1.00 ± 0.02	$0.75 \pm 0.05 \pm 0.1$	0.98 ± 0.02
χ^2/ NDF	939/729	1031/1061	470/395	374/376
Events	33,000	-	10,000	-

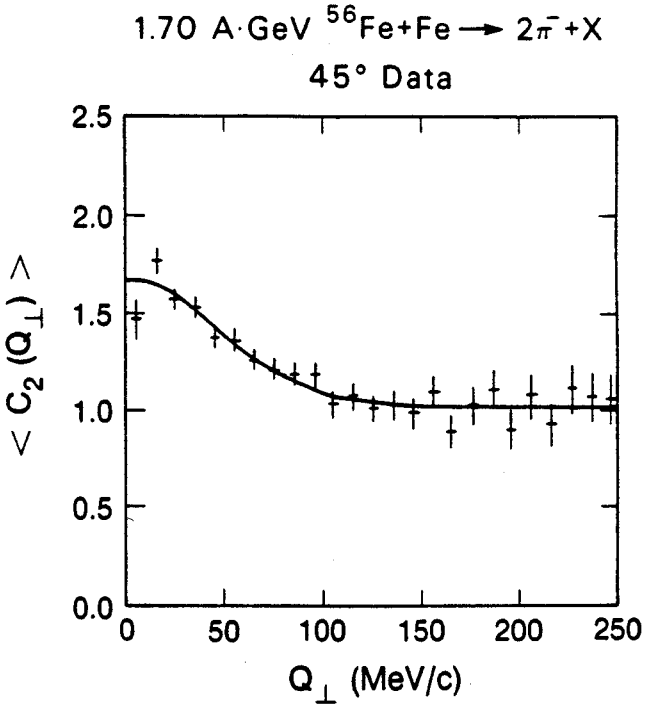

Fig. 2 Projection of the experimental correlation function and its Gaussian fit onto the $q_\perp$ axis for the 45° data. Only statistical errors are indicated.

dominated by the statistical uncertainties. Spectrometer resolution has less than a 1% effect on the correlation function.

Also listed in Table I are source parameters derived from intranuclear cascade calculations.[8] Our procedure was: Cugnon's CASCADE code[9] was run to produce a set of pions that survive to the end of the calculation, recording their momenta and space-time creation point. The experimental acceptance criteria were then imposed. Then randomly-selected pion pairs from each event were weighted by $|\Psi^s|^2$, the symmetrized plane-wavefunction, to impose Bose statistics. Finally, the two-pion correlation function was formed and parameters extracted.

For both acceptance angles and all momentum cuts, $R_\perp / R_{||}$ is significantly greater than 1. A spherical source shape was measured with a 4π acceptance[10] for 1.5-AGeV ^{40}Ar + KCl and for 1.8-AGeV ^{40}Ar + Pb. Using different analysis techniques, prolate source shapes have been measured[11] for pp and $p\bar{p}$ collisions, and oblate shapes[12] for p + Xe and $\bar{p}$ + Xe. The λ parameters were all significantly less than 1. We do not observe a significant dependence of the source size on the pion momentum for either acceptance angle.

Although CASCADE predicts an oblate source, for 45° $R_{||}$ is overpredicted (underpredicting the oblateness), and for 0° $R_\perp$ is underpredicted and $R_{||}$ overpredicted. For 45° τ is predicted reasonably well, although uncertainties are large because of the small sample size.

Possible causes of the excess oblateness, small source size, and small λ relative to CASCADE are: Transverse collective flow of nuclear matter[13] could reduce $R_{||}$ and increase $R_\perp$ with respect to CASCADE. Simple pion shadowing effects in excess of CASCADE could push the pion source toward the strong absorption limit. An expanding source can be important for the correlation function.[14] Dynamical correlations from other effects, such as the decay of Δ resonances, could cause the small λ. We will continue trying to analyze these phenomena theoretically.

---

a. A.D. Chacon, J.A. Bistirlich, R.R. Bossingham, H.R. Bowman, C.W. Clawson, K.M. Crowe, T.J. Humanic, J.M. Kurck, C.A. Meyer, J.O. Rasmussen (LBL); O. Hashimoto (Tokyo); Wm. C. McHarris (MSU); J.P. Sullivan (TAMU); W.A. Zajc (Pa.)

* This is a condensation of LBL-18709 (1987), which has been accepted for publication in Phys. Rev. Lett.

References

1. R. Stock et al., Phys. Rev. Lett. 49, 1236 (1982).
2. R. Hanbury-Brown and R.Q. Twiss, Nature 177, 27 (1956); 178, 1046 (1956).
3. G. Goldhaber et al., Phys. Rev. 120, 300 (1960); G. Kopylov, Phys. Lett. 50B, 472 (1974).
4. F.B. Yano and S.E. Koonin, Phys. Lett. 78B, 556 (1978).
5. M. Gyulassy, Phys. Rev. Lett. 48, 454 (1982).
6. W.A. Zajc et al., Phys. Rev. C 29, 2173 (1984); A.D. Chacon et al., to be submitted to Phys. Rev. C.
7. M. Gyulassy and S.K. Kauffmann, Nucl. Phys. A362, 503 (1981).
8. T.J. Humanic, Phys. Rev. C 34, 191 (1986).
9. J. Cugnon, D. Kinet, and J. Vandermeulen, Nucl. Phys. A379, 553 (1982).
10. D. Beavis et al., Phys. Rev. C 27, 910 (1983); 34, 757 (1986).
11. T. Åkesson et al., Phys. Lett. B 187, (1987).
12. C. De Marzo et al., Phys. Rev. D 29, 363 (1984).
13. H. Kruse, B. Jacak, and H. Stöcker, Phys. Rev. Lett. 54, 289 (1985); J. Molitoris et al., Phys. Rev. C 33, 867 (1986).
14. S. Pratt, Phys. Rev. Lett. 53, 1219 (1984).

DECAY OF NEUTRON UNSTABLE STATES FROM HEAVY ION COLLISIONS

L. Heilbronn, F. Deak[a], A. Galonsky, A. Kiss[a], B. Remington[b], H.R. Schelin[c], Z. Seres[d], and X. Yang

Recent measurements have determined the populations of particle unbound states for light nuclei ($6 \leq A \leq 15$) created in heavy ion collisions[1-3]. These populations were then fitted with a Boltzmann distribution to obtain a temperature. The fitted temperatures, which ranged from 1 MeV to 5 MeV, were obtained by fitting only two states (or groups of states). A more convincing test of the validity of using a Boltzmann population distribution to obtain a temperature would be to fit three states to a single temperature. In order to measure three separate groups of states, resolution must be improved. Also, a detailed knowledge of branching ratios between competing modes of decay must be obtained.

An experiment was conducted that measured the populations of neutron unbound states in fragments created by bombarding ^{nat}Ag with 35 MeV/nucleon ^{14}N. Neutron velocities were determined by a time of flight technique that used the coincident fragment signal as the start of the timing circuit and the neutron signal as the stop. Fragment energies and isotope identification were determined by a ΔE-E silicon telescope. By using a colinear geometry between the fragment detectors and neutron detectors and a long flight path (3.5-4.5 meters) to the neutron detectors, resolution was good enough to separate 3 groups of states of ^{13}C which decay by neutron emission.

Figure 1 shows a relative velocity plot for neutrons in coincidence with ^{12}C fragments at 15°. For each state of ^{13}C that decays into ^{12}C + n, two peaks appear on the plot (provided the relative velocity between fragment and neutron is greater than ~0.3 cm/ns), and these peaks should have the same absolute value of relative velocity. A negative value of relative velocity

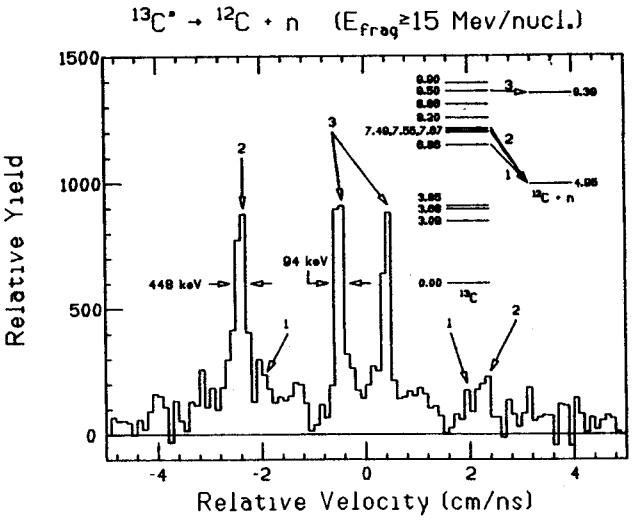

Fig. 1: Relative velocity spectrum for ^{12}C + n at 15° in the lab. Bin sizes are 0.1 cm/ns. An energy level diagram for ^{13}C is shown in the upper right hand corner, along with some decays to the ^{12}C + n system. The corresponding peaks are indicated in the spectrum.

indicates that the neutron velocity as measured in the lab (v_n) is greater than the fragment velocity (v_f), and a positive value indicates $v_f > v_n$. These two peaks have different heights with respect to each other since the geometrical efficiency for collecting neutrons differs between forward emission of a neutron ($v_n > v_f$) and backward emission ($v_n < v_f$).

Also shown in Fig. 1 is an energy level diagram for ^{13}C. The small peaks at ±2.0 cm/ns come from the decay of the 6.864 MeV state of ^{13}C ($J^\pi = 5/2^+$) to the ground state of ^{12}C + n, which lies 4.946 MeV above the ground state of ^{13}C. The peaks at ±2.4 cm/ns come from the decay of a group of three states of ^{13}C at 7.492 MeV ($J^\pi = 7/2^+$), 7.547 MeV ($J^\pi = 5/2^-$), and 7.686 MeV ($J^\pi = 3/2^+$). As one goes higher in energy in ^{13}C, the geometrical efficiency becomes too low

to reliably measure the decay of a state. However, at 9.500 MeV ($J^{\pi}=9/2^{+}$), decay into the first excited state of ^{12}C (9.385 MeV above the ground state of ^{13}C) is possible. The peaks at ±0.5 cm/ns are from this decay. The fwhm of these peaks is 0.2 cm/ns, which corresponds to an energy resolution of 94 keV. Although the peaks at ±2.4 cm/ns also have a fwhm of 0.2 cm/ns, this corresponds to an energy resolution of 448 keV, which explains why we are unable to separate the states within that group.

A relative velocity plot for ^{11}B + n at 31° is shown in Fig. 2. The spectrum is dominated by a single peak centered at 0.0 cm/ns, which is due to the decay of the 3.388 MeV ($J^{\pi}=3^{-}$) state of ^{12}B. Since the relative velocity of this decay is so low (0.2 cm/ns), the geometrical efficiency for detecting it is almost 100%. One should note that our resolution is almost good

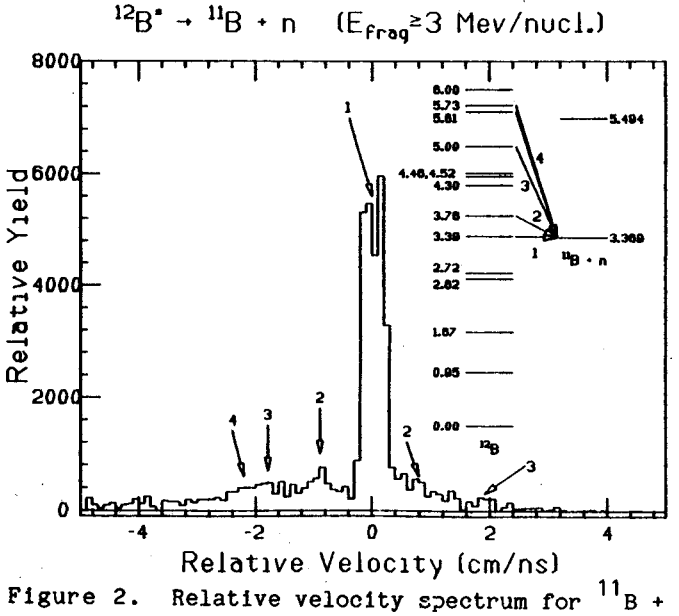

Figure 2. Relative velocity spectrum for ^{11}B + n at 31° in the lab. Bin sizes are 0.1 cm/ns. An energy level diagram for ^{12}B is shown in the upper right hand corner, along with some decays to the ^{11}B + n system. The locations of the corresponding relative velocities are indicated in the spectrum.

enough to separate forward and backward emission of the neutron, even though the decay energy is only 19 keV. The locations of neutron decays from other states of ^{12}B are shown in Fig. 2. Of these decays, only the #2 peaks appear to be statistically significant.

The next step in the analysis will be to calculate the background found in our relative velocity plots. One method for determining this background can be found in reference 4. Once this background has been incorporated into our relative velocity plots, attempts will be made to fit these peaks according to a Boltzmann population distribution.

---

a. Eötvös Lorand University, Budapest, Hungary.
b. Lawrence Livermore National Laboratory.
c. Centro Tecnico Aerospacial and FAPESP, Brazil.
d. Central Research Lab. for Physics, Budapest, Hungary.

References

1. A. Galonsky, G. Caskey, L. Heilbronn, B. Remington, H. Schelin, F. Deak, A. Kiss, Z. Seres, J. Kasagi, Phys. Lett. B 197 (1987) 511.
2. J. Pochodzalla, W.A. Friedman, C.K. Gelbke, W.G. Lynch, M. Maier, D. Ardouin, H. Delagrange, H. Doubre, C. Gregoire, A. Kyanowski, W. Mittig, A. Peghaire, J. Peter, F. Saint-Laurent, Y.P. Viyogi, B. Zwieglinski, G. Bizard, F. Lefebvres, B. Tamain, J. Quebert, Phys. Rev. Lett. 55 (1985) 177.
3. J. Pochodzalla, W.A. Friedman, C.K. Gelbke, W.G. Lynch, M. Maier, D. Ardouin, H. Delagrange, H. Doubre, C. Gregoire, A. Kyanowski, W. Mittig, A. Peghaire, J. Peter, F. Saint-Laurent, Y.P. Viyogi, B. Zwieglinski, G. Bizard, F. Lefebvres, B. Tamain, J. Quebert, Phys. Lett. 161B (1985) 275.
4. C. Bloch, W. Benenson, A.I. Galonsky, E. Kashy, J. Heltsley, L. Heilbronn, M. Lowe, B. Remington, D.J. Morrissey, J. Kasagi, Annual Report, Cyclotron Laboratory, Michigan State University (1986) 25.

POPULATION DISTRIBUTIONS OF NUCLEAR STATES AT LOW BOMBARDING ENERGIES

J.H. Lee, W. Benenson, R.A. Blue, Y.M. Chen, E. Kashy,
M.F. Mohar, R.M. Ronningen, C. Bloch[a], D.J. Morrissey

In low energy heavy-ion collisions, from the neighborhood of the Coulomb barrier up to around 10 MeV/nucleon, complete momentum transfer to give a compound nucleus is a dominant entrance channel. In this process, light fragments ($Z \geq 3$) and intermediate fragments are produced mainly through the asymmetric or symmetric binary fission of the highly excited nuclear compound. The residual heavy fragments are very slow moving sources, and the population distribution in this regime depends heavily on the rotational motion as well as the excitation energy. The concept of the nuclear temperature in this region of the bombarding energy is rather well defined, but as the beam energy increases slightly over around E/A = 10 MeV, the role of the complete fusion process in the entrance channel becomes less dominant while an increasing dominance of deep-inelastic scattering or incomplete fusion processes take place. The nuclear temperature deduced from the population distribution in this energy region does not, in general, seem to reflect the nuclear reaction mechanism effectively because the mechanism of the fragment-forming processes is not well defined.

Reverse kinematics were employed in the present experiment as a continuation of the new type of temperature measurement experiments[1-4]. In this new method, it is assumed that the population distribution of the nuclear states in the heavy ion collision is given by a Boltzmann distribution, and a nuclear temperature can be obtained from the gamma-ray intensity observed in the particle-gamma coincidences runs. The fraction of the nuclei that emit the specific gamma-rays by a transition from an excited state to another lower state can be formulated from Boltzmann factor, and, by comparing this with the observed gamma fraction in the experiment, the nuclear temperature can be deduced using a simple program. Temperature measurements of this type can be broadly divided into two parts according to the bombarding energy: E/A > 10MeV[1,2,4] and E/A < 10MeV[3]. The temperatures derived from the excitations of the light fragments (^{7}Li, ^{7}Be, and ^{10}B) at E/A > 10MeV were significantly lower than those expected from Fermi Gas Model and the slope parameters of the particle inclusive spectra while at E/A < 10MeV the temperatures indicated a rough agreement with those predicted. This may indicate that, at the high bombarding energy (E/A > 10MeV), the preferential feeding to especially the ground state[1,2] from the unbound states of the larger nuclei was important in populating the states of the nucleus, hence lowering the observed temperature. In the present experiment, we performed a measurement of the population distribution of the nuclear states, hence the nuclear temperature, at the bombarding energies around E/A = 10MeV. The use of reverse kinematics avoided the detection of projectile-like light fragments and direct reaction fragments. In addition, we extended the particle-gamma coincidence runs to the much heavier fragments.

Beams of 320MeV $^{40}Ar^{+6}$ and 400 and 480MeV $^{40}Ar^{+7}$ ions were provided by the K500 cyclotron. The target was a self-supporting foil of ^{12}C, 490 $\mu m/cm^2$ thick. Charged particles were detected in three element silicon surface barrier telescopes each with a 50 mm^2 area. The three elements (Δ_1E - Δ_2E - E) of each particle telescope were 30 μm, 75μm, and 1000 μm thick, respectively. A two dimensional particle identification spectra with $\Delta_1E+\Delta_2E$ vs E gave excellent identification of the fragments up to

^{23}Na. In addition, a combination of $\Delta_1 E$ vs $\Delta_2 E$ provided identification for the heavy fragments from Z=16 to Z=20. However, because of the narrow energy range in the $\Delta_2 E$ element compared to the energy loss of the heavy fragments in it, the useful statistics at E/A=10MeV and 12MeV were limited. A set of eight NaI(Tl) scintillation detectors, 7.62cm x 7.62cm right cylinders, and a pair of Ge counters, 4.71cm x 4.36cm cylinders, were used to detect gamma-rays in coincidence with the particles.

The particle inclusive spectra obtained for each of the light fragments and the intermediate fragments showed the change from the Maxwellian shape for the very light fragments to the Gaussian-like shape for the heavy fragments as predicted in Ref. 5. The slope parameters in the energy spectra transformed into the center-of-mass frame were roughly estimated to be 2.7MeV-3.7MeV at E/A=8MeV, 3.4MeV-4.2MeV at E/A=10MeV, and 3.5MeV-4.5MeV at E/A=12MeV, using a Boltzmann-Maxwell function. However, these were rather sensitive to the magnitude of the Coulomb correction. The average temperatures calculated from the Fermi Gas Model with consideration of the rotational energy were $\langle \kappa T \rangle$= 2.76MeV, 3.10MeV, and 3.46MeV for E/A= 8MeV, 10MeV, and 12MeV, respectively, and these were close to the slope parameters at each beam energy. This rough agreement between the slope parameter in the particle inclusive spectra and the calculated temperature from Fermi Gas Model suggested an assumption that the nuclear temperature in the present reaction system can be characterized by Fermi Gas Model. When the deduced temperature is around an order of one MeV, it is very sensitive to the variation of the statistics in the gamma fraction, and it depends on the structure of the excited states. We tried a comparison of the gamma fraction that was calculated with the temperature from Fermi Gas Model with that from the observed value as well.

Fig. 1 shows the result of the deduced temperatures for ^{7}Li, ^{7}Be, and ^{10}B in terms of the beam energy per nucleon. The solid line in Fig. 1 is the variation of the temperature calculated from Fermi Gas Model before subtracting the rotational energy and the dotted line is that after subtracting the average rotational energy which was calculated by means of a simple kinematic consideration. In this simple calculation, the maximum angular momenta were 50 hbar, 56 hbar, and 61 hbar at E/A=8MeV, 10MeV, and 12MeV, respectively, while Ref. 6 predicts that the critical angular momentum for ^{52}Cr will be 52 hbar. The temperature variation in Fig. 1 agrees with the Ref. 3, while at E/A=12MeV the temperatures differ from one fragments type to another. The gamma fractions, hence the temperatures, of ^{7}Li and ^{7}Be at E/A=12MeV were significantly lower than expected.

Table 1 shows a comparison of the calculated gamma fractions with the observed values for ^{18}O, ^{19}F, ^{20}Ne, ^{21}Ne, and ^{22}Ne. The statistics were not sufficient to be able to

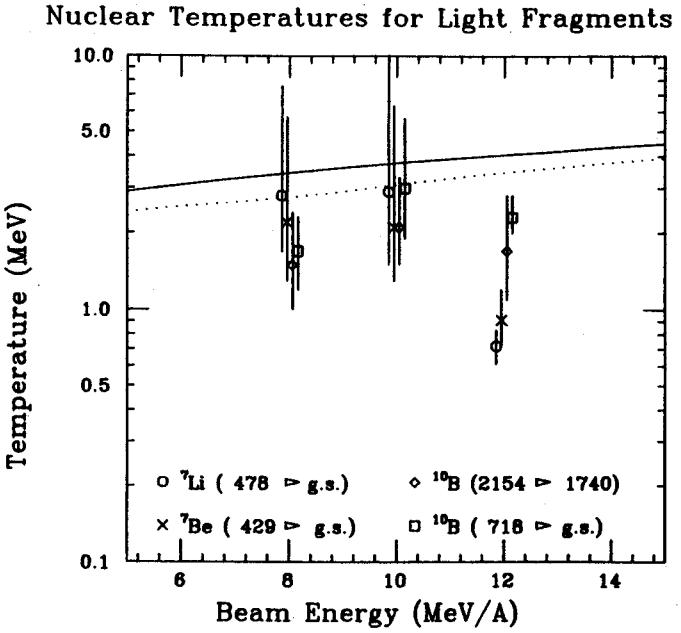

Fig. 1: Temperature variation of the light fragments. The four data points at each beam energy are separated to avoid folding one to another. The curves are explained in the text.

extract the temperatures in this mass region. However, an attempt was made, and the result was the widely ranged temperatures which are shown in Table 1. The contamination of the E_γ=1937KeV level into E_γ=1982KeV was taken account.

Table 1

Deduced population distribution

E/A[a]	Isotope	E_γ[b]	f_C[c]	f	κT[a]
8	^{18}O	1982	1.003	0.865(221)	$1.5^{+\infty}_{-0.4}$
	^{19}F	1236	0.225	0.256(52)	$1.9<\kappa T<\infty$
	^{20}Ne	1630	0.874	0.772(131)	$1.7^{+2.3}_{-0.4}$
	^{21}Ne	350	0.744	0.666(71)	$1.4^{+1.1}_{-0.4}$
	^{22}Ne	1270	0.908	0.750(162)	$1.2^{+1.8}_{-0.3}$
10	^{18}O	1982	1.013	0.727(243)	$1.2^{+1.0}_{-0.3}$
	^{19}F	1236	0.230	0.178(48)	$1.4^{+1.4}_{-0.4}$
	^{20}Ne	1630	0.886	0.488(98)	$0.91^{+0.18}_{-0.14}$
	^{21}Ne	350	0.749	0.549(61)	$0.78^{+0.24}_{-0.18}$
	^{22}Ne	1270	0.914	0.541(107)	$0.79^{+0.18}_{-0.14}$
12	^{18}O	1982	1.021	0.740(180)	$1.2^{+0.6}_{-0.2}$
	^{19}F	1236	0.233	0.243(47)	$5.6^{+\infty}_{-3.9}$
	^{20}Ne	1630	0.895	0.466(55)	$0.87^{+0.09}_{-0.08}$
	^{21}Ne	350	0.754	0.561(19)	0.82±0.07
	^{22}Ne	1270	0.919	0.726(53)	1.2±0.1

a. Units in MeV

b. Units in KeV

c. Calculated gamma fraction. See the text.

As a conclusion, in the case of the light fragments and the intermediate fragments, the population distributions are consistent with thermal equilibrium at E/A=8MeV, but apparently not at E/A=12MeV, while the inconsistency at E/A=10MeV resembles the latter rather than the former.

The coincidence gamma-ray spectra with the heavy fragments at E/A=8MeV were obtained with the Ge counters. The gamma-ray peaks were identified by means of both the CASCADE code[7] for the simulated residual cross sections and the calculated gamma-intensities with the known level and gamma-branching ratio information. A Boltzmann distribution with the temperature κT=2.76MeV was assumed in the calculation of the gamma-ray intensities in order to see whether the population distribution of the nuclear states in the heavy fragments resembles that in the light fragments. The result of ^{42}Ca is given in Table 2. The calculated gamma-ray intensities were normalized to E_γ=145KeV [6553(9^-)→6408(8^-)]. The result in table 2 shows that the gamma-ray decay along the yrast line was much stronger than that between the low spin states, and this indicates the important role of the rotational energy in heavy fragment population. One noticeable fact in Table 2 is that the gamma intensity of the low-lying transitions was much lower than the calculated value, even after considering the long-lived state (3190KeV), while that of the high-lying state transition was much larger than the predicted. Neither increasing nor decreasing the temperature in the calculation made the discrepancy much narrower. Hence the Boltzmann distribution was obviously not an important factor in populating the states of the heavy fragments and another model calculation is needed badly for this regime. A comparison of the experimentally observed data from many other heavy fragments including ^{42}Ca with the results from CASCADE code is being carried out currently, and the result will be published soon.

Table 2

Gamma intensity of ^{42}Ca (E/A=8MeV)

E_γ(KeV)	Decay	I_γ(dedu.)	I_γ(calc.)
928	8296→7368($11^-\rightarrow 10^-$)		
+916	6408→5492($8^-\rightarrow 6^-$)	806±185	1180
+909	4099→3190($5^-\rightarrow 6^+$)		
382	7750→7368($11^-\rightarrow 10^-$)	167± 39	86
815	7368→6553($10^-\rightarrow 9^-$)	548± 90	364
810	6553→5743($9^-\rightarrow 7^-$)	447± 90	447
145	6553→6408($9^-\rightarrow 8^-$)	174± 12	174
1644	5743→4099($7^-\rightarrow 5^-$)	483±231	399
439[a]	3190→2751($6^+\rightarrow 4^+$)	632± 68	3587
1227	2751→1524($4^+\rightarrow 2^+$)	1465±217	5488
1524	1524→ 0($2^+\rightarrow 0^+$)	1608±142	8859
1462	4715→3253($6^+\rightarrow 4^+$)	378±156	361
1729	3253→1524($4^+\rightarrow 2^+$)	502±209	594

a. $\tau_{1/2}$(3190KeV) = 5.4ns

a. Present address, Indiana University Cyclotron Facility, Bloomington, IN.

References

1. D.J. Morrissey, W. Benenson, E. Kashy, B. Sherrill, A.D. Panagiotou, R.A. Blue, R.M. Ronningen, J. van der Plicht, and H. Utsunomiya, Phys. Lett. 148B, 423 (1984).
2. D.J. Morrissey, W. Benenson, E. Kashy, C. Bloch, M. Lowe, R.A. Blue, R.M. Ronningen, B. Sherrill, H. Utsunomiya, and I. Kelson, Phys. Rev. C 32, 877 (1985).
3. D.J. Morrissey, C. Bloch, W. Benenson, E. Kashy, R.A. Blue, R.M. Ronningen, and R. Aryaeineyad, Phys. Rev. C 34, 761 (1986).
4. C. Bloch, W. Benenson, E. Kashy, D.J. Morrissey, R.A. Blue, R.M. Ronningen, and H. Utsunomiya, Phys. Rev. C 34, 850 (1986).
5. Luciano G. Moretto, Nucl. Phys. A247, 211 (1975).
6. S. Cohen, F. Plasil, and W.J. Swiatecki, Ann. Phys. (N.Y.) 82, 557 (1974).
7. F. Puhlhofer, Nucl. Phys. A280, 267 (1977).

SMALL RELATIVE MOMENTUM CORRELATIONS BETWEEN LIGHT AND HEAVY EJECTILES IN $^{14}N+^{nat}Ag$ REACTIONS AT 35 MEV/NUCLEON

Tetsuya Murakami, T.K. Nayak, W.G. Lynch, K. Swartz, D.J. Fields, C.K. Gelbke, Y.D. Kim, J. Pochodzalla, M.B. Tsang, F.Zhu, and K. Kwiatkowski[a]

Recently a new method based on the relative population of states has been employed to determine the "emission temperature" T_{em} in nuclear collisions, i.e. the temperature at the time when the particles leave the thermally equilibrated nuclear subsystem.[1-7] According to the statistical model, the ratio of populations, N_1/N_2, of two narrow excited states of a certain fragment is given approximately by

$$N_1/N_2 = (2J_1+1)/(2J_2+1)\ \exp(-\Delta E/T_{em}). \quad (1)$$

Here $\Delta E=E_1-E_2$ and J_i and E_i are the spin and excitation energy, respectively, of the i^{th} state of the fragment. If this is a reasonable approximation and the feeding to those excited states of interest from the sequential decay of heavier particle unstable nuclei is not significant, one may determine T_{em} from the populations of only two states of a given fragment. Such a simple approximation, however, does not allow one to test the internal consistency of this approach. For a detailed test, the relative populations of many (>>2) states of a given fragment should be examined, requiring the study of fragments which have many well resolved excited states.

In order to investigate the validity of this approximation, we have performed an experiment using a newly developed high resolution hodoscope[8], which can resolve the populations of many particle unstable states of light heavy nuclei ($10 \leq A \leq 16$) emitted in energetic nuclear reactions.

The experiment was carried with a ^{14}N beam of E/A=35 MeV/nucleon from the K500 cyclotron. A natural silver target of approximately 0.5 mg/cm^2 thickness was used. The size of the beam spot on target was about 3×3 mm^2. Light particles ($Z \leq 2$) and heavy fragments ($Z \geq 3$) were measured by a close-packed tetragonal array of 13 ΔE-ΔE-E telescopes; nine of them (LP-telescopes) consisting of a 200 μm silicon surface barrier detector, a 5 mm Si(Li) detector, and a 10 cm-thick NaI(Tl) detector, and the other four (HF-telescopes) consisting of 75 μm and 100 μm silicon surface barrier detectors and a 5 mm Si(Li) detector. Position information was provided by 13 pairs of X-Y single wire gas proportional counters attached just in front of each telescope. Details about this position sensitive heavy fragment hodoscope are given elsewhere.[8] The center of the hodoscope was set at laboratory angle of 38.4°. The angular separation between nearest neighbour telescopes was $\Delta\theta$=8.0°; the one between farthest neighbours was 32.0°. The solid angles of LP- and HF-telescopes were approximately 4.5 msr and 5.7 msr, respectively. Using this position sensitive hodoscope we achieved an angular resolution of better than 0.2° and a decay energy resolution of about 150 keV.

We present the data taken with the hodoscope in terms of the correlation function $R(E_{rel})$, defined for a particle pair (1,2) by

$$Y_{1,2}(\vec{p}_1,\vec{p}_2)=CY_1(\vec{p}_1)Y_2(\vec{p}_2)[1+R(E_{rel})] \quad (2)$$

where $Y_{1,2}$ denotes the coincidence yield, Y_1 and Y_2 the singles yields. The laboratory momenta of particles 1 and 2 are $\vec{p}_1$ and $\vec{p}_2$, respectively and E_{rel} is the kinetic energy of relative motion. The normalization constant C is determined by the requirement that $R(E_{rel})=0$ at large relative energies.

A sample correlation function is shown in Fig. 1. In this measured p-^{13}C correlation function distinct structures were observed at E_x=7.97, 8.49, 8.96, 9.39, 10.08, 10.43, and 10.81 MeV, which correspond to excited states with J ≥ 2; the excited states with J = 0 are not strongly populated. In order to obtain the coincidence yield, $Y_{^{14}N}$, resulting from the decay of excited ^{14}N nuclei we subtracted the background shown by the solid curve in Fig. 1, due to coninicident ^{13}C and protons which do not proceed through a particle unstable excited state in ^{14}N. The result of background subtraction is shown in Fig. 2.

The yield $Y_{^{14}N}$ is related to the energy spectrum, dn(E)/dE, in the ^{14}N center-of-mass frame by the equation

$$Y_{^{14}N}(E^*) = \int \varepsilon(E^*,E)\,\frac{dn(E)}{dE}\,dE. \qquad (3)$$

Here, ε(E*,E) is the efficiency function for the position sensitive hodoscope to detect p-^{13}C pairs with an actual relative energy E; E* denotes the measured excitation energy.

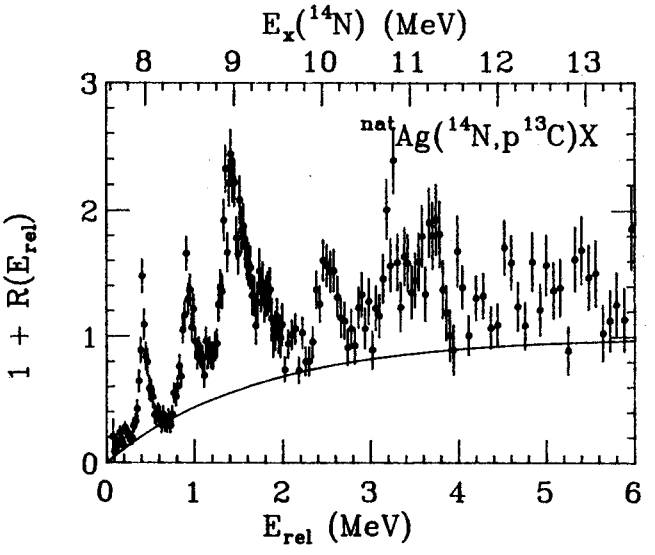

Fig. 1 Correlation function for coincident protons and ^{13}C particles for ^{14}N-induced reactions on ^{nat}Ag at E/A = 35 MeV. The curve is an estimated background.

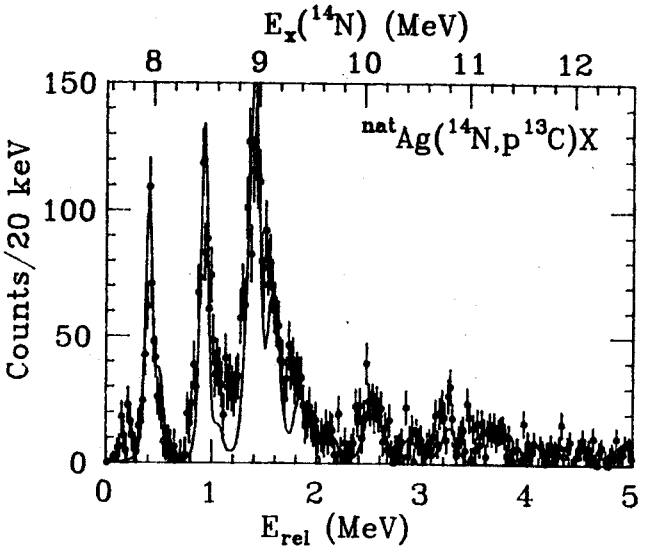

Fig. 2 Energy spectrum resulting from the decay of particle-unbound states in ^{14}N. The curve corresponds to a thermal distribution with T_{em} = 5 MeV in Eq. (3), taking the response of the hodoscope into account.

The efficiency function for our hodoscope was calculated by using the precise geometry, the energy thresholds for proton and ^{13}C, and the detector energy and position resolutions that were determined during the experiment.

Assuming an excitation energy spectrum dn/dE for thermally emitted ^{14}N nuclei of the form

$$\frac{dn(E)}{dE} = N \sum_i \left[\frac{(2J_i+1)\,\Gamma_i/2\pi}{(E-E_i)^2 + \Gamma_i^2/4}\,\frac{\Gamma_{p,i}}{\Gamma_i}\right] \times e^{-E/T_{em}} \qquad (4)$$

where N is a normalization constant, one can simulate the experimental yield $Y_{^{14}N}$ via Eq. (3). Preliminary results using T_{em} = 5 MeV together with the level information from the literature[9] are indicated by solid curve in Fig. 2. The general trend of the spectrum is well reproduced, however, it may be necessary to include more complicated decay processes, like $^{14}N^* \rightarrow {}^{13}C^* + p$, as well before drawing a definite conclusion.

a. Department of Chemistry and Physics and Indiana University Cyclotron Facility, Indiana University, Bloomington, IN 47405

References

1. D.J. Morrisey et al., Phys. Lett. 148B, 423 (1984); Phys. Rev. C32, 877 (1985).
2. J. Pochodzalla et al., Phys. Rev. Lett. 55, 177 (1985); Phys. Lett. 161B, 275 (1985); Phys. Rev. C35, 1695 (1987).
3. D.J. Morrisey et al., Phys. Rev. C34, 761 (1986).
4. C.B. Chitwood et al., Phys Lett. 172B, 27 (1986).
5. A. Kyanowski et al., Phys. Lett. 181B, 43 (1986).
6. H.M. Xu et al., Phys. Lett. 182B, 155 (1986).
7. Z. Chen et al., Phys. Rev. C36, 2297 (1986).
8. T. Murakami et al., to be published.
9. F. Ajzenberg-Slove, Nucl. Phys. A449, 1 (1986).

POPULATION OF PARTICLE UNBOUND STATES FOR THE REACTION ^{16}O+Au AT E/A=94 MeV

Z. Chen, C.K. Gelbke, W.G. Gong, Y.D. Kim, W.G. Lynch, M.R. Maier, J. Pochodzalla[a], M.B. Tsang, F. Saint-Laurent[b], D. Ardouin,[c] H. Delagrange[b], H. Doubre[b], J. Kasagi[d], A. Kyanowski,[b] A. Péghaire[b], J. Péter[b], E. Rosato[e], G. Bizard[f], F. Lefèbvres[f], B. Tamain[f], J. Québert[g] and Y.P. Viyogi[h]

Complex particle emission in intermediate energy heavy ion induced reactions is often treated in terms of models based on the assumption of statistical emission from highly excited nuclear subsystems characterized in terms of their average velocity, space-time extent, and excitation energy.[1-4] In order to explore the limitations of such simplifying assumptions, we have measured the populations and decays of highly excited states of light nuclei for ^{16}O induced reactions on Au at E/A=94 MeV.

The experiment was performed at the Laboratoire Grand Accélérateur National d'Ions Lourds (GANIL) at Caen, France. Light particles ($Z \leq 3$) were detected by a close-packed hexagonal array of 18 ΔE-E telescopes, each consisting of a 300 μm thick planar surface barrier detector of 450 mm^2 active area and a 10 cm thick NaI(Tl) scintillator. The angular separation between the centers of adjacent telescopes was Θ_{min}=2.7°; the maximum relative angle was 11.9°. Each telescope subtended a solid angle of 0.44 msr corresponding to a resolution of the relative angle of $\Delta\Theta_{fwhm}$= 1.2°. The center of the hodoscope was positioned at a laboratory angle of Θ_{av}= 45°.

The two-particle coincidence yield, $Y_{12}(\vec{p}_1,\vec{p}_2)$, contains contributions from the sequential decay of particle unstable states as well as from the coincident, but non-resonant emission of two (or more) particles. These two components can be most easily separated by constructing the two-particle correlation function, R(q):

$$\sum Y_{12}(\vec{p}_1,\vec{p}_2) = C_{12}\cdot[1+R(q)]\cdot\sum Y_1(\vec{p}_1)\cdot Y_2(\vec{p}_2) ,$$

where $Y_1(\vec{p}_1)$ and $Y_2(\vec{p}_2)$ denote the single particle yields of particles 1 and 2 with laboratory momenta $\vec{p}_1$ and $\vec{p}_2$, respectively, and q is the momentum of relative motion. The coincidence yield, Y_c, resulting from the decay of particle unbound states is extracted by assuming that the total coincidence yield, Y_{12}, is given by

$$Y_{12}(\vec{p}_1,\vec{p}_2)=Y_c(\vec{p}_1,\vec{p}_2) + C_{12}Y_1(\vec{p}_1)Y_2(\vec{p}_2)[1+R_b(q)],$$

where $R_b(q)$ denotes the "background" correlation function.[5]

The left hand panel of Fig. 1 shows the d-α correlation function measured in this experiment. The background correlation function[5] is shown by the solid curve. The dashed line shows a theoretical correlation function[6] calculated for a Gaussian source of negligible lifetime and radius parameter of r_o=4.0 fm. The right hand side of the figure shows the extracted excitation energy spectrum for particle unstable ^{6}Li nuclei, plotted here as a function of relative kinetic energy between the coincident deuteron and α particle. The curves show the theoretical yield for thermally distributed particle unstable ^{6}Li nuclei.[5] From the coincidence yields, Y_L and Y_H, integrated over the energy ranges of $T_{c.m.}$ = 0.3-1.45 and 1.5-6.25 MeV, apparent emission temperatures of $T(^6Li)$ = 5.0±1.3 MeV were extracted. The uncertainty in T reflects primarily the uncertainty in the normalization of the background correlation function. The extracted emission temperature was not corrected for possible perturbations due to feeding from higher lying states.

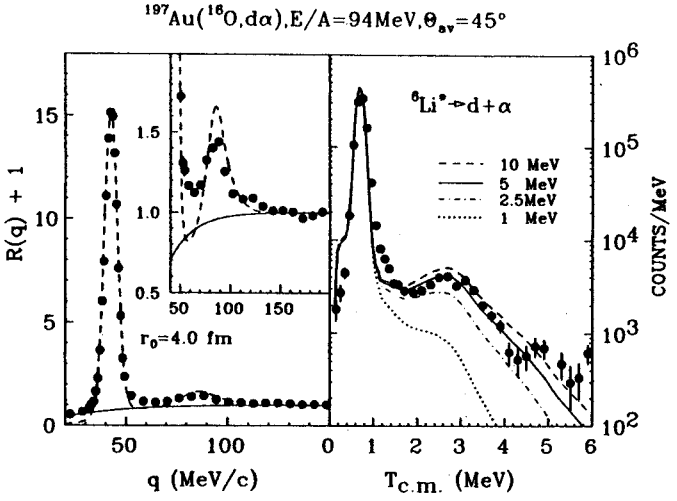

Fig. 1: Left hand panel: Energy integrated d-α correlation function for the ^{16}O+Au reaction at E/A=94 MeV and θ_{av}=45°. The dashed curve shows a theoretical correlations function;[6] the solid curve shows the background correlation function, $R_b(q)$. Right hand panel: Dependence of the coincidence yield from the decay of particle unstable ^{6}Li nuclei on the relative kinetic energy, $T_{c.m.}$, of the coincident particles. The curves show yields predicted for thermal distributions corresponding to various temperatures.

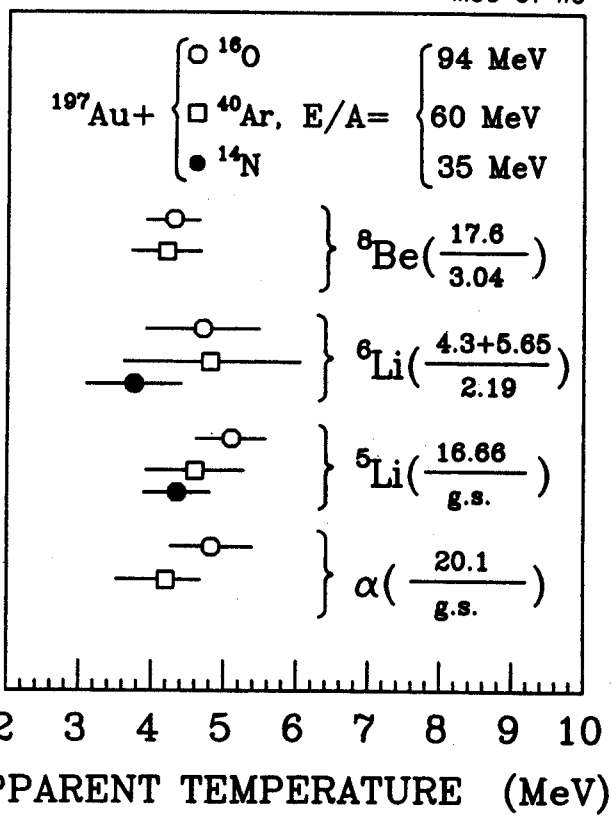

Fig. 2: Apparent emission temperatures extracted from the relative populations of states in ^{4}He, ^{5,6}Li and ^{8}Be nuclei emitted in the reactions: ^{14}N+^{197}Au at E/A=35 MeV, θ_{av}= 35° (solid points), ^{40}Ar+^{197}Au at E/A=60 MeV, θ_{av}= 30° (open squares), and ^{16}O+^{197}Au at E/A=94 MeV, θ_{av}= 45° (open circles).

More accurate determinations of emission temperatures can be made[7] by measuring the relative populations of states separated by significantly larger energy intervals, ΔE>>T. Apparent emission temperature extracted from states in ^{4}He, ^{5}Li, and ^{8}Be are consistent with that extracted from particle unbound states in ^{6}Li. Most remarkable, however, is the comparison of values extracted from the relative population of states in this experiment with those measured[8,9] for the reactions ^{14}N+^{197}Au at E/A=35 MeV and ^{40}Ar+^{197}Au at E/A=60 MeV. As shown in Fig. 2, very similar values are extracted for all three reactions, indicating that the relative populations of states are surprisingly insensitive to the incident energy. This result stands in marked contrast to the systematic energy dependence[10] of the kinetic temperature parameters (τ≈10-12 MeV for ^{14}N+Au at E/A=35 MeV, τ≈16-19 MeV for ^{40}Ar+Au at E/A=60 MeV, and τ≈17-20 MeV for ^{16}O+Au at E/A=94 MeV) which characterise the slopes of the kinetic energy spectra of light particles emitted at intermediate rapidity.

In the presence of large collective velocity components, kinetic temperatures extracted from fits to single particle inclusive distributions can be significantly larger than temperatures characterising the internal energy of the fragmenting system at breakup.[11] Relative kinetic energy spectra of coincident particles, both resonant and non-resonant, should be less sensitive to collective velocity

components, provided both particles are emitted from a portion of the interacting system which is undergoing uniform collective motion. Figure 3 shows the experimental relative kinetic energy spectrum for coincident deuterons and alpha particles. Decays of particle unstable states in ^{6}Li contribute only for $T_{c.m.} \lesssim 5$ MeV. To provide some perspective, the shapes of relative kinetic energy spectra were calculated by folding Maxwellian distributions of 10, 20, 30, and 40 MeV temperatures with the detection efficiency of the experimental apparatus. The similarity between the observed spectrum and those calculated for temperatures ranging from 20-40 MeV suggests that adequate internal energies were available to excite high lying states of intermediate mass fragments. Relative populations of states characterized by emission temperatures of 5 MeV may, therefore, not be due to a lack of internal energy.

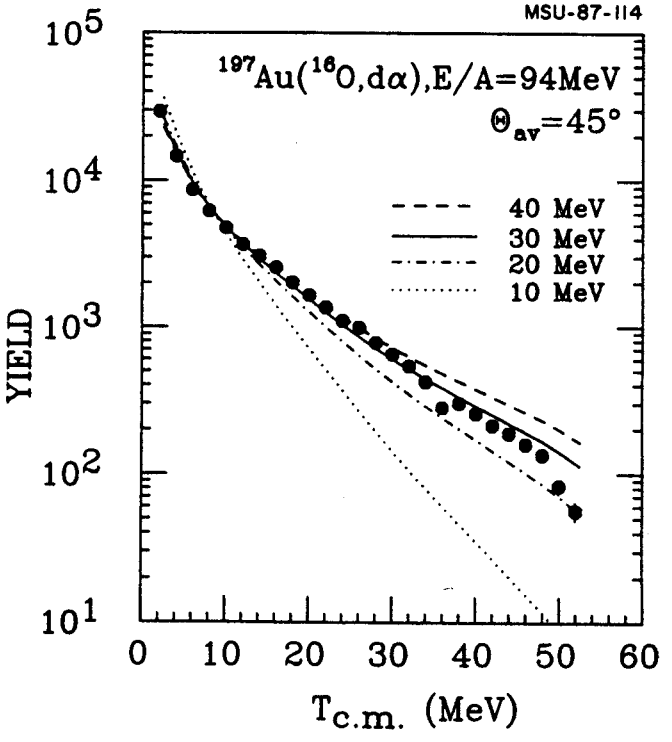

Fig. 3: Experimental d-α coincidence yield as a function of the relative kinetic energy, $T_{c.m.}$, of the two coincident particles. The curves show yields expected for Maxwellian distributions of different temperatures folded by the detection efficiency of the experimental apparatus.

a. Universität Frankfurt, Federal Republic of Germany.
b. Laboratoire Ganil, BP 5027, 14021 Caen Cedex, France
c. University of Nantes, France.
d. Tokyo Institute of Technology, Japan.
e. University of Naples, Italy.
f. Université de Caen, 14032 Caen Cedex, France
g. Centre d'Etudes Nucléaires de Bordeaux, 33170 Gradignan Cedex, France
h. Variable Energy Cyclotron Centre, Calcutta 700064, India

References

1. G.D. Westfall, et al., Phys. Rev. Lett. 37 (1976) 1202.
2. J. Gosset, et al., Phys. Rev. C18 (1978) 844.
3. J. Knoll, Phys. Rev. C30 (1979) 773.
4. D.J. Fields, et al., Phys. Rev. C30 (1984) 1912.
5. J. Pochodzalla, et al., Phys. Rev. Lett. 55 (1985) 177.
6. D.H. Boal, and J.C. Shillcock, Phys. Rev. C33 (1986) 549.
7. J. Pochodzalla, et al., Phys. Lett. B161 (1985) 275.
8. C.B. Chitwood, et al., Phys. Lett. B172 (1986) 27.
9. J. Pochodzalla, et al., Phys. Rev. C35 (1987) 1695.
10. G.D. Westfall, et al., Phys. Lett. B116 (1982) 118.
11. C.B. Chitwood, et al., Phys. Rev. C34 (1986) 858.

POSSIBLE DYNAMICAL LIMITATIONS TO EXCITATION ENERGY STORAGE IN NUCLEI

D. Ardouin[a], G. Bizard[b], H. Delagrange[a], H. Doubre[a], C.K. Gelbke, C. Grégoire[a], A. Kyanowski[a], F. Levèbvres[b], W. Lynch, M. Maier, W. Mittig[a], A. Péghaire[a], J. Péter[a], J. Pochodzalla, J. Québert[c], F. Saint-Laurent[a], B. Tamain[b], and Y.P. Viyogi[d]

Intermediate-energy heavy-ion induced reactions are of considerable interest since they provide the opportunity to study unknown features of highly excited nuclear matter. If the final disintegration stages of these reactions may be approximated in terms of statistical emission from equilibrated subsystems, the relative populations of excited states in emitted clusters would carry information about the emission temperature[1,2].

We have investigated the dependence of the relative populations of particle unbound states on the multiplicity of coincident light charged particles emitted at forward angles (θ = 5°-30°), and on the total kinetic energy of the two decay products. The light charged-particle multiplicity is used to characterize the violence of the collision. The total kinetic energy of the cluster may reveal possible cooling effects of the system.

Collisions of 60 MeV/nucleon ^{40}Ar particles with gold were studied at the GANIL facility. Coincident fragments resulting from the decay of particle unstable light clusters were detected and identified in a 13 element hodoscope located at an average laboratory angle of 30°. At this angle, the kinetic energy spectra of the emitted particles exhibit structureless near-exponential shapes indicating that contributions from quasi-elastic projectile fragmentation reactions are of minor importance[3]. Coincident with these fragments, light charged particles were observed in a large multi-detector plastic wall[4] covering a laboratory angle range from 5° to 30°. The data were analyzed event-by-event, and sorted according to the observed charged-particle multiplicity (O.M.) in the plastic wall, and the total kinetic energy of the coincident particles.

Fig. 1 shows the dependence of emission temperatures on the charged-particle multiplicity observed in the plastic wall. These values were extracted from the populations of the ground and 16.66 MeV states in ^{5}Li and of the 3.04 MeV and 17.64 MeV states in ^{8}Be. The extracted temperature values of T ≈ 4-5 MeV are consistent with those extracted from inclusive measurements[3]. Surprisingly, they exhibit little sensitivity to the coincident charged-particle multiplicity measured with the plastic wall. On the other hand, two-particle correlation functions were found[5] to depend strongly on this quantity. In addition, the extracted emission temperatures exhibit little, if any, sensitivity on the total kinetic energy per nucleon of the two decay products, see Fig. 2.

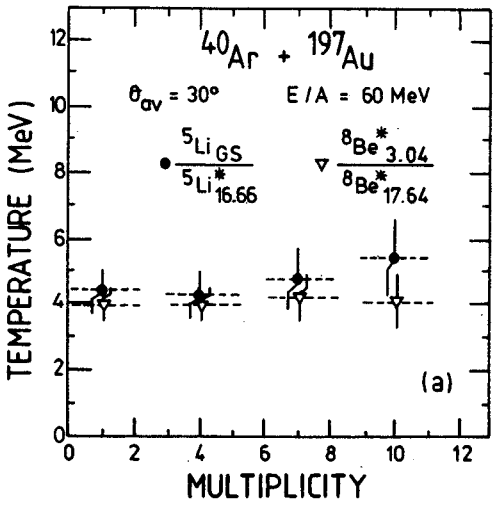

Fig. 1: Emission temperatures extracted from relative populations of widely separated states as a function of the multiplicity of light-charged particles detected in a forward direction ($\theta \leq 30°$). The horizontal dashed lines span the range over which the coincidence yields were summed.

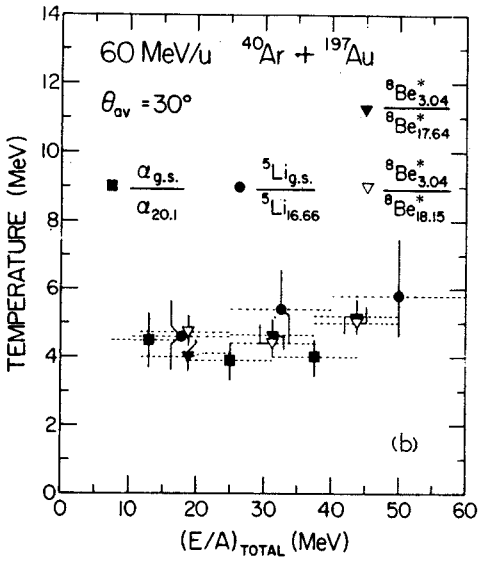

Fig. 2: Emission temperatures extracted from populations of widely separated states as a function of the total kinetic energy per nucleon of the emitted particles. The horizontal dashed lines indicate the range over which the coincidence yields were summed.

The measured insensitivities of emission temperatures to the observed charge particle multiplicity as well as to the total kinetic energy of the emitted particles are inconsistent with predictions of the participant-spectator model[7]. In this model, light-charged particles emitted at $\theta \approx 30°$ with $E/A \geq 10$ MeV originate primarily from the participant zone characterized by temperatures between 11-15 MeV. Dissipation effects[7] could lower these values to about 7-10 MeV with the exact values depending on impact parameter, these values are still inconsistent with our measurements.

In view of these difficulties, two alternative explanations could be envisaged: 1) The relative populations of states could only be sensitive to the late stages of the reaction, at which the system has already cooled by particle emission or expansion. 2) The amount of thermal energy per nucleon deposited in the reaction zone could be dynamically limited by direct, nonequilibrium particle emission. Indeed, there is some evidence for such an effect from Landau-Vlasov simulations indicating that the deposition of thermal energy could be limited in nuclear collisions. Such limitations reflect the dynamic competition between fast preequilibrium decays, excitation of collective modes, and thermalisation.

---

a. Laboratoire National GANIL, Caen, France.
b. Laboratoire de Physique Corpusculaire, Universite de Caen, France.
c. Centre d'Etudes Nucleaires de Bordeaux, Gradignan, France.
d. Variable Energy Cyclotron Centre - CALCUTTA, India and Laboratoire National GANIL, Caen, France.

References

1. J. Pochodzalla et al, Phys. Lett. 148B (1984) 423.
2. D.J. Morrissey et al, Phys. Lett. 148B (1984) 423.
3. J. Pochodzalla et al, Phys. Rev. C35, (1987) 1695.
4. G. Bizard et al, Nucl. Inst. and Meth. A244 (1986) 549.
5. A. Kyanowski et al, Phys. Lett. 181B (1986) 43.
6. R. Dayras et al, Nucl. Phys. A460 (1986) 299.
7. A. Bonasera et al, Nucl. Phys. A463 (1987) 653.

UNSTABLE RESONANCES FROM 500 MEV P + AG

D.A. Cebra, W. Benenson, Y. Chen, R. Helmer[a], E. Kashy, R. Korterling[b], D.J. Morrissey, A. Pradhan, R. S. Tickle[c], A. Vander Molen, G.D. Westfall, and W.K. Wilson

The collision between two nuclei at incident energies greater than the Fermi energy creates a thermalized interaction zone in the region of overlap between the projectile and the target.[1,2] The slope parameter of the fragment kinetic energy spectra has been used to extract the temperature of this thermal region.[3] One may also extract the temperature of the source by measuring the relative populations of excited states of the intermediate mass fragments produced in the collision. If the source is in thermal equilibrium, the ratio of two states of an isotope will be given by the Boltzmann distribution. Measurements of the relative populations of gamma emitting states of lithium and beryllium yielded temperatures an order of magnitude lower than those suggested by the slope of the energy spectra.[4] It was suggested that preferential feeding of the ground state by the decay of particle unbound states of heavier fragments caused one to underestimate the temperature, the measurements were therefore extended to particle unstable states.[5,6,7,8] The temperatures extracted from these states were still much lower than those suggested by the slope parameters of the energy spectra. In addition, the temperature did not scale with beam energy, but remained constant at 5 MeV.

We performed an experiment to study the system 500 MeV p + Ag at the Tri-University Meson Facility (TRIUMF) in Vancouver, British Columbia. This system has the same target and the same total beam energy as the 35 MeV/nucleon ^{14}N + Ag system that was studied extensively in the earlier work. It has also been demonstrated that the two systems produce similar outgoing fragment spectra[8,9]; the proton induced reactions yield a 17 MeV slope while the nitrogen on silver system yields a 14 MeV slope. The two systems both possess similar input and output characteristics, however the proton induced reaction is simpler and better understood.

We used a large solid angle (165 msr) three plane multi-wire proportional chamber (MWPC) to determine the positions of the particles emitted from the reaction. The MWPC had a position resolution of 5mm in the x and y planes (angular resolution of 0.7°). The third plane was used to resolve ambiguities that arise when several particles hit the detector simultaneously. Behind the MWPC was a four-by-four stacked array of fast/slow plastic scintillator phoswich telescopes. This allowed us to detect both fragments that are associated with the decay of a particle unstable state. The central angle of this detector array was positioned at $\theta = 60°$.

The figures display two-particle correlation functions. This correlation function is defined as the ratio of the cross section for emission of two particles in coincidence divided by the cross sections for emission of each particle individually. The solid lines correspond to calculations of expected correlations between particles emitted from a thermalized source of a given radius R_0. The emitted particles are allowed to undergo both nuclear and Coulomb final state interactions[10]. The first figure displays the proton-proton correlation function. The peak at 20 MeV/c corresponds to a final state nuclear interaction. The apparent source size for the emission of two protons from this reaction lies between 5 and 6 Fermis, note that this source size is comparable to that extracted from the

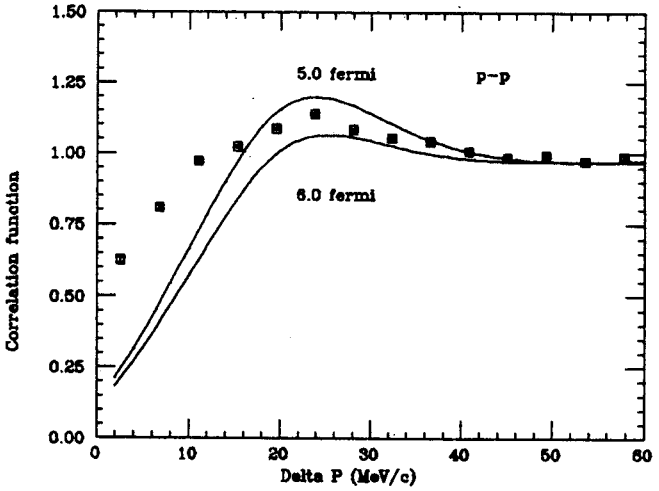

Fig. 1: Proton-proton correlation function. The solid curves represent emission from a thermal source of 5 and 6 Fermis.

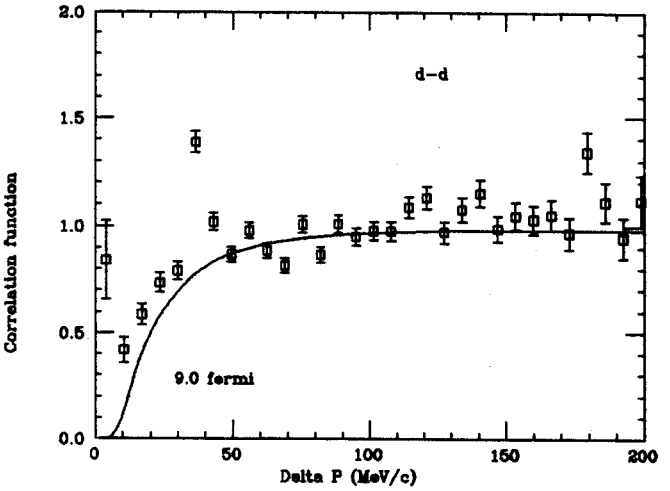

Fig. 2: The deuteron-deuteron correlation function. The solid curve represents emission from a thermal source of 9 Fermis.

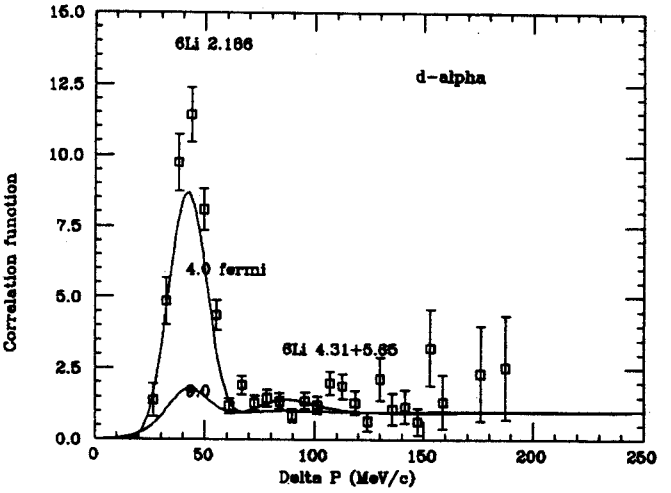

Fig. 3: The deuteron-alpha correlation function. The solid curves represent emission from a source of 4 and 9 fermi.

nitrogen on silver system in ref. 8.

Figure 2 displays the deuteron-deuteron correlation function. There is no nuclear resonance possible for this pair of particles, thus the particles undergo only Coulomb final state interactions. We feel that determination of source size from a pair that does not exhibit resonances yields a reliable measurement of the size of the interaction region. The best fit for source size is 9 Fermis.

Figure 3 displays the deuteron-alpha correlation function. One can clearly see the peaks associated with the decay of ^{6}Li. The first peak comes from the decay of the 2.186 MeV state while the second much smaller and broader peak comes from both the 4.31 and the 5.65 MeV states. The solid curves represent emission from a 4 Fermi source and from a 9 Fermi source. The source of deuteron-alpha pairs is less than 4 Fermis in size; this is an underprediction of the size of the interaction region because many of these events are the product of decay of ^{6}Li.

Having determined the size of the thermal source from the deuteron-deuteron correlation function, one can subtract out the portion of the center of mass energy spectrum that can be accounted for by emission of two light fragments independently from the source. The portion of the energy spectrum that is left must come from light particles produced in the decay of excited states. By a determination of the ratios for the production of excited states, one can determine the temperature of the thermal source as was done in ref. 5,6,7 and 8. This analysis is under way at the present time.

a. Tri-University Meson Facility, Vancouver, British Columbia.
b. Simon Fraser University, Burnaby, British Columbia.
c. University of Michigan, Ann Arbor, Michigan.

References

1. G.D. Westfall et al., Phys. Rev. Lett. 37, 1202 (1976).
2. J. Gosset et al., Phys. Rev. C18, 844 (1978).
3. B.V. Jacak et al., Phys. Rev. Lett. 51, 1846 (1983).
4. D.J. Morrissey et al., Phys. Lett. 148B, 423 (1984).
5. J. Pochodzalla et al., Phys. Rev. Lett. 161B, 275 (1985).
6. C.B. Chitwood et al., Phys. Rev. Lett. 172B, 27 (1986).
7. C. Bloch, MSU PhD thesis.
8. D. Fox et al., submitted for publication.
9. R. Green and R. Korteling, Phys. Rev. C22, 1594 (1980).
10. D. Boal and Shillcock, Phys. Rev. C33, 549 (1986).

STUDY OF THE PRODUCTION OF BOUND AND PARTICLE UNSTABLE LIGHT NUCLEI FROM 800 MeV/NUCLEON ^{40}Ar-INDUCED REACTIONS

G.D. Westfall, D.A. Cebra, W.K. Wilson, A.M. Vander Molen, C. Djalali, H. Wieman[a], W. Mueller[a], D. Olson[b], W. Christie[c], C. Tull[c], P. Brady[c], and J. Romero[c]

The study of the entropy produced and the temperatures reached in intermediate energy nucleus-nucleus collisions has produced several surprises in recent years. Temperatures extracted from the relative populations of excited states have consistently fallen in the range of 3 to 5 MeV while the kinetic energy spectra of bound fragments from the same reactions show temperatures ranging from 10 to 30 MeV. The kinetic energy temperatures scale smoothly with bombarding energy and can be explained in terms of simple kinematic and thermodynamic arguments. The temperatures extracted from these reactions from the distributions of excited states show a weak dependence on incident energy. However, most of these measurements have been carried out in the relatively small energy range of 35 to 100 MeV/nucleon.

We have extended measurements of the relative population of excited states and kinetic energy spectra of bound fragments to the much higher energy of 800 MeV/nucleon. The systems studied were ^{40}Ar+Au and KCl. These systems have been studied at 20, 30, 41, 92, and 137 MeV/nucleon where inclusive measurements of light particles and intermediate mass fragments were obtained. The measurements were carried out at the Lawrence Berkeley Laboratory (LBL) Bevalac using the Heavy Ion Spectrometer System (HISS).

The apparatus consisted of: a large, superconducting dipole magnet, a large (1.5 x 2 x 3 m) 15 plane drift chamber, and two time-of-flight (TOF) scintillator walls. Each TOF wall consisted of 20 plastic scintillators, each 10 cm wide, 2.5 cm thick, and 10 m tall. The target was placed in the center of the dipole. The positions of the drift chamber and the TOF walls, as well as the value of the magnetic field, were adjusted to maximize the acceptance of intermediate rapidity fragments. A schematic diagram of the apparatus is shown in Fig. 1.

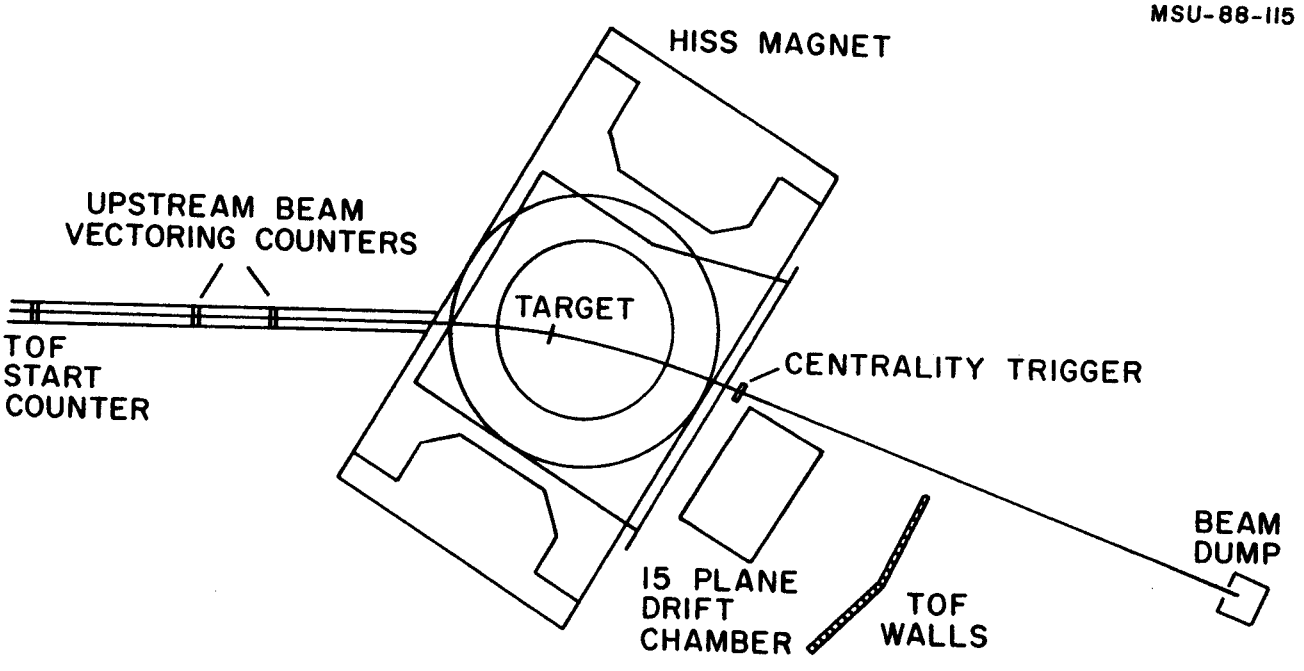

Fig. 1: The configuration of detectors around the Heavy Ion Spectrometer.

The 40 TOF scintillators provided information on the charge and the time-of-flight of each fragment. The drift chamber along with the magnetic field provided a measurement of the emission angle of the particles as well as their rigidity.

The trigger for the system consisted of one upstream scintillator, two beam vectoring devices, and an anti-coincidence scintillator. An event was accepted if a good beam particle was identified in the upstream counters and no large signal was observed in the downstream anti counter. This trigger provided central collisions in a way similar to previous streamer chamber experiments. In addition, measurements were made with a variety of less restrictive triggers including a beam trigger to provide overall absolute normalization of the cross sections.

The average multiplicity of tracks observed in the drift chamber was about 6 and an equal number of hits in the TOF wall scintillators was observed.

Currently the analysis has progressed to the stage of tracking particles through the large drift chamber and matching these tracks with the corresponding TOF wall scintillators as well as calibrating and identifying the various charges in the TOF scintillators.

---

a. Lawrence Berkeley Laboratory, Berkeley, CA 94720.
b. University of California at Riverside, Riverside, CA 92521.
c. University of California at Davis, Davis, CA 95616.

SOURCE DIMENSIONS FROM TWO-PARTICLE CORRELATION FUNCTIONS

Z. Chen, C.K. Gelbke, W.G. Gong, Y.D. Kim, W.G. Lynch, M.R. Maier, J. Pochodzalla[a], M.B. Tsang, F. Saint-Laurent[b], D. Ardouin[c], H. Delagrange[b], H. Doubre[b], J. Kasagi[d], A. Kyanowski[b], A. Péghaire[b], J. Péter[b], E. Rosato[e], G. Bizard[f], F. Lefèbvres[f], B. Tamain[f], J. Québert[g], and Y.P. Viyogi[h]

When two particles are emitted in close proximity in space and time, their wave function of relative motion can be modified by their mutual interaction.[1,2] Quantum statistical symmetries introduce further restrictions for the case of identical particles.[3] With decreasing overlap of the wavepackets of the two emitted particles, these effects become less important. Measurements of two-particle correlations at small relative momenta can, therefore, provide information about the space-time characteristics of the emitting system. Two-particle correlation functions at small relative momenta have been published[4-6] for the reactions $^{16}O+^{197}Au$ at E/A=25 MeV, $^{14}N+^{197}Au$ at E/A=35 MeV, and $^{40}Ar+^{197}Au$ at E/A=60 MeV. Here, we report the results of similar measurements for the reaction $^{16}O+^{197}Au$ at E/A=94 MeV.

The experiment was performed at the Laboratoire Grand Accélérateur National d'Ions Lourds (GANIL) at Caen. The experimental setup and the definition of the experimental correlation function are given on page 53.

If, in a thermal model, the interactions between two particles are much more important than the interactions with the rest of the system, the correlation function can be approximated as:[2]

$$R(q) = \frac{2\pi}{(2s_1+1)(2s_2+1)\cdot Vq^2} \cdot \sum_{J,\alpha} (2J+1)\cdot\frac{\partial\delta_{J,\alpha}}{\partial q} \quad .$$

Here, J is the total angular momentum and $\delta_{J,\alpha}$ is the scattering phase shift for channel α. In this approximation, the two-particle correlation function depends only on the volume, V, of the emitting system. It is independent of its temperature. This sensitivity of two-particle correlation functions to the space-time extent of the emitting system was originally derived from the modifications of the plane waves describing the relative motion of the two particles by their respective interactions[1] and, for the case of identical particles, by the restrictions imposed by quantum statistical symmetries.[3] If the time dependence of the emission process is neglected, one can express the two-particle correlation function in terms of the single particle source function, $\rho(\vec{r})$, and the two-body wave function $\Psi(\vec{r}_1,\vec{r}_2)$:[1]

$$R(q) = \int d^3r_1 d^3r_2 \{|\Psi(\vec{r}_1,\vec{r}_2)|^2-1\}\cdot\rho(\vec{r}_1)\rho(\vec{r}_2) \times \left(\int d^3r\ \rho(\vec{r})\right)^{-2}.$$

The equivalence of these two expressions was proved in ref. 2. Most analyses of two-particle correlations have been based on the model of ref. 1, with $\rho(r) \propto \exp(-r^2/r_0^2)$. For fixed spatial source dimensions, the magnitude of two-particle correlations decreases when the particles are emitted at larger time intervals. The simplifying assumption of negligible lifetime can, therefore, only provide upper limits for the spatial dimensions of the emitting system.

Figure 1 shows two-proton correlation functions measured in this experiment. The attractive singlet S-wave interaction between the two coincident protons gives rise to a maximum in the correlation function at a relative momentum of q≈20 MeV/c. This maximum becomes larger with increasing total kinetic energy, E_1+E_2, of the two coincident particles

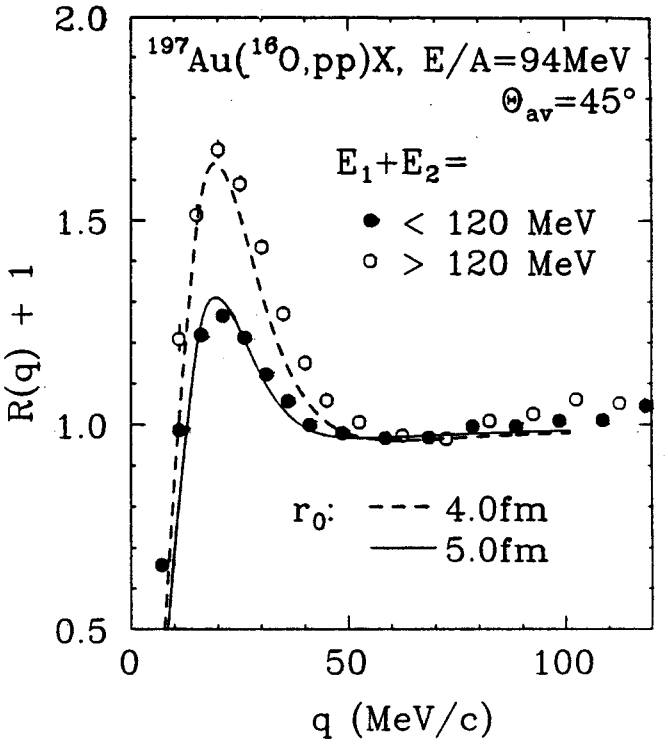

Fig. 1: p-p correlation functions measured for ^{16}O induced reactions on ^{197}Au at E/A=94 MeV and an average emission angle of θ_{av}=45°. The constraints on the total kinetic energy, E_1+E_2, of the two coincident particles are indicated in the figure. The curves show calculations with the model of ref. 1.

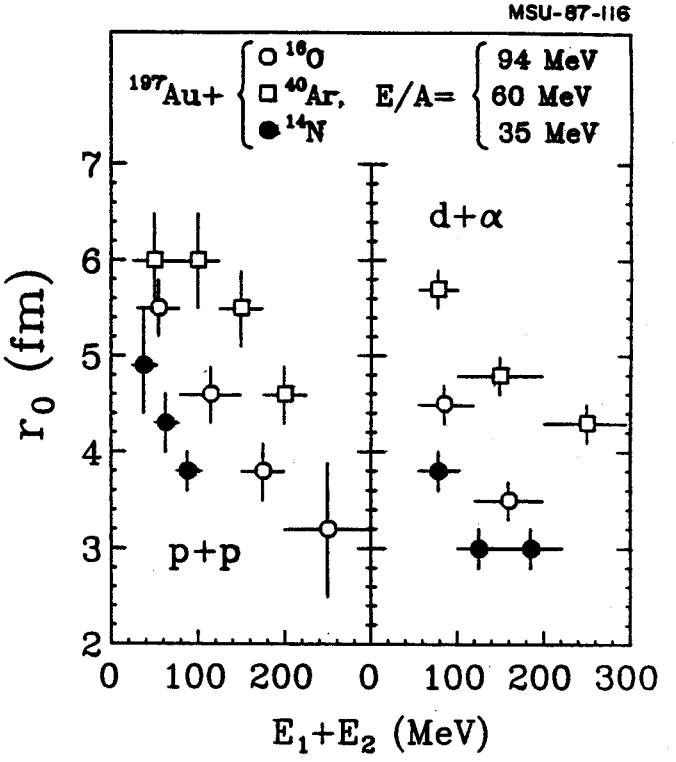

Fig. 2: Source parameters, r_0, extracted from p-p correlation functions (left hand side) and α-d correlation functions (right hand side) for the reactions: ^{14}N+^{197}Au at E/A=35 MeV (solid points, ref. 5), ^{40}Ar+^{197}Au at E/A=60 MeV (open squares, ref. 6), and ^{16}O+^{197}Au at E/A=94 MeV (open circles, this work). The dependence on the total kinetic energy, E_1+E_2, of the two coincident particles is shown.

indicating that more energetic light particles are emitted from sources which are more localized in space-time. A more quantitative scale is provided by the dashed and solid curves which represent theoretical correlation functions predicted[1] for r_0 = 4 and 5 fm, respectively.

Figure 2 compares source radii extracted in terms of the zero-lifetime final state interaction model from p-p (left hand side) and α-d (right hand side) correlation functions measured for ^{14}N, ^{40}Ar, and ^{16}O induced reactions on ^{197}Au at E/A = 35, 60, and 94 MeV, respectively. Since there is strong experimental evidence[7] that finite lifetime effects cannot be ignored, these source radii only provide upper limits for the spatial dimensions of the emitting system. In all cases, smaller source radii are extracted for more energetic particles indicating that these particles are emitted at shorter time intervals and/or from smaller sources. For the most energetic particles emitted in ^{14}N and ^{16}O induced reactions, the extracted upper limits of the source dimensions are smaller than the size of the target nucleus ($r_0(Au) = \sqrt{2/3}\cdot r_{rms}(Au) \approx 4.3$ fm). Larger values for r_0 are deduced for ^{40}Ar induced reactions. For particles of a fixed total kinetic energy, the source dimensions can be ordered as $r_0(^{14}N+Au) < r_0(^{16}O+Au) < r_0(^{40}Ar+Au)$. Qualitatively, this ordering is to be expected from the relative dimensions of the geometrical regions of overlap formed for an average collision. However, it

does not appear that the extracted source dimensions depend only on the size of the initial reaction zone. Indeed, for correlations at fixed sum energy, E_1+E_2, the source dimensions also depend on the incident energy, with increasing space-time dimensions being observed at higher projectile energies. Source radii extracted from two-proton correlation functions exhibit an interesting dependence on the quantity

$$\frac{E_1 + E_2}{A_1 + A_2} \times \frac{A_p}{E_p},$$

the total kinetic energy per nucleon of the two coincident protons measured in units of the kinetic energy per nucleon of the incident projectile, see Fig. 3. For projectiles of comparable dimensions, such as ^{14}N and ^{16}O, the extracted values of r_o appear to depend primarily on this parameter. Alternative methods for scaling two-particle correlation functions should be explored. Clearly, more data are needed to establish the systematic dependence of two-particle correlation functions on beam energy and projectile-target combination.

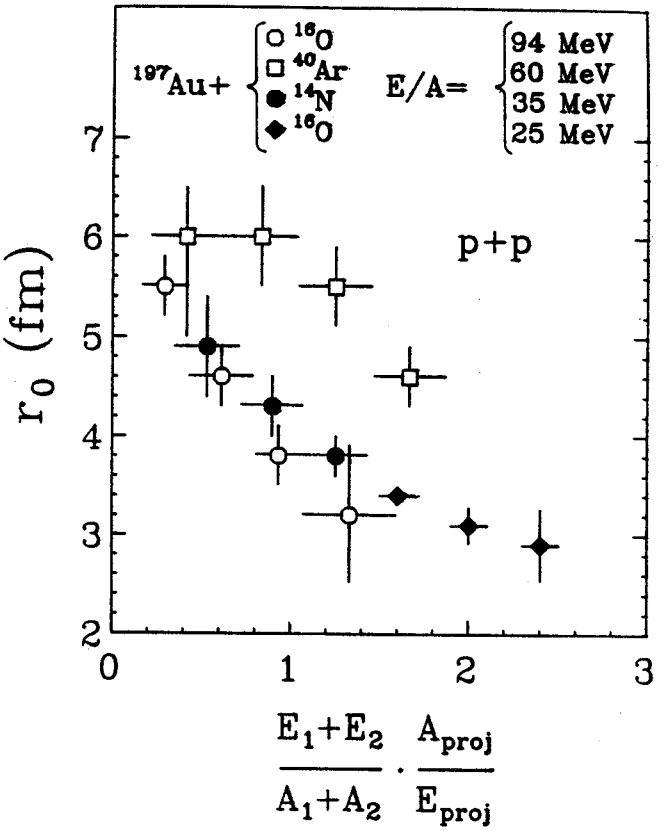

Fig. 3: Source parameters extracted from p-p correlation functions measured for the reactions: $^{14}N+^{197}Au$ at E/A=35 MeV (solid points, ref. 5), $^{40}Ar+^{197}Au$ at E/A=60 MeV (open squares, ref. 6), and $^{16}O+^{197}Au$ at E/A=25 MeV (solid diamonds, ref. 4) and E/A=94 MeV (open circles, this work). Shown is the dependence on the total kinetic energy per nucleon of the two coincident particles measured in units of the projectile energy per nucleon, $(E_1+E_2)A_p/[(A_1+A_2)E_p]$.

a. Universität Frankfurt, Federal Republic of Germany.
b. Laboratoire Ganil, BP 5027, 14021 Caen Cedex, France
c. University of Nantes, France.
d. Tokyo Institute of Technology, Japan.
e. University of Naples, Italy.
f. Université de Caen, 14032 Caen Cedex, France
g. Centre d'Etudes Nucléaires de Bordeaux, 33170 Gradignan Cedex, France
h. Variable Energy Cyclotron Centre, Calcutta 700064, India

References

1. S.E. Koonin, Phys. Lett. B70, 43 (1977).
2. B.K. Jennings, et al., Phys. Rev. C33, 1303 (1986).
3. G.I. Kopylov, Phys. Lett. B50, 472 (1974).
4. W.G. Lynch, et al., Phys. Rev. Lett. 51, 1850 (1983).
5. J. Pochodzalla, et al., Phys. Lett. 174B, 36 (1986).
6. J. Pochodzalla, et al., Phys. Rev. C35, 1695 (1987).
7. Z. Chen, et al., Phys. Lett. B186, 280 (1987).

TARGET RESIDUES FROM THE INTERACTION OF COPPER AND SILVER WITH ^{12}C IONS

S.Y. Cho[a], Y. H. Chung[b], D.J. Morrissey, and N.T. Porile[a]

We are investigating the interaction of 15-45 MeV/nucleon ^{12}C ions with copper and silver by γ-ray spectrometry of target residues. The experiments provide information on the isobaric-yield and mass yield distributions as well as on the longitudinal momentum transfer. During the past year, we performed experiments with 15 and 45 MeV/nucleon ^{12}C ions. The copper data have been analyzed and, along with earlier data at intermediate energies, will be written up for publication. The silver data are still being analyzed.

An article describing the experimental procedure and the results obtained for 35 MeV/nucleon interactions with copper has been published.[1]

---

a. Department of Chemistry, Purdue University, W. Lafayette, IN
b. Department of Chemistry, Hallym University, Chooncheon, Korea

References

1. S.Y. Cho, Y.H. Chung, N.T. Porile, and D.J. Morrissey, Phys. Rev. C36, 2349 (1987).

ELASTIC SCATTERING OF 35 MeV/A ^{6}Li IONS FROM ^{28}Si AND ^{40}Ca

A. Nadasen[a], M. McMaster[a], J. Tavormina[a], F.D. Becchetti[b], J.W. Janecke[b], P. Schwandt[c], R.E. Warner[d], and J. Winfield

Measurements of the elastic scattering of 35 MeV/A ^{6}Li from ^{28}Si and ^{40}Ca were carried out using the S320 spectrometer. Differential cross sections were obtained for center-of-mass angles of 4° to 46° for ^{28}Si and 4.5° to 43.5° for ^{40}Ca (Fig. 1). The data ranged over seven orders of magnitude. The angular distributions exhibit diffractive oscillations at the forward angles, which are very similar to lower energy data. However, at the larger angles smooth exponential fall-off, characteristic of rainbow scattering, is observed. The large-angle rainbow scattering data are expected to provide unique ^{6}Li potentials for these targets. This has already been demonstrated for ^{12}C and ^{58}Ni.[1] Additional measurements have been made for the ^{90}Zr target in order to eliminate inconsistencies in earlier measurements and to define more clearly the angular dependence of the data. Coupled with earlier measurements,[1,2] data for six targets ranging from ^{12}C to ^{208}Pb are available for the elastic scattering for 35 MeV/A ^{6}Li ions. Unique potentials are expected to be extracted for all targets except ^{208}Pb. If a target-mass dependence of the potentials could be determined, then the unique potential for ^{208}Pb can also be obtained. Further, with the aid of these results, unique potentials at lower energies could be selected from the families of ambiguous ones. Finally, the energy dependence of ^{6}Li elastic scattering for energies up to 210 MeV could be clearly defined.

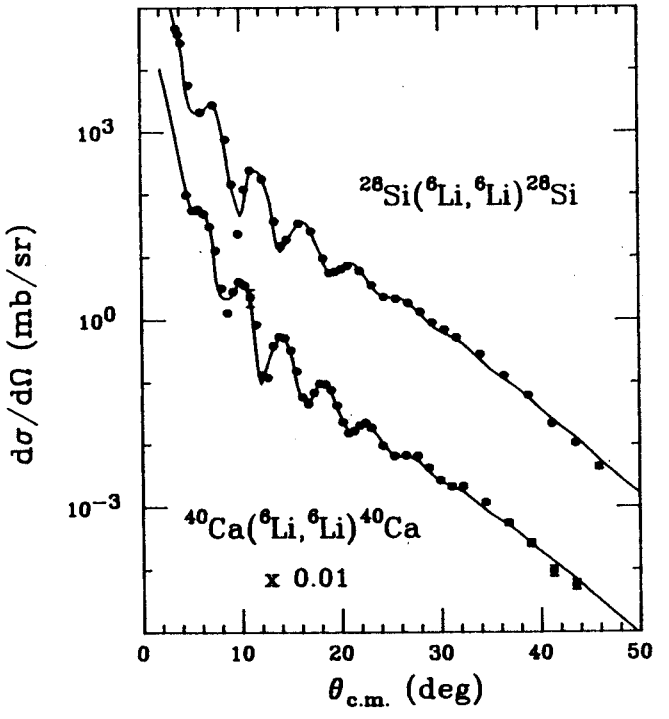

Fig. 1: Differential cross sections for 35 MeV/A ^{6}Li scattering from ^{28}Si, and ^{40}Ca.

a. University of Michigan, Dearborn, MI.
b. University of Michigan, Ann Arbor, MI.
c. IUCF, Bloomington, IN.
d. Oberlin College, Oberlin, OH.

References

1. A. Nadasen, et al., Phys. Rev. C37, 132 (1988).
2. A. Nadasen, et al., BAPS 30, 1280 (1985).

STATISTICAL MODEL OF $p\bar{p}$ ANNIHILATION AT REST

H. Toki[a] and G.F. Bertsch

In view of the interest in phase transitions in hot hadronic matter, it is worthwhile to reexamine $p\bar{p}$ annihilation, which produces very high energy density in a small volume. Fermi's statistical model of the decay[1] is characterized by a single parameter, the spatial volume of the decaying equilibrated source. His original model considered only pion degrees of freedom and required an unreasonably large equilibration volume, $V \approx 75$ fm^3, i.e. a spherical volume of radius 2.6 fm. When higher mesons were included via a bootstrap model,[2] the necessary volume was reduced to a more reasonable value. However, the strangeness production was greatly overestimated.

We have reexamined the statistical model using only the known meson degrees of freedom in recently compiled data.[3] The N-body phase space is calculated allowing the following 14 mesons: π, η, ρ, ω, η', a_0, ϕ, h_1, b_1, f_2, a_1, f_1, f_0, and a_2. The mesons heavier than the π decay into pi's and K's with known branching ratios.

Figure 1 shows the predicted multi-pion branches in the $p\bar{p}$ annihilation, compared to experiment[4] and also compared to a microscopic quark model.[5] Both models describe the data fairly well. The size parameter in the statistical model, R=1.5, is close to the value found in Ref. 2, and represents a somewhat expanded state. One important difference in our results as compared to ref. 2) is that we reproduce the K production much better. We conclude that the statistical model is as good an explanation of the decay branches as the microscopic model.

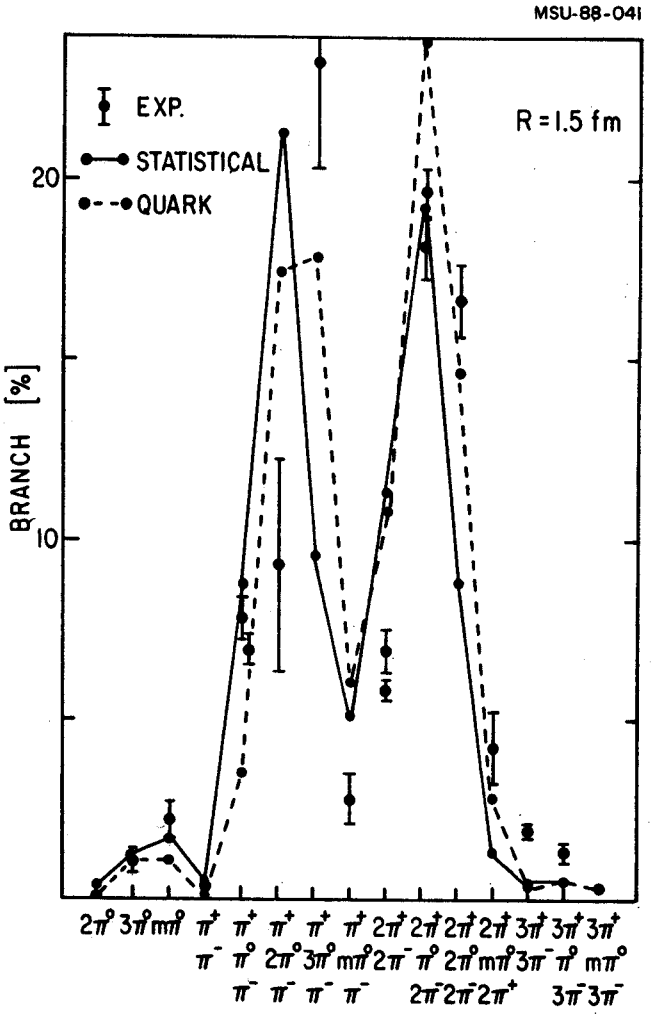

Fig. 1

a. Permanent address: Department of Physics, Tokyo Metropolitan University, Setagaya, Tokyo 158, Japan

References

1. E. Fermi, Prog. Theor. Phys. 5,570(1950).
2. C.J. Hamer, Nuovo Cimento 12A,162(1972).
3. Particle Data Group, Phys. Lett. 56,1 (1986).
4. P. Pavlopoulos, et al., Nucleon-Nucleon Interactions--1977, (AIP Conf. Proc. 41,340 (1978)).
5. S. Furui, A. Faessler and S.B. Khadkikar, Nucl. Phys. A424,495(1984); A. Faessler, TÜbingen preprint, 1987.